UNITED STATES AIR FORCE

SUMMER RESEARCH PROGRAM -- 1997

SUMMER RESEARCH EXTENSION PROGRAM FINAL REPORTS

VOLUME 5

ARNOLD ENGINEERING CENTER
AIR LOGISTICS CENTERS
UNITED STATES AIR FORCE ACADEMY
WILFORD HALL MEDICAL CENTER

RESEARCH & DEVELOPMENT LABORATORIES

5800 Uplander Way

Culver City, CA 90230-6608

Program Director, RDL
Gary Moore

Program Manager, AFOSR
Major Linda Steel-Goodwin

Program Manager, RDL
Scott Licoscos

Program Administrator, RDL
Johnetta Thompson

Program Administrator, RDL
Rebecca Kelly-Clemmons

Submitted to:

AIR FORCE OFFICE OF SCIENTIFIC RESEARCH

Bolling Air Force Base

Washington, D.C.

December 1997

PREFACE

This volume is part of a five-volume set that summarizes the research of participants in the 1997 AFOSR Summer Research Extension Program (SREP.)

Reports presented in this volume are arranged alphabetically by author and are numbered consecutively – e.g., 1-1, 1-2, 1-3; 2-1, 2-2, 2-3. Reports in the five-volume set are organized as follows:

VOLUME	TITLE
1	Armstrong Laboratory
2	Phillips Laboratory
3	Rome Laboratory
4A	Wright Laboratory
4B	Wright Laboratory
5	Arnold Engineering Development Center Air Logistics Centers United States Air Force Academy Wilford Hall Medical Center

REPORT DOCUMENTATION PAGE

AFRL-SR-BL-TR-00-

0713

1. AGENCY USE ONLY *(Leave blank)*	2. REPORT DATE	3. REP
	December, 1997	

4. TITLE AND SUBTITLE
1997 Summer Research Program (SRP), Summer Research Extension Program (SREP), Final Report, Volume 5, Arnold Eng. Development Center (AEDC), Air Logistics Centers, USAF Academy, and Wilford Hall Medical Center (WHMC)

5. FUNDING NUMBERS
F49620-93-C-0063

6. AUTHOR(S)
Gary Moore

7. PERFORMING ORGANIZATION NAME(S) AND ADDRESS(ES)
Research & Development Laboratories (RDL)
5800 Uplander Way
Culver City, CA 90230-6608

8. PERFORMING ORGANIZATION REPORT NUMBER

9. SPONSORING/MONITORING AGENCY NAME(S) AND ADDRESS(ES)
Air Force Office of Scientific Research (AFOSR)
801 N. Randolph St.
Arlington, VA 22203-1977

10. SPONSORING/MONITORING AGENCY REPORT NUMBER

11. SUPPLEMENTARY NOTES

12a. DISTRIBUTION AVAILABILITY STATEMENT
Approved for Public Release

12b. DISTRIBUTION CODE

13. ABSTRACT *(Maximum 200 words)*

The United States Air Force Summer Research Program (SRP) is designed to introduce university, college, and technical institute faculty members to Air Force research. This is accomplished by the faculty members, graduate students, and high school students being selected on a nationally advertised competitive basis during the summer intersession period to perform research at Air Force Research Laboratory (AFRL) Technical Directorates and Air Force Air Logistics Centers (ALC). AFOSR also offers its research associates (faculty only) an opportunity, under the Summer Research Extension Program (SREP), to continue their AFOSR-sponsored research at their home institutions through the award of research grants. This volume consists of a listing of the participants for the SREP and the technical report from each participant working at the Arnold Engineering Development Center (AEDC), Air Logistics Centers, United States Air Force Academy (USAFA), and Wilford Hall Medical Center (WHMC).

14. SUBJECT TERMS
Air Force Research, Air Force, Engineering, Laboratories, Reports, Summer, Universities, Faculty, Graduate Student, High School Student

15. NUMBER OF PAGES

16. PRICE CODE

17. SECURITY CLASSIFICATION OF REPORT	18. SECURITY CLASSIFICATION OF THIS PAGE	19. SECURITY CLASSIFICATION OF ABSTRACT	20. LIMITATION OF ABSTRACT
Unclassified	Unclassified	Unclassified	UL

GENERAL INSTRUCTIONS FOR COMPLETING SF 298

The Report Documentation Page (RDP) is used in announcing and cataloging reports. It is important that this information be consistent with the rest of the report, particularly the cover and title page. Instructions for filling in each block of the form follow. It is important to ***stay within the lines*** to meet ***optical scanning requirements.***

Block 1. Agency Use Only *(Leave blank)*.

Block 2. Report Date. Full publication date including day, month, and year, if available (e.g. 1 Jan 88). Must cite at least the year.

Block 3. Type of Report and Dates Covered. State whether report is interim, final, etc. If applicable, enter inclusive report dates (e.g. 10 Jun 87 - 30 Jun 88).

Block 4. Title and Subtitle. A title is taken from the part of the report that provides the most meaningful and complete information. When a report is prepared in more than one volume, repeat the primary title, add volume number, and include subtitle for the specific volume. On classified documents enter the title classification in parentheses.

Block 5. Funding Numbers. To include contract and grant numbers; may include program element number(s), project number(s), task number(s), and work unit number(s). Use the following labels:

C - Contract	**PR** - Project
G - Grant	**TA** - Task
PE - Program Element	**WU** - Work Unit Accession No.

Block 6. Author(s). Name(s) of person(s) responsible for writing the report, performing the research, or credited with the content of the report. If editor or compiler, this should follow the name(s).

Block 7. Performing Organization Name(s) and Address(es). Self-explanatory.

Block 8. Performing Organization Report Number. Enter the unique alphanumeric report number(s) assigned by the organization performing the report.

Block 9. Sponsoring/Monitoring Agency Name(s) and Address(es). Self-explanatory.

Block 10. Sponsoring/Monitoring Agency Report Number. *(If known)*

Block 11. Supplementary Notes. Enter information not included elsewhere such as: Prepared in cooperation with....; Trans. of....; To be published in.... When a report is revised, include a statement whether the new report supersedes or supplements the older report.

Block 12a. Distribution/Availability Statement. Denotes public availability or limitations. Cite any availability to the public. Enter additional limitations or special markings in all capitals (e.g. NOFORN, REL, ITAR).

DOD -	See DoDD 5230.24, "Distribution Statements on Technical Documents."
DOE -	See authorities.
NASA -	See Handbook NHB 2200.2.
NTIS -	Leave blank.

Block 12b. Distribution Code.

DOD -	Leave blank.
DOE -	Enter DOE distribution categories from the Standard Distribution for Unclassified Scientific and Technical Reports.
	Leave blank.
NASA -	Leave blank.
NTIS -	

Block 13. Abstract. Include a brief *(Maximum 200 words)* factual summary of the most significant information contained in the report.

Block 14. Subject Terms. Keywords or phrases identifying major subjects in the report.

Block 15. Number of Pages. Enter the total number of pages.

Block 16. Price Code. Enter appropriate price code *(NTIS only)*.

Blocks 17. - 19. Security Classifications. Self- explanatory. Enter U.S. Security Classification in accordance with U.S. Security Regulations (i.e., UNCLASSIFIED). If form contains classified information, stamp classification on the top and bottom of the page.

Block 20. Limitation of Abstract. This block must be completed to assign a limitation to the abstract. Enter either UL (unlimited) or SAR (same as report). An entry in this block is necessary if the abstract is to be limited. If blank, the abstract is assumed to be unlimited.

1997 SREP Final Technical Report Table of Contents

Armstrong Laboratory

Volume 1

1997 SREP Final Technical Report Table of Contents

Armstrong Laboratory

Volume 1 (cont.)

1997 SREP Final Technical Report Table of Contents

Phillips Laboratory

Volume 2

1997 SREP Final Technical Report Table of Contents

Phillips Laboratory

Volume 2 (cont.)

1997 SREP Final Technical Report Table of Contents

Rome Laboratory

Volume 3

1997 SREP Final Technical Report Table of Contents

Rome Laboratory

Volume 3 (cont.)

1997 SREP Final Technical Report Table of Contents

Wright Laboratory

Volume 4A

1997 SREP Final Technical Report Table of Contents

Wright Laboratory (cont.)

Volume 4A

1997 SREP Final Technical Report Table of Contents

Wright Laboratory (cont.)

Volume 4B

1997 SREP Final Technical Report Table of Contents

Volume 5

ANALYSIS OF LASER VAPOR SCREEN FLOW VISUALIZATION SYSTEM IN 16 T

Frank G. Collins
Professor
Department of Mechanical and Aerospace Engineering and Engineering Mechanics

The University of Tennessee Space Institute
Tullahoma, TN 37388-8898

Final Report for:
Summer Research Extension Program
Arnold Engineering Development Center

Sponsored by:
Air Force Office of Scientific Research
Boling Air Force Base, DC

and

Arnold Engineering Development Center

March 1998

ANALYSIS OF LASER VAPOR SCREEN FLOW VISUALIZATION SYSTEM IN 16 T

Frank G. Collins
Professor
Department of Mechanical and Aerospace Engineering
and Engineering Mechanics
The University of Tennessee Space Institute

Abstract

A laser vapor screen (LVS) flow visualization apparatus has been installed in the AEDC 16T subsonic/transonic wind tunnel and used during two tests. Previous wind tunnel use of the vapor screen method is examined with emphasis on the improvements that have been made over time, leading to the present use of a laser light sheet to illuminate the water droplets. Naturally occurring vaporization patterns are used to illustrate flow features that could be made visible using the method in the wind tunnel. Natural vaporization usually occurs in vortices on vehicles that are at large angles-of-attack. The components of a LVS system are enumerated. Mie scattering patterns for various droplet sizes are computed to illustrate the benefits of viewing the laser light sheet from 50° rather than 90°. Equations needed for analyzing the humidity conditions in a wind tunnel are given and used to analyze the humidity conditions of two 16T tests. It is shown that the method depends on the total amount of water vapor in the tunnel circuit rather than the specific humidity. Relative humidity approaching 1.0 in the stilling chamber is required to apply the technique to low subsonic flow fields but must be reduced to very low values for supersonic flow fields. Tentative limits of applicability of LVS in the 16T wind tunnel are determined from the two tests. Recommendations for continued improvement of LVS in 16T are given.

ANALYSIS OF LASER VAPOR SCREEN FLOW VISUALIZATION SYSTEM IN 16 T

Frank G. Collins

Introduction

Vapor screen is a means for making certain aspects of a flow field within a plane in a wind tunnel visible. It is particularly useful for exploring the properties of flows that have embedded vortices, such as flows over aircraft with strakes or other sharp-edged geometries that generate strong vortices or missile configurations at high angles of attack. The method is also useful when shock waves exist.

The vapor screen method operates by introducing an intense sheet of light into a wind tunnel, which is then scattered by water droplets (or sometimes ice crystals) that have been generated in the flow field. Scattered light is recorded at an appropriate angle to the light sheet by a video or still camera. The light sheet is generally introduced perpendicular to the free stream flow direction. Regions of concentrated vorticity are observed as white patches in subsonic flow or dark areas within a white sheet in supersonic flow. The water vapor can be supplied either by the wind tunnel free stream or from spray nozzles positioned upstream of the test section.

Vapor screen requires that the local relative humidity exceeds 1.0 (in this report relative humidity is given as a decimal) and the air is supersaturated. The supersaturated water vapor will then nucleate and condense to form small water droplets. The accompanying latent heat release brings the flow to a new equilibrium condition at a higher stagnation temperature, which is approximately saturated. The scattered light intensity distribution can be described by Mie scattering theory assuming spherical water droplets. If the number density and size of the droplets are large enough, then the light scattered by the water droplets is sufficient to be recorded by the camera and a vapor screen image can be recorded. The success of the vapor screen method depends on both generating great numbers of large water droplets at the appropriate point in the flow field and on introducing an intense light sheet into the wind tunnel.

First consider the vapor screen that relies upon the condensation of the wind tunnel free stream moisture. In subsonic flow the free stream relative humidity must be increased

sufficiently to allow condensation to occur within local regions of the flow over a model, such as in the core of vortices. These regions appear as white regions within the light sheet. Local condensation occurs because the local temperature in the vortex is decreased; the relative humidity is much more sensitive to changes in the local static temperature than to changes in pressure (Ref. 1 and Eq. (29)). In supersonic flow the entire flow field saturates within the nozzle, allowing droplets to be formed in the free stream upstream of the model. The droplets are then partially removed by the intense circular motion within the core of the vortices, which appear as dark regions, devoid of water droplets, contained within a white sheet. The vapor screen method has recently found great value in studying vortical flows for free-stream Mach numbers greater than 0.6 (Ref. 2 to 5); it has also been used with some success at lower Mach numbers (Ref. 6).

Campbell, et al. (Ref. 1) collected around 300 photographs of aircraft which displayed natural water condensation while the aircraft were in flight. These photographs were collected to obtain a more complete understanding of flow features that can be observed due to condensation. Naturally-occurring patterns could be classified as spanwise "gull" patterns from swept wing-bodies, expansion and shock patterns for transonic flow, and leading-edge separation-induced vortex flow from slender wings and bodies. Generally the vehicles were at high angles-of-attack. The same types of flow features should be observable by the vapor screen method in the wind tunnel. Unfortunately, no atmospheric temperature, pressure, or humidity data accompanied the photographs.

Campbell, et al. used existing CFD solutions for similar aircraft configurations to obtain approximate flow field information and then added a humidity prediction to the computation assuming that the atmosphere had a temperature of 280 K and a relative humidity of 0.85. They concluded that homogeneous nucleation of water vapor did not occur before the relative humidity reached 4.0 locally, and that otherwise heterogeneous nucleation (on foreign bodies) occurred. Once condensation occurred, then it was thought that the relative humidity remained in the range 1 to 4 as a result of the latent heat release.

Some of their results are of interest. For flow over a transonic airfoil, they predicted that the relative humidity reached 20.0 just before the shock wave on the upper airfoil surface. Then the relative humidity decreased through the shock due to the rapid increase in temperature, even

though the pressure also increased. Since the temperature was higher in the boundary layer, the relative humidity was very low there. Supercritical conditions, with the relative humidity greater than 1.0, were predicted to extend far upward from the wing surface in the region of transonic flow, explaining the observation of large patches of condensation in some regions of transonic flow conditions.

For M = 0.3 flow over a delta wing at 25° angle-of-attack, the relative humidity increased to 1.25 in some portions of the vortices but it was predicted to be less than 1.0 within the vortex core, which appeared clear in the photograph. This may offer an additional explanation to why the core of vortices in supersonic flow are clear (or appear as dark spots in vapor screen images) other than due to centrifugal effects on the core droplets. The computer program predicted that within the vortex core the temperature increased and the pressure decreased.

Condensation was found to occasionally occur in the streamwise vorticity that is shed from the leading edge of a wing at high angle-of-attack. These vortices are caused by a three-dimensional cross-flow instability. The vortices were observed to disappear at mid-chord, not because they no longer existed, but because the local temperature increased in the compression above the wing causing the droplets to evaporate. Condensation was also observed to disappear at the point where a vortex bursts, probably due to the fact that there is an adverse pressure gradient and deceleration of the flow which causes a rise in temperature and pressure great enough to evaporate the droplets. The same occurs for flows that pass through shock waves. This suggest that caution should be exercised when comparing flows visualized by condensation with those obtained by seeding with dyes or smoke, because whereas the seeding particles cannot disappear, the water vapor can both condense and evaporate.

Usually it is desirable to operate a wind tunnel at free stream conditions far from saturation. Vapor screen flow visualization can still be utilized by introducing streamtubes of very moist air which are positioned to pass over the model. The streamtubes are created by spraying water from nozzles that are strategically placed at the upstream end of the stilling chamber. Large water droplets from the spray nozzles fall to the tunnel floor before reaching the wind tunnel nozzle and the smaller droplets evaporate, resulting in a streamtube of high humidity air which then will re-condense in the vortices and other flow features created by the model.

This report describes the humidity considerations of the laser vapor screen flow visualization system that has been implemented in the AEDC 16T wind tunnel. Results of both natural and seeded vapor screen condensation will be described from two wind tunnel tests in which the flow visualization tests were piggy-backed onto the other measurements.

Previous Applications of Vapor Screen Flow Visualization

The vapor screen flow visualization method was developed by Allen and Perkins (Ref. 7) in 1950 to examine the vortex system created by an ogive-cylinder at high angles-of-attack in supersonic flow (M = 2) in the NASA Ames 1- by 3-foot supersonic wind tunnel. They added water vapor to the tunnel, in a manner not described, which condensed in the nozzle to form a fine fog in the test section. The fog was illuminated by a narrow beam of light from a mercury vapor lamp. The vortices were observed as dark patches in a white sheet. It was speculated that the droplets were removed from the core of the vortex by the circular motion within the vortices, thus leaving a dark patch in the light sheet. Shock waves were also observed as a change in light intensity.

The vapor screen method was thoroughly investigated later by McGregor (Ref. 8) in the 3-Foot R. A. E. Bedford tunnel. While most of his investigation was performed on the flow over a delta wing in the Mach number range of 1.3 to 2.0, some examination was made using the same model at Mach numbers of 0.8-0.85. The tunnel air was very thoroughly dried and then measured amounts of water vapor were added to the circuit. For supersonic flow the air/vapor mixture cooled in the nozzle to form a fog in the test section. The fog was illuminated by a beam of white light from a mercury-vapor lamp. The degree of condensation was found to depend upon the amount of water in the tunnel circuit and not on the value of the specific humidity. Rather the frost point was found to give a unique relation between the amount of water in the tunnel circuit and the tunnel volume. Scattered light could be initially observed at a supersaturation ratio of just greater than 15, but useful photographs could not be obtained until additional water had been added to the circuit.

Considerably more water vapor was required to generate a useful vapor screen image at subsonic Mach numbers. At M = 0.8, the specific humidity had to be increased to 0.0588 with a

stilling chamber relative humidity was 0.78, but a specific humidity of only 0.0394 ($\phi_o = 0.53$; ϕ_o = stilling chamber relative humidity) was required at M= 0.85

Keener (Ref. 9) performed a comprehensive examination of flow separation patterns on various symmetrically-shaped forebodies using several flow visualizations techniques, including vapor screen. The tests were conducted in the NASA Ames 6- by 6-Foot Transonic/Supersonic Wind Tunnel over the Mach number range 0.6 to 2 with angle-of-attack greater than 30°. The light sheet was formed from twelve mercury-vapor lamps.

Erickson (Ref. 2, 4) performed a series of tests in the 7- by 10-Foot Transonic Tunnel at David Taylor Research Center. These studies were performed on various generic delta wing configurations and on the F/A-18 fighter. The tests were conducted over a wide subsonic Mach number range and to large angles-of-attack. Some models included leading-edge flap deflections and forebody strakes, which generated additional vortices. Originally the tunnel humidity was controlled by putting water vapor in the tunnel before the test (Ref., 2) but later it was injected into the settling chamber with a spray nozzle during the tests (Ref. 4). The light sheet was generated by an 18-watt argon-ion laser, located outside the tunnel. The laser light was steered into the tunnel with mirrors. The models were painted black to increase contrast (in Ref. 4 the tunnel interior was also painted).

The laser light was admitted from various directions for the different tests. Initially (Ref. 2) it was admitted from one side of the tunnel but the model caused shadows on the far side and so in later tests it was admitted from above the model, through the tunnel ceiling (Ref. 4). In all cases the plane of the laser light was somewhat adjustable in the axial direction and with respect to the plane of the model, to keep it approximately perpendicular to the model plane. The scattered light was generally photographed or recorded on video tape from an angle on the order of 45° from the forward scattering direction as well as by a sting-mounted camera at 90° to the light plane. Condensation in vortices could frequently be observed with only the wind tunnel test section interior lights (Ref. 4). Photographs were published of vapor screen images for Mach numbers as low as 0.4.

Erickson performed similar tests in the NASA Ames 6- by 6-Foot Transonic/Supersonic Wind Tunnel (Ref. 3). Water was injected into the tunnel from a single orifice on the tunnel

ceiling. The laser light sheet was introduced through the side of the tunnel and the vapor screen image was recorded from downstream.

Most recently Erickson has added an improved version of the laser vapor screen (LVS) flow visualization technique to the 8-Foot Transonic Pressure Tunnel (TPT) and the 7- by 10-Foot High-Speed Tunnel (HST) at NASA Langley (Ref. 6). While most of the details of the installation apply to the TPT, some information was given for the HST. The TPT is a continuous flow, closed-return tunnel, with stagnation pressure of 0.25 to 2.0 atmospheres, and Mach number from 0.2 to 1.2. Water was added from six atomizing nozzles located in the ceiling of the diffuser; deionized water was used. The full-cone spray patterns encompassed most of the diffuser cross section under tunnel-off conditions. The diffuser section was chosen for the water spray nozzles because of the relatively high cross flow velocity in the diffuser that would assist in the atomization of the water droplets. It could not be determined if complete vaporization occurred in the diffuser. The LVS method was used over the Mach number range of 0.6 to 1.2. It is estimated that a test section relative humidity of 0.98 was required in the test section at M = 0.6 for successful application of the vapor screen. The HST is a continuous-flow, subsonic/transonic (M = 0.06 to 0.94) tunnel that operates at ambient pressure and temperature and continuously exchanges air with the atmosphere. The humidity was measured with a hygrometer in the settling chamber. A measured relative humidity in the settling chamber as low as 0.30 yielded satisfactory vapor screen images and frequently is was unnecessary to add additional water to the flow. LVS images were obtained on vortex-dominated models at high angles-of-attack for M= 0.2 to 0.85. The optical details of the LVS installations in these tunnels will be described in a later section.

Elements of a Laser Vapor Screen System

The modern vapor screen application such as described in Ref. 6. uses a laser to generate the light sheet. It is thus referred to as the laser vapor screen (LVS) method. A typical system consists of the following elements:

- a multi-mode high-power laser, using all spectral lines to maximize the output power;
- a fiber optic cable (single fiber, step-index, multi-mode);
- laser sheet optics, including light sheet steering controls;

- video equipment for recording the scattered light;
- water injection system to increase (and control) the specific humidity in the wind tunnel;
- means for measuring the relative humidity in the free stream of the tunnel test section.

The laser sheet optics must have the capability to control the focus (thickness) of the laser sheet, the spread (width) of the laser sheet, and to steer the light sheet within the flow direction to illuminate different portions of the flow over a model. Frequently the laser must be outside the wind tunnel under ambient conditions. Since a laser and fiber optics is an extended luminous source, as opposed to a point source, the light can only be imaged to a waist.

The LVS system in the AEDC 16T wind tunnel possesses all of these elements and is closely patterned after the system at NASA Langley Research Center.

Mie Scattering Patterns

The size of the water droplets in the 16T tunnel are unknown but the size measurements made in other wind tunnels indicate that they are probably small enough to be assumed to be spherical in shape. Assuming that this is true, Mie scattering patterns from individual scattering spheres were computed using the program MIE01.FOR given in Bohren and Huffman (Ref. 10), as modified by Dr. Robert A. Reed, Sverdrup Technology, Inc., AEDC Group. The code computes k^2S_{11}, where k is the wave number and S_{11} is the component of the amplitude scattering matrix (part of the Mueller matrix for the scattering of a single particle) that gives the intensity ratio. For an incident wave of intensity I_o watts/cm^2, the scattered intensity (watts/sr) is k^2S_{11}. A laser light wavelength of 0.515 μm was used in the computations along with the index of refraction for water of n = 1.335 + 0 i (Ref. 11 & 12). In this case $k^2 = 148.85$. Scattering intensity distributions were computed for droplet radii from 0.1 μm to 12.5 μm. Some of the results are compared in Figure 1. It can be seen that observing the scattered light at 50° from the forward direction would increase the observed scattered intensity by a factor greater than 10 for all droplet sizes, making it much easier to record the vapor screen images. That was the angle (approximately) that had been used by many previous investigators.

The Mie scattering patterns described above were computed for a single scattering sphere. Stein (Ref. 13) analyzed the scattering from a cloud of spheres. The differential cross section for the cloud is equal to n times the differential cross section for an individual sphere if two

conditions are met. First, the incident light must be attenuated through the scattering volume by a factor $e^{-\tau}$ with $\tau < 0.1$, where τ is the optical depth. If this true, then single photon scattering occurs. Second, if

$$\frac{4\pi\ell}{\lambda}\sin\left(\frac{\theta}{2}\right) \succ\succ 1 \tag{1}$$

then independent scattering occurs in which intensities, and not amplitudes, of the scattering waves are added. Durbin (Ref. 14) estimated that single scattering existed if the droplets were separated by at least 100 times the radius of the droplets. The assumption of single scattering was assumed to be valid for tests in the 16T wind tunnel and the Mie scattering computations were used to position the video cameras at optimal angles with respect to the laser light sheet.

16T Wind Tunnel Humidity Relations

This section will derive the equations that are used to determine the humidity levels in the stilling chamber and test section of the 16T wind tunnel at AEDC. A general discussion of humidity is given in Ref. 15. The following notation is used. A(b) means that the quantity A is a function of the quantity b, and $\hat{A}$ indicates the quantity A per mole. In this section subscript a designates air and subscript w designates water.

A. Specific Humidity

Specific humidity is defined for a volume of moist air as

$$\omega = \frac{mass\ of\ water\ vapor}{mass\ of\ dry\ air} = \frac{m_w}{m_a}. \tag{2}$$

The number of moles for a unit volume of gas mixture is given by

$$\hat{N} = \hat{N}_a + \hat{N}_w. \tag{3}$$

This relation can be rewritten in terms of the mole fractions,

$$1 = x_a + x_w, \quad x_i = \hat{N}_i / \hat{N}. \tag{4}$$

Since

$$\hat{N}_i = m_i / \hat{M}_i = \frac{mass\ of\ component\ i}{molecular\ weight\ of\ component\ i} \tag{5}$$

then

$$m_i = \hat{N}_i \hat{M}_i. \tag{6}$$

Using this relation the specific humidity can be written as

$$\omega = \frac{\hat{M}_w \hat{N}_w}{\hat{M}_a \hat{N}_a} = \frac{18.015 \hat{N}_w}{28.964 \hat{N}_a} = 0.621979 \frac{\hat{N}_w}{\hat{N}_a}, \tag{7}$$

or, equivalently,

$$\omega = 0.621979 \frac{x_w}{1 - x_w}. \tag{8}$$

It is assumed that the air and water vapor mix as perfect gases. Thus, for each component mixed in a volume V at temperature T,

$$p_i V = \hat{N}_i \hat{R} T \tag{9}$$

In this equation $\hat{R}$ is the universal gas constant or the gas constant per mole. For a mixture of perfect gases Dalton's Law holds, or

$$p = \sum_i p_i \tag{10}$$

where p is the mixture pressure and p_i is the partial pressure of component i. These equations can be rearranged to yield

$$\frac{p_i}{p} = x_i. \tag{11}$$

Then Equation (8) can be written in terms of the partial pressure of the water vapor

$$\omega = 0.621979 \frac{p_w}{p - p_w}. \tag{12}$$

B. Relative Humidity

We assume that the partial pressure of water in saturated moist air is equal to the vapor pressure of pure water at saturation. At saturation, the specific humidity is given by

$$\omega_s(T_{dp}) = 0.621979 \frac{p_s(T_{dp})}{p - p_s(T_{dp})}. \tag{13}$$

where the subscript s refers to saturation conditions at the moist air temperature T_{dp}, the dew point temperature (to be defined below). The ratio ω/ω_s at the same temperature and total

pressure is called the degree of saturation. The relative humidity is defined as the ratio of the actual partial pressure of the water vapor to the saturated partial pressure of the water vapor at the same temperature and total pressure of the moist air mixture. For a mixture of perfect gases,

$$\phi(T) = \frac{p_w}{p_s(T)} = \frac{x_w p}{p_s}, \tag{14}$$

where p_w is the partial pressure of water vapor in the moist air mixture and p_s is the vapor pressure of the pure water vapor at the moist air temperature. The degree of saturation and the relative humidity are related by the equation

$$\frac{\omega}{\omega_s} = \frac{\phi}{\left[1 + 1.60777(1-\phi)\omega_s\right]}. \tag{15}$$

If moist air with a degree of saturation less than unity is cooled at constant pressure and constant composition, it will become saturated at some temperature which is called the thermodynamic dew point temperature T_{dp}. Since the amount of water vapor remains constant per mass of mixture, the specific humidity must satisfy the relation

$$\omega_s\left(p, T_{dp}\right) = \omega(p, T). \tag{16}$$

C. Humidity Relations for Wind Tunnel Stilling Chamber

During the 16-T wind tunnel tests the following parameters are provided to the investigator:

- Stilling chamber pressure in psf, p_o = PT
- Stilling chamber temperature in °F, $T_o = T_{vp}$ = TT (TTR is the stilling chamber temperature in degrees R)
- Stilling chamber dew point temperature in °F, T_{dp} = TDP (not needed or used);
- Tunnel specific humidity, SH = $10^3\omega$;
- The difference between the test section static and dew point temperatures, DTDPS == TTS-TDPTS;
- Mach number of the tunnel nozzle, M.

The partial pressure of water in the stilling chamber is equal to the partial pressure of water at the dew point temperature and the stilling chamber pressure. They are related to the measured specific humidity by the equation

$$\omega = 0.621979 \frac{pdp}{PT - pdp} \tag{17}$$

where pdp is the dew point pressure in the stilling chamber.

If the water vapor was saturated at the stilling chamber temperature TT, then its pressure, $p_s(TT)$, is given by the vapor pressure-temperature relation given in the next section. Then the relative humidity in the stilling chamber is given by

$$\phi = pdp / p_s(TT). \tag{18}$$

D. Vapor Pressure of Water and Ice

The vapor-temperature is given by the following three relations that apply to different temperature regions (Ref. 16).

$$T_s(^\circ F) = -17.958 + 40.562P + 3.7421P^2 + 0.3938P^3, \quad T < 32^\circ F \tag{19}$$

$$T_s(^\circ F) = -21.001 + 38.964P + 8.122P^2, \quad T > 32^\circ F. \tag{20}$$

The following equation, obtained by fitting a cubic equation to the vapor pressure data for ice in Ref. 17, can be used for temperatures less than 32 °F (within the range -55 °F to 32 °F). Comparison of the use of this equation with Eq. 20 is excellent.

$$T_s(^\circ F) = -18.009 + 40.5606P + 3.8148P^2 + 0.8861P^3, \quad T < 32^\circ F, ice. \tag{21}$$

In these three equation

$$P = \log_{10}(p_s), \quad p_s \, in \, psf, \tag{22}$$

where the subscript s indicates saturated conditions. Temperature is given in °F and the pressure in psf.

An alternative relation that is valid over the temperature range $(268K \le T \le 647.27K)$ (Ref. 18):

$$\log_{10} pvp(atm) = A + \frac{B}{T} + \frac{Cx}{T}\left(10^{Dx^2} - 1\right) + E\left(10^{Fy^{3/4}}\right) \tag{23}$$

where

$$x = T^2 - K$$
$$y = 647.27 - T$$
$$A = 5.4266514$$
$$B = -2005.1$$
$$C = 1.3869 \times 10^{-4}$$
$$D = 1.1965 \times 10^{-11}$$
$$E = -4.4 \times 10^{-3}$$
$$F = -5.7148 \times 10^{-3}$$
$$K = 2.937 \times 10^{5}$$

These nonlinear equations are solved for p_s using a Newton-Raphson procedure.

E. Humidity Relations for Wind Tunnel Test Section

The temperature and static pressure in the test section are determined from the following equations, which assume that $\gamma = 1.4$.

$$TTS(^\circ F) = -459.67 + \frac{TTR}{(1+0.2M^2)}, \tag{24}$$

$$PTS = PT/(1+0.2M^2)^{3.5}. \tag{25}$$

The specific humidity is the same in the test section and stilling chamber if no water has been added or removed between them. This conservation of water vapor can be used to determine the partial pressure of the water vapor in the test section, pvts, by solving Equation (12) using p = PTS.

$$pvts = \frac{\omega(PTS)}{(0.621979+\omega)}. \tag{26}$$

Then we have to find the vapor pressure if the test section is saturated, i.e., if TTS=TDPTS (dew point temperature in the test section). The vapor pressure relations in the previous section can be solved to obtain pdts(TDPTS) (saturated vapor pressure in the test section at the test section temperature and pressure). The test section relative humidity is given by the equation

$$\phi_{ts} = \frac{pvts}{pdts}. \tag{27}$$

Finally, the parameter DTDPS is determined by using the vapor pressure relations to find the test section dew point temperature corresponding to the test section water vapor pressure pvts(T_{dpts}), given above. This is obtained from Equation (26). Then DTDPS is given by.

$$DTDPS = TTS - T_{dpts}. \tag{28}$$

The computed value of DTDPS is compared to the value given by the wind tunnel operator as a check on the computations, in particular, a check that the correct vapor pressure equation has been used for the corresponding temperature.

A number of assumptions have been made in writing these equations. It has been assumed that moist air is a mixture of calorically and thermally perfect gases (see Ref. 15, 19 to 21). The equilibrium between the liquid and its vapor is not influenced by the presence of the air. The partial pressure of the water vapor is equal to the saturation pressure corresponding to the temperature of the mixture (assuming a planar interface between the two phases). The dew point is the temperature at which the water vapor condenses on a plane when it is cooled at constant pressure. The partial pressure of the vapor, and thus its mole fraction, remains constant until condensation begins. $\gamma = 1.4$ is assumed for the air/vapor mixture (see Ref. 22).

An approximation to the test section relative humidity for given stagnation chamber relative humidity was given in Ref. 1. Using the ideal gas relations for p_{ts}/p_o, T_{ts}/T_o for given Mach number, the expression is

$$\phi_{ts} = \phi_o \left(\frac{p_{ts}}{p_o} \right) 10^{-\left\{ \frac{2263}{T_o(K)} \left(\frac{T_{ts}/T_o - 1}{T_{ts}/T_o} \right) \right\}}. \tag{29}$$

This equation is not accurate for very large values of relative humidity but it does illustrate the fact that the relative humidity is directly proportional to pressure but logrithmically proportional to temperature. Thus the relative humidity is much more sensitive to changes in temperature than to changes in pressure.

Analysis of Previous Vapor Screen Applications

McGregor (Ref. 8) was the first to observed that the degree of condensation in the wind depends only on the amount of water in the tunnel circuit. Since moist air is a perfect gas mixture of air and water vapor, equilibrium condensation requires that the water vapor pressure be greater than the saturation pressure at the local temperature. The relative humidity in the test

section depends on the relative humidity and temperature in the stilling chamber, and the Mach number. The relative humidity in the stilling chamber is representative of the relative humidity in the tunnel circuit. But from Eq. (14), the relative humidity is proportional to the partial pressure of water in the tunnel circuit and the temperature ($p_s = p_{s(T)}$) and since $p_w V_w = m_w R_w T$, it is proportional to the mass of water in the tunnel circuit. Thus, condensation depends upon the amount of water in the tunnel circuit and the temperature and not upon the specific humidity.

A number of additional observations of previous investigators are worthy of discussion at this point, especially those relating to the required levels of stilling chamber relative humidity. McGregor (Ref. 8) plotted the amount of water required to produce 15-fold supersaturation in his tunnel. A further increase in water was required before the first condensation could be detected by the eye and even more water was required to obtain suitable photographs. This indicates that the water droplets must grow to a suitable size before the vapor screen visualization is useful. In a subsonic tunnel, this means that the droplets must progress downstream for a finite period of time before they can be usefully observed. Williams, et al. (Ref. 23) observed this effect in a subsonic tunnel with Rayleigh scattering from water droplets. Their tunnel was operated at fixed stilling chamber conditions and the test section Mach number was varied by varying the downstream pressure. During one test the relative humidity reached 1.0 at test section conditions corresponding to M= 0.3 and the first scattering signal was observed at M=0.35, where the relative humidity was 1.126. However, the droplets could not be observed visually until the flow reached conditions such that M=0.65, where the relative humidity was 2.70, and the local flow temperature was 26.8 °F below the local dew point temperature (Figure 2). The vapor was observed from a generally forward direction using only tunnel building lights. It was estimated that the flow time from the point in the nozzle where the flow saturated to the nozzle exit where the droplets were seen was 2 ms. This time is characteristic of the temperature gradient existing in their wind tunnel and should not be extrapolated to tunnels or flow fields with other temperature gradients.

The work of McGregor (Ref. 8) also allows the computation of the relative humidity in the stilling chamber and in the test section under optimum viewing conditions. At a tunnel test section Mach number of 0.8, the stilling chamber and test section relative humidities were 0.78 and 4.62, respectively. The stilling chamber temperature was 40 °F below the dew point

temperature. At M=0.85, the relative humidities were 0.54 and 4.01, respectively and the delta temperature was 32.6 °F. McGregor observed the vapor screen with a light sheet from a mercury vapor lamp. A laser light sheet would have allowed the vapor sheet to have been observed with a lesser amount of water in the tunnel circuit.

The relative humidity in the Langley tunnel under good vapor screen conditions can only be estimated from the work of Erickson and Inenaga (Ref. 6). At a tunnel Mach number of 0.6, assuming that the stagnation pressure was one atmosphere and that the stagnation temperature was 80 °F, the test section relative humidity would have been 0.35 and the test section relative humidity would have been 0.98. Assuming the same stagnation conditions (they were not stated in the reference), then at a test section Mach number of 1.2, the stilling chamber relative humidity would have been 0.07 and the test section relative humidity would have been 8.07.

To aid in the understanding of the 16T wind tunnel tests that were analyzed for this work, the humidity relations for typical tunnel parameters are presented in Figures 3 to 5. The relative humidity in the stilling chamber is nearly a linear function of the specific humidity and the stagnation temperature and pressure.

$$\phi_\circ = f(\omega, p_\circ, T_\circ). \tag{30}$$

This relation is plotted in Figure 3. On the other hand, the relative humidity in the test section is also a function of the wind tunnel Mach number.

$$\phi_{TS} = f(\omega, p_\circ, T_\circ, M). \tag{31}$$

This relation is plotted in Figures 4 and 5. Note that at supersonic Mach numbers, very small values of specific humidity and stilling chamber relative humidity result in a supersaturated state in the test section. At 100 °F in the stilling chamber the saturation vapor pressure is 136.8 psf. Expanding that mixture to a Mach number of 0.6 drops the saturation vapor pressure to 39.6 psf, expanding to M = 0.85 drops the saturation vapor pressure to 11.1 psf, and expanding to M = 1.55 drops the saturation vapor pressure to 0.015 psf, a drop by a factor of 900 from the stilling chamber value. Consequently the test section relative humidity must be significantly lowered to prevent test section condensation at high Mach numbers.

AEDC 16T Wind Tunnel

16T is a closed-circuit, continuous-flow subsonic/transonic wind tunnel that can be operated with the stagnation pressure above or below the atmospheric pressure. The humidity is controlled by passing the tunnel make-up air through a dryer. The temperature is controlled by a heat exchanger (cooler) located upstream of the turning vanes that are upstream of the stilling chamber. The water flow through the cooler is carefully controlled so that the air temperature distribution, measured by thermocouples placed downstream of the heat exchanger, is uniform. The stilling chamber temperature is measured by RTV's located on a strut downstream of the exit plane of the cooler. An example of the measure temperature distribution in the 55-foot diameter pipe leading to the stilling chamber is shown in Figure 6. The nominal measured temperature was 95 °F whereas the measured stagnation temperature was 100 °F. A uniform test section temperature is a requirement for the successful application of the vapor screen method.

The wind tunnel air was generally dried to the point that natural condensation could not occur in the flow over the models examined. In this case stream tubes of nearly saturated air, which passed over the model, were created by spray nozzles of water placed on the trailing edges of the turning vanes upstream of the stilling chamber. Nozzles were placed at five vertical locations so that various combinations could be turned on to optimize the observed vapor screen pattern. Rarely was the wind tunnel so dry that the moist stream tubes did not cause observable condensation over the model.

The laser light sheet was introduced from the test section ceiling. The width of the sheet could be varied to change the light intensity and the sheet could be swept in the stream direction to illuminate different flow features over or downstream of a model. The condensation pattern was recorded using video cameras placed on the sting (viewing the light sheet at roughly 90°) and on the test section side wall (approximately 45° to the sheet). The Mie scattering calculations showed that these cameras should see different flow features.

AEDC 16T Wind Tunnel Tests

Laser vapor screen (LVS) flow visualization tests were performed during two tunnel entries in 1997. In each test the humidity conditions were recorded and moist air created by upstream spray nozzles which generated moist streamtubes which passed over the model.

Generally the wind tunnel humidity conditions were under the control of the test engineer so that a systematic study of LVS under controlled humidity conditions could not be performed. Nevertheless, much useful information was obtained from these tests. The humidity conditions during these tests will be discussed in this section.

A. TST Tests

The first test was the Technology Wing Demonstration (TST) Test, which was a joint BMDF/USAF test. A transonic fighter configuration was used as a test bed for advanced wing development. The model did not possess strakes or other vortex-generating surfaces so vortices and separation surfaces were not observed at small angles-of-attack.

The TST laser vapor screen tests consisted primarily of seven runs. Conditions for the runs are summarized in the following table, with detailed conditions given in Appendix A. The humidity conditions for the runs are given in Figures 7 to 10.

TST Test Conditions

Run No.	Mach No.	p_o (psf)	$\overline{\omega}$	$\overline{\phi}_{TS}$
940	0→0.209	1500	0.019	0.80
127	0.6; 0.6→0	1000	0.020	0.69
273	0→0.34	1600	0.017	0.67
294	0.835	1240	0.0044	0.06
297	0.60	1490	0.0131→0.0158	0.56→0.74
460	0.6→0.848→0	1400	See Figures	See Figures

T_o = 100 °F for all tests

Run 940 was performed during tunnel start-up with the water spray nozzles off (number 1 to 20 in Appendix A). Condensation could be observed during the initial phases of the tunnel start-up.

Run 127 (number 21 to 30 in Appendix A) was performed with and without the water spray nozzles. LVS images were observed only with water seeding. Different flow features were observed with different water spray nozzle combinations. While the test section relative

humidity was very constant during the run, the specific humidity increased from 0.0184 to 0.0223 as a result of the water added by the spray nozzles. The tunnel was shut down at the end of the test. No condensation was observed after a ten second delay (the time it took to evaporate all of the water from the stilling chamber screens) when the water spray nozzles were turned off, which included the tunnel shut-down. The moisture that is observed during the wind tunnel start-up is removed before the tests are performed by the wind tunnel driers.

Run 273 (numbers 31 to 38 in Appendix A) was conducted during the wind tunnel start-up. Condensation was observed only during the initial start-up. No water spray nozzles were turned on.

Run 294 (numbers 39 and 40 in Appendix A) was performed at a high Mach number after considerable drying of the wind tunnel air. LVS could be observed only when the water spray nozzles were turned on.

Run 297 (numbers 41 to 50 in Appendix A) was performed at a fixed Mach number with the water spray nozzles turned on. Both the specific humidity and the test section relative humidity rose during the test due to the water input from the spray nozzles.

Run 460 (numbers 51 to 73 in Appendix A) was performed as the Mach number was increased from 0.6 to 0.85 and then the wind tunnel was shut down. The humidity data are plotted in Figure 10. With increasing Mach number the test section relative humidity increased and when the relative humidity was around 1.0 natural condensation without the spray nozzles was observed, starting at number 57, M = 0.755. Quickly, though, the wind tunnel became too moist since the saturation vapor pressure decreases quickly with decreasing temperature (between a Mach number increase from 0.6 to 0.85, the saturation vapor pressure decreases from 39.6 psf to 11.1 psf, a decrease by a factor of 3.6). This occurred at M = 0.808 (number 59) and the wind tunnel remained too wet until the Mach number was decreased to M = 0.827 (number 63). The process was roughly repeated for decreasing Mach numbers

B. Missile Tests

The second test was performed on a missile which contained many vortex-generating surfaces. The angle-of-attack was varied from 0° to 42.5°, causing large changes in the exterior vortex and separation pattern. The pattern appeared to be steady at all angles-of-attack. As a

result, this was an ideal flowfield to be explored with the laser vapor screen flow visualization and LVS was performed during twelve runs. In general, the runs were performed at Mach numbers of 0.8, 0.95, 1.15, and 1.55. The stagnation pressure was considerably lower than for the TST tests (Appendix B), the stilling chamber relative humidity was very low, and thus there was less water vapor in the wind tunnel circuit than for the TST tests. Also, the wind tunnel was dried considerably for the tests with $M \geq 1$. The humidity conditions for the tests are summarized in Figures 11 to 14. The specific humidity values were varied over a wide range at $M = 0.95$ and $M = 1.15$. This resulted in a wide variation in test section relative humidity at the same Mach number. At $M = 0.95$, the wind tunnel was never too wet and good vapor screen images could be observed with the spray nozzles on. At $M = 1.15$, the spray nozzles were used except for numbers 32 and 33, where the test section relative humidity was too great and there was considerable background fogging that interfered with the LVS image. At $M = 1.55$ (number 44 to 47) the wind tunnel was too wet to use LVS. Between $M = 0.95$ and $M = 1.55$ the saturation vapor pressure had dropped by a factor of 360 but a corresponding amount of water had not been removed from the tunnel circuit.

C. Relative Humidity Requirements for LVS

One of the primary objectives of the present work was to determine the wind tunnel requirements for application of the laser vapor screen flow visualization in the AEDC 16T wind tunnel. It was determined that the degree of condensation in the test section depends on the relative humidity in the test section and not on the specific humidity. Then the TST and missile tests were examined to determine the following limits: tunnel too dry for LVS even with water spray nozzles; LVS is usable with water spray nozzle seeding of stream tubes; natural condensation with moisture contained within the tunnel flow stream; too much water in the tunnel circuit to yield usable condensation images. Several of the tests allowed placing points on the approximate boundaries of these regions. These boundaries are shown in Figure 15. This result should be considered to be very tentative until considerably more data can be obtained. The boundaries have been drawn as straight lines since there was considerable scatter in the few points that existed on each boundary and a different curve could not justified. Undoubtedly the upper curve for too wet conditions is nonlinear.

Most of the runs for the TST and missile tests were performed in the region needing seeding with the water spray nozzles. This coincidence must arise because this is the moisture region that AEDC tries to achieve for 16T wind tunnel tests because natural condensation will not occur; drying the wind tunnel air to the point where even seeding will not work is too expensive and not necessary.

Conclusions

The success of the laser vapor screen method depends on the total amount of water in the tunnel circuit rather than the value of the specific humidity. This is measured by the relative humidity in the test section. Naturally occurring condensation requires around 100% relative humidity in the test section but the LVS method can be used at much lower levels of tunnel moisture by seeding streamtubes, which pass over the model, with water vapor. The stream tubes originated upstream of the stilling chamber.

A very concentrated and intense sheet of laser light is mandatory for vapor screen flow visualization. The optics should be able to change the spread of the light sheet and steer the sheet in the flow direction.

Mie scattering computations suggest that it would be easier to observe the scattered light from an angle closer to the forward scattering direction than 90°, such as 50°. The scattering intensity is increased by an order of magnitude at this lower angle for droplets of all sizes. It proved useful to place video camera at several locations around the test section to observe the scattering pattern from different directions.

Limits of applicability of LVS flow visualization, as tentatively determined from two 16T wind tunnel tests, indicate that the method is generally applicable using seeded streamtubes for the wind tunnel humidity conditions that are usually specified by the tunnel operators. Considerably more data is needed to make a definitive map of the applicable humidity range as a function of Mach number.

At higher values of test section relative humidity natural condensation can be used for the LVS method but very quickly the wind tunnel becomes too wet and naturally occurring condensation is not recommended.

Recommendations

Fred Heltsley has recommended the development of a Flow Diagnostic Development Station which would be placed within the 16T test section (Ref. 24). The station would consist of a model which is permanently mounted to the wall of the transition region of 16T, downstream of the test section cart (Fig. 16). A streamtube of moist air would be created upstream of the stilling chamber and positioned to pass over the model. The laser would be mounted on the side of the transition region with the video camera mounted at an angle to the laser light sheet on the opposite side. The LVS system would then be out of the way of all wind tunnel tests and could be used during all wind tunnel tests to accurately determine humidity conditions for which LVS could be used. It is strongly recommended that this suggestion be implemented.

Since it has been determined that the applicability of the LVS flow visualization method depends on the value of the relative humidity in the test section, this quantity should be directly measured. Humidity measuring instruments should have time constants that are short compared to the time required to change wind tunnel flow conditions. A means should be found for accurately and rapidly measuring the test section relative humidity at a location outside of the test section boundary layers.

All temperatures should be measured to a tenth of a degree Fahrenheit since vapor pressure is such a strong function of temperature.

An indication of the status of the water spray nozzles (off; number of those nozzles on) should be added to the CRT screen that records the other humidity data and the LVS images.

Flow fields should be simultaneously examined using vapor screen flow visualization and a local flow measurement method, such as laser velocimetry or PLIF, to determine the relation between the vapor screen image and the flow field feature. For example, it would be of interest to know the relation between the image recorded in a vortex by vapor screen and the extent of the vortex velocity field.

References

1. J. F. Campbell, J. R. Chambers, and C. L. Rumsey, "Observation of Airplane Flow Fields by Natural Condensation Effects," AIAA 88-1091, January, 1988; J. F. Campbell and J. R. Chambers, Patterns in the Sky, NASA SP-514, 1994.
2. G. E. Erickson and L. W. Rogers, "Effects of Forebody Strakes and Mach Number on Overall Aerodynamic Characteristics of Configuration with 55° Cropped Delta Wing," NASA TP-3253, November 1992.
3. G. E. Erickson, "Wind Tunnel Investigation of the Interaction and Breakdown Characteristics of Slender-Wing Vortices at Subsonic, Transonic, and supersonic Speeds," NASA TP-3114, November 1991.
4. G. E. Erickson, "Wind Tunnel Investigation of Vortex Flows on F/A-18 at Subsonic Through Transonic Speeds," NASA TP-3111, December 1991.
5. G. E. Erickson and D. G. Murri, "Forebody Strakes for High-Angle-of-Attack Vortex Flow Control: Mach Number and Strake Performance Effects," *High-Angle-of-Attack Technology*, Vol. I, J. R. Chambers, W. P. Gilbert, and L. T. Nguyen, Editors, NASA CP-3149, Part 1, 1992, pp. 381-480.
6. G. E. Erickson and A. S. Inenaga, "Fiber-Optic-Based Laser Vapor Screen Flow Visualization System for Aerodynamic Research in Larger Scale Subsonic and transonic Wind Tunnels," NASA TM 4514, January 1994.
7. H. J. Allen and E. W. Perkins, "A Study of Effects of Viscosity on Flow Over Slender Inclined Bodies of Revolution," NACA Report 1048, 1951.
8. I. McGregor, "The Vapor-Screen Method of Flow Visualization," J. Fluid Mech. Vol. 11, Part 4, December, 1961, pp. 481-511.
9. E. R. Keener, "Flow-Separation Patterns on Symmetric Forebodies," NASA TM 86016, January 1986.
10. C. F. Bohren and D. R. Huffman, Absorption and Scattering of Light by Small Particles, Wiley-Interscience, New York, 1983.
11. G. M. Hale and M. R. Querry, "Optical Constants of Water in the 200-nm to 200-μm wavelength Region," Appl. Optics, Vol. 12, No. 3, 1973, pp. 555-563.

12. S. G. Warren, "Optical Constants of Ice from the Ultraviolet to the Microwave," Appl. Optics, Vol. 23, No. 2, 1984, pp. 1206-1223.

13. G. D. Stein, "Angular and Wavelength Dependence of the Light Scattered from a Cloud of Particles Formed by Homogeneous Nucleation," J. Chem. Phys., Vol. 51, no. 3, pp. 938-942, 1969.

14. E. J. Durbin, "Optical Methods Involving Light Scattering for Measuring Size and Concentration of Condensation Particles in Supercooled Hypersonic Flow," NACA TN 2441, August, 1951.

15. G. V. Van Wylen and R. E. Sonntog, Fundamentals of Classical Thermodynamics, 3rd Edition, Wiley, New York, 1986.

16. Anonymous, "Tunnel 16T Test Conditions Standard Program," Program number PDP 10001, Arnold Engineering Development Center.

17. J. Hilsenrath, et al., "Tables of Thermodynamic Properties of Gases," NBS Circular 564, November 1, 1955.

18. N. S. Osborne and C. H. Meyers, J. Res. Bur. Stand., Vol. 13, pp 1-20, 1934; "A Formula for the Saturation Pressure of Steam in the Range 0 to 234 °C," Mech. Eng., Vol. 56, pp. 207-209, 1934.

19. J. A. Goff and S. Gratch, "Thermodynamic Properties of Moist Air," Heating, Piping & Air Conditioning, June, 1945, pp. 334-348.

20. J. A. Goff and S. Gratch, "Low-Pressure Properties of Water from -160 to 212 F," Heating, Piping & Air Conditioning, February, 1946, pp. 125-136.

21. J. A. Goff, "Standardization of Thermodynamic Properties of Moist Air," Heating, Piping & Air Conditioning, November, 1949, pp. 118-128.

22. P. P. Wegener and L. M. Mach, "Condensation in Supersonic and Hypersonic Wind Tunnels," Advances in Applied Mechanics, Vol. V, 1958, pp. 307-445.

23. W. D. Williams, D. W. Sinclair, and L. L. Price, "Laser-Raman/Rayleigh Flow Diagnostic Techniques Applied to Subsonic Flow," AEDC-TR-80-20, October 1980.

24. F. L. Heltsley, Private Communication, March, 1998.

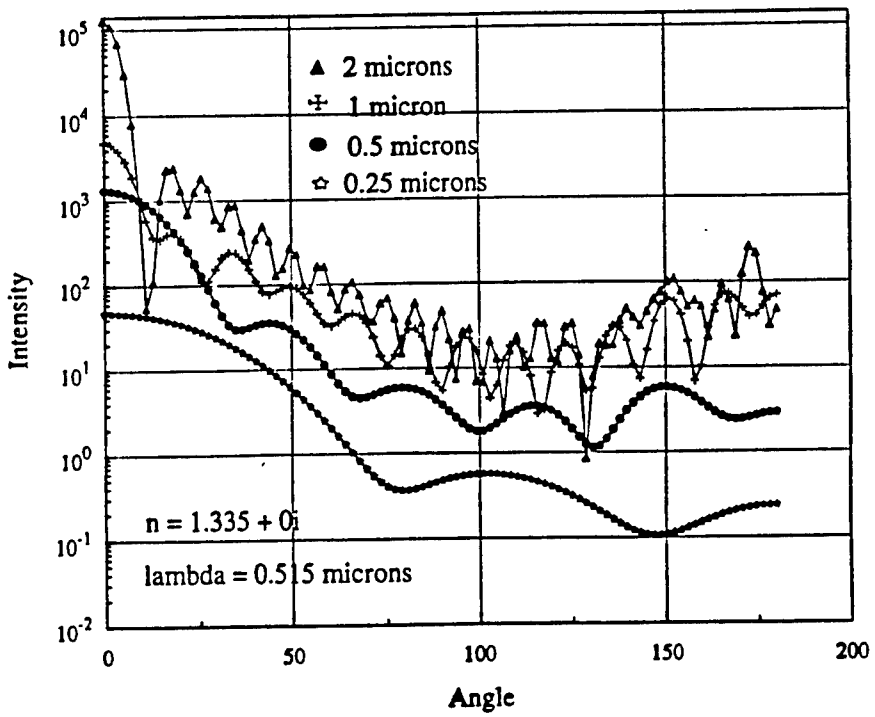

Figure 1. Mie scattering from spherical water droplets.

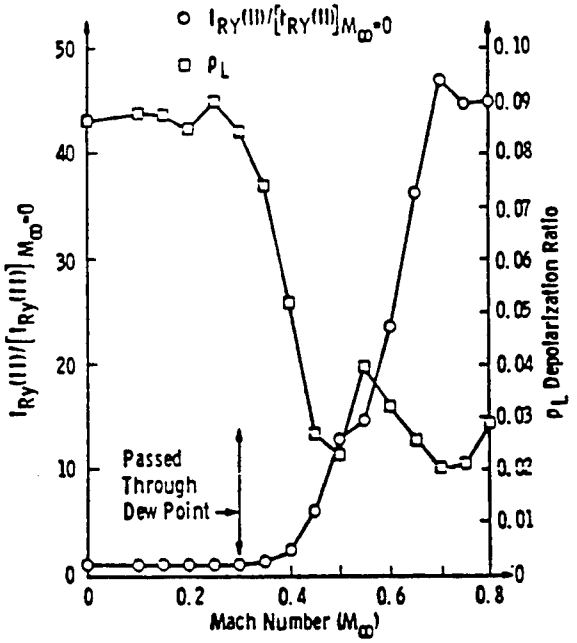

Figure 2. Test section Rayleigh scattering data as a function of Mach number. y = 2 in. (Ref. 23).

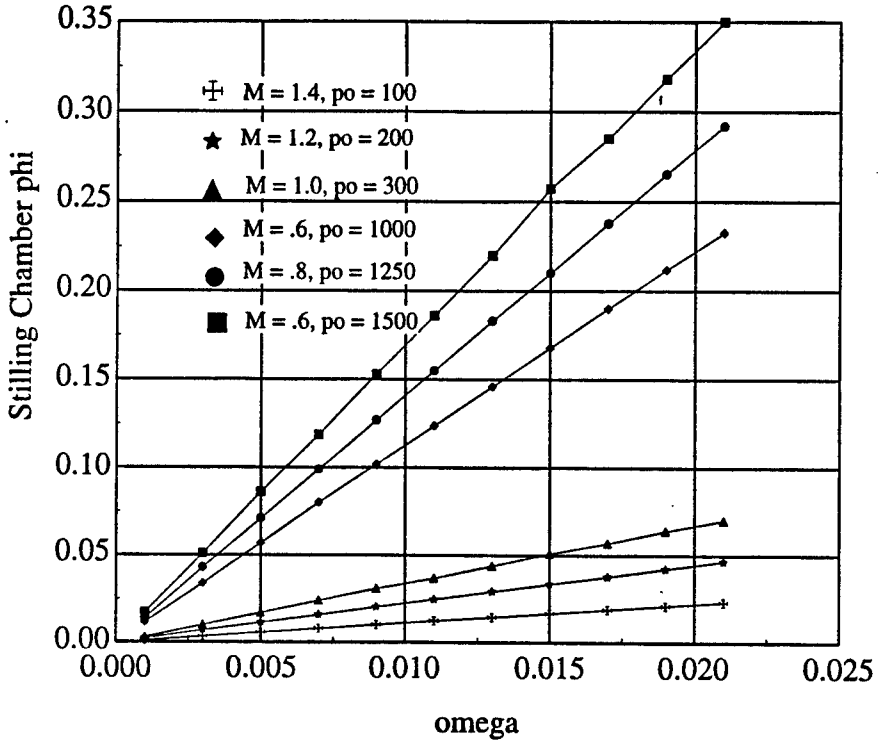

Figure 3. Stilling chamber relative humidity vs. specific humidity for typical 16T run conditions. $T_o = 100$ °F.

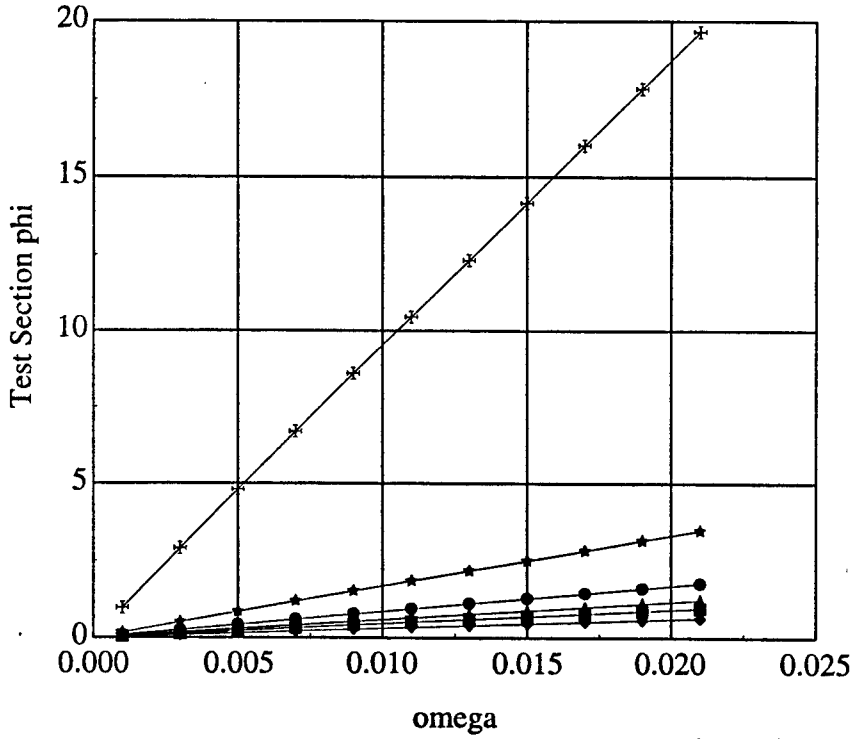

Figure 4. Test section relative humidity vs. specific humidity for typical 16T run conditions. $T_o = 100$ °F. Symbols defined in Figure 3.

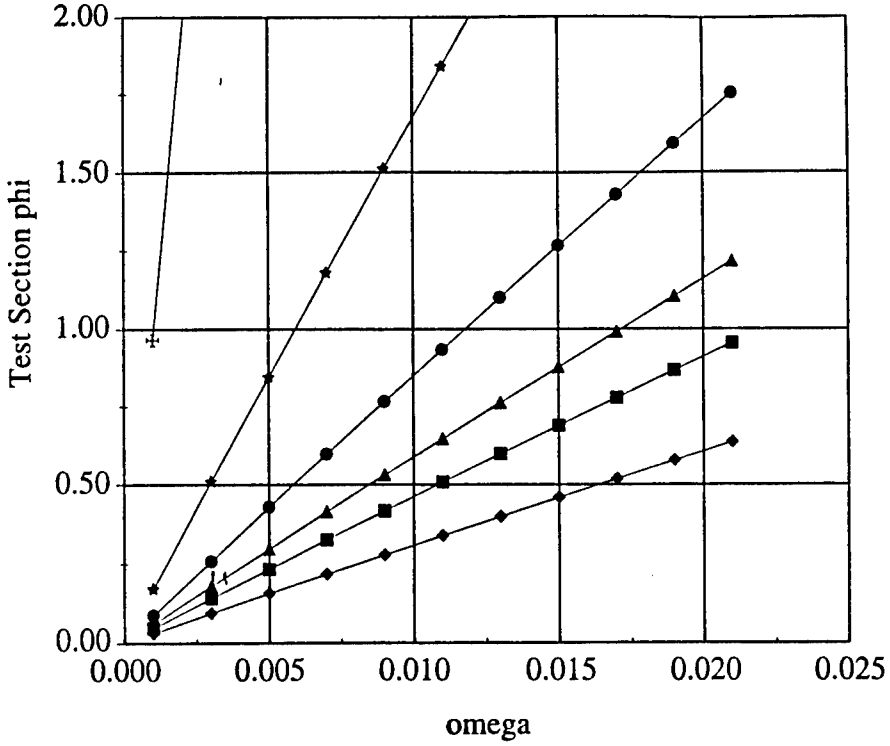

Figure 5. Test section relative humidity vs. specific humidity for typical 16T run conditions. T_o = 100 °F. Symbols defined in Figure 3.

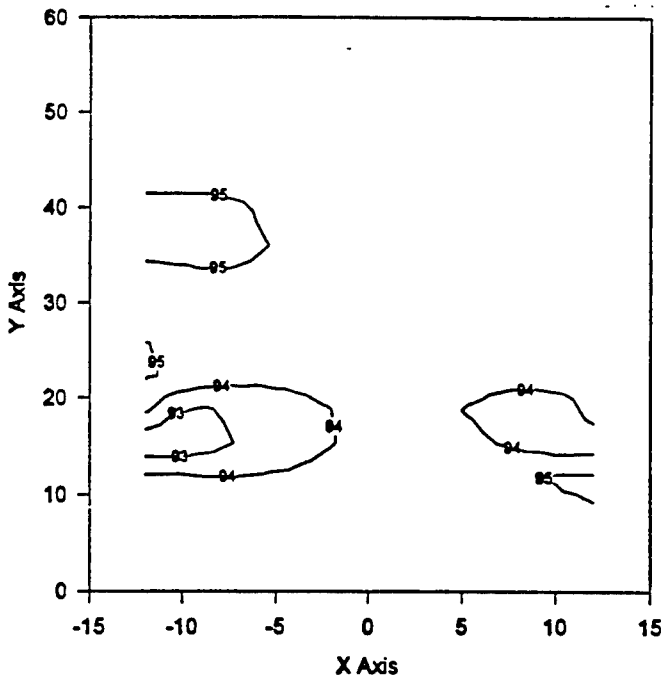

Figure 6. Typical measured stream temperature distribution in 16T tunnel, measured downstream of the cooler. M = 0.8, p_o = 600 psf, T_o = 100 °F.

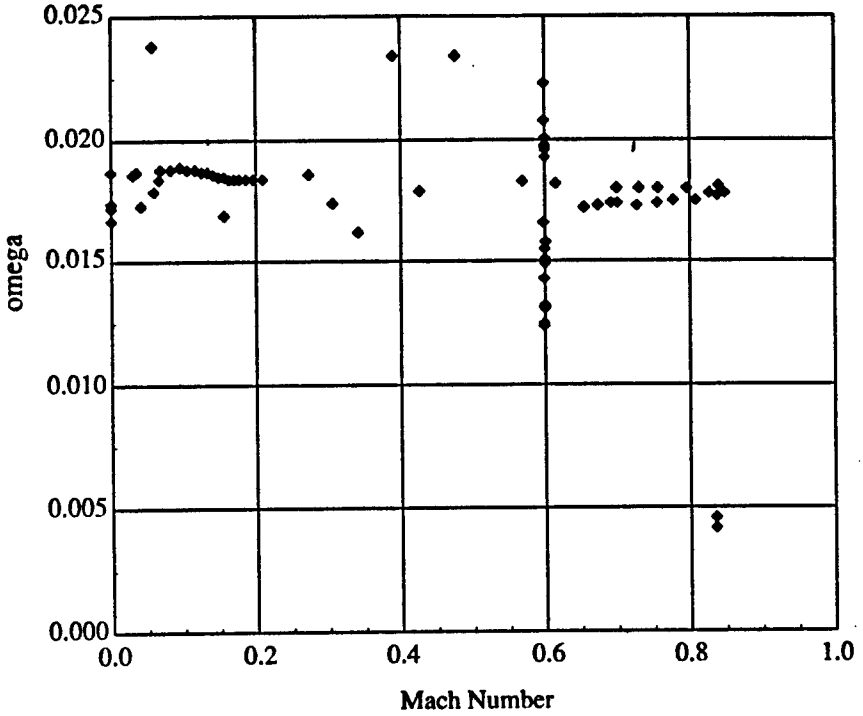

Figure 7. Specific humidity for TST tests.

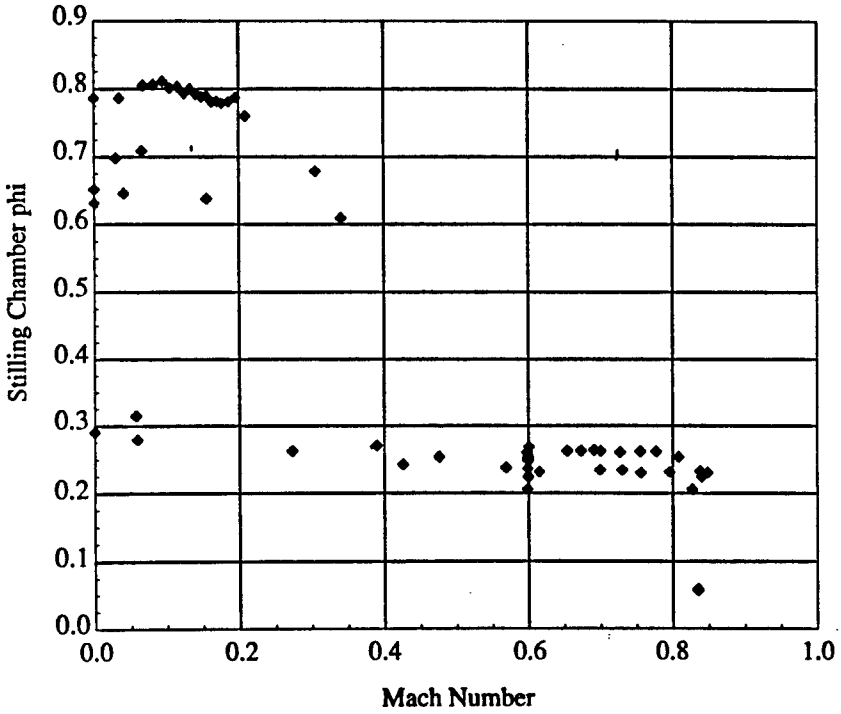

Figure 8. Stilling chamber relative humidity for TST tests.

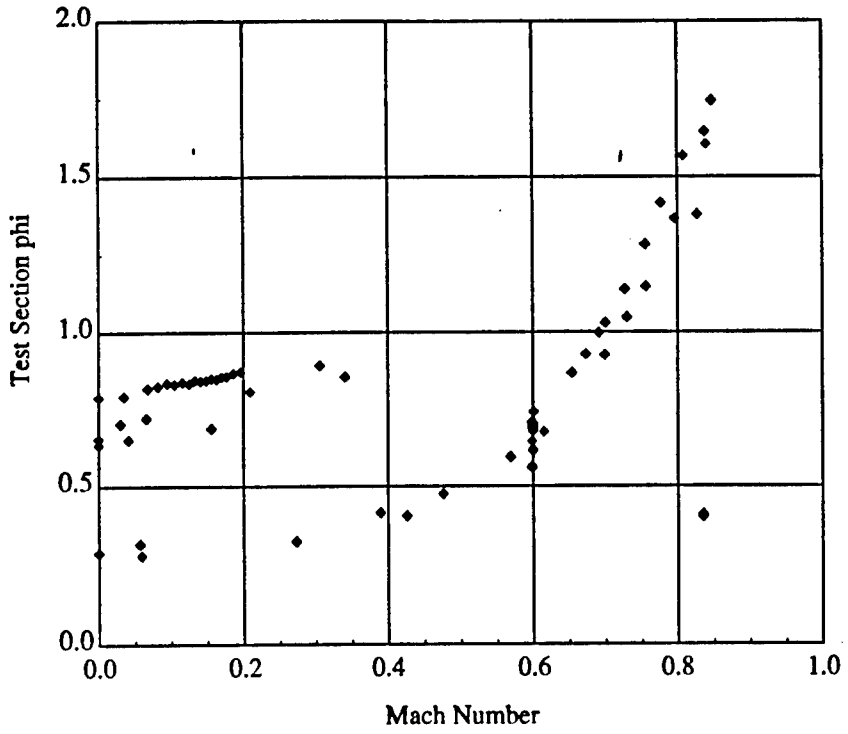

Figure 9. Test section relative humidity for TST tests.

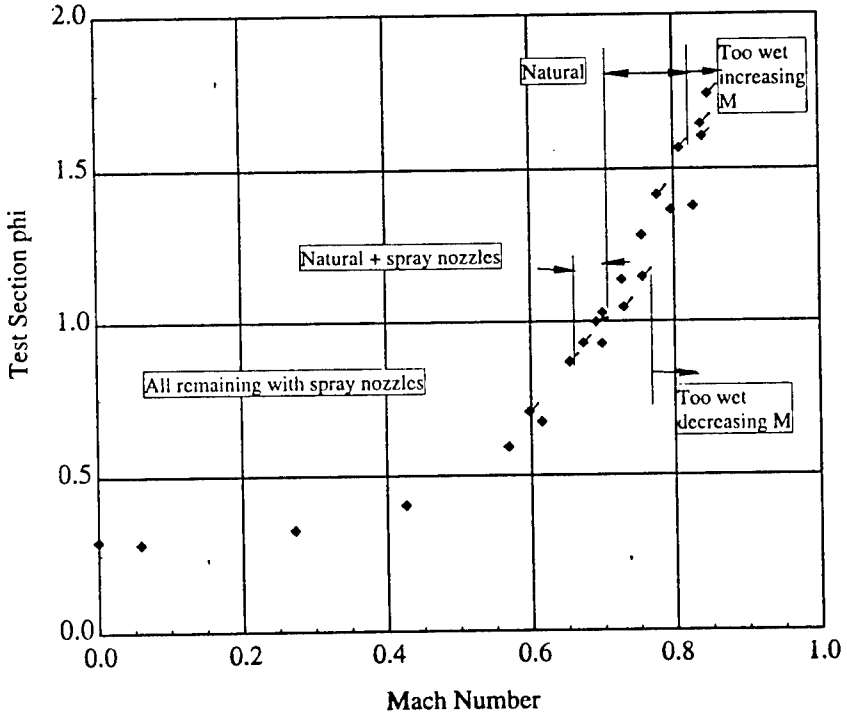

Figure 10. Test section relative humidity for run 460 of TST tests. Flagged symbols represent increasing Mach number portion of the run.

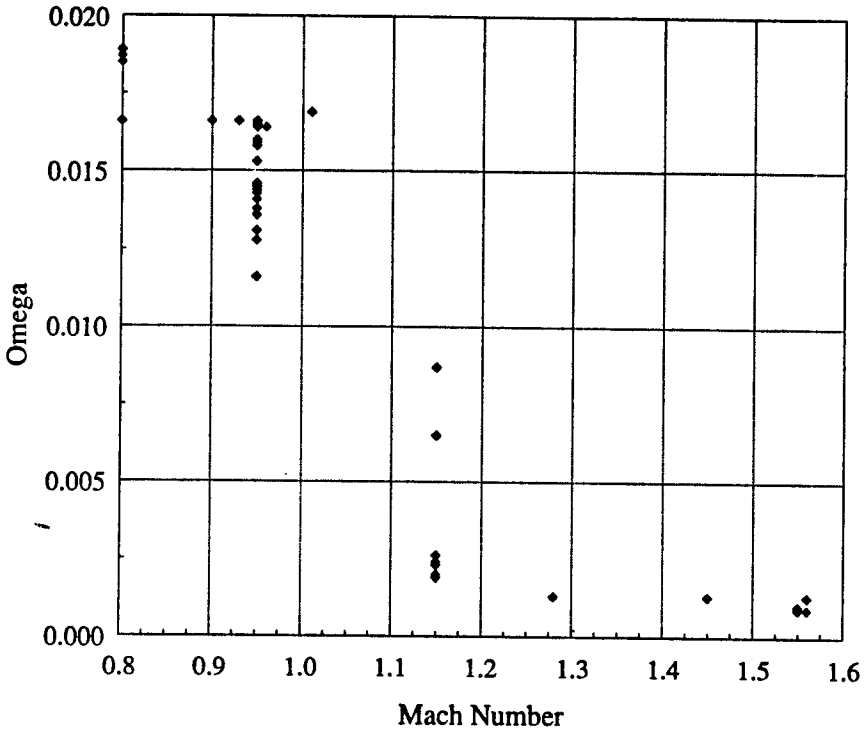

Figure 11. Specific humidity for missile tests.

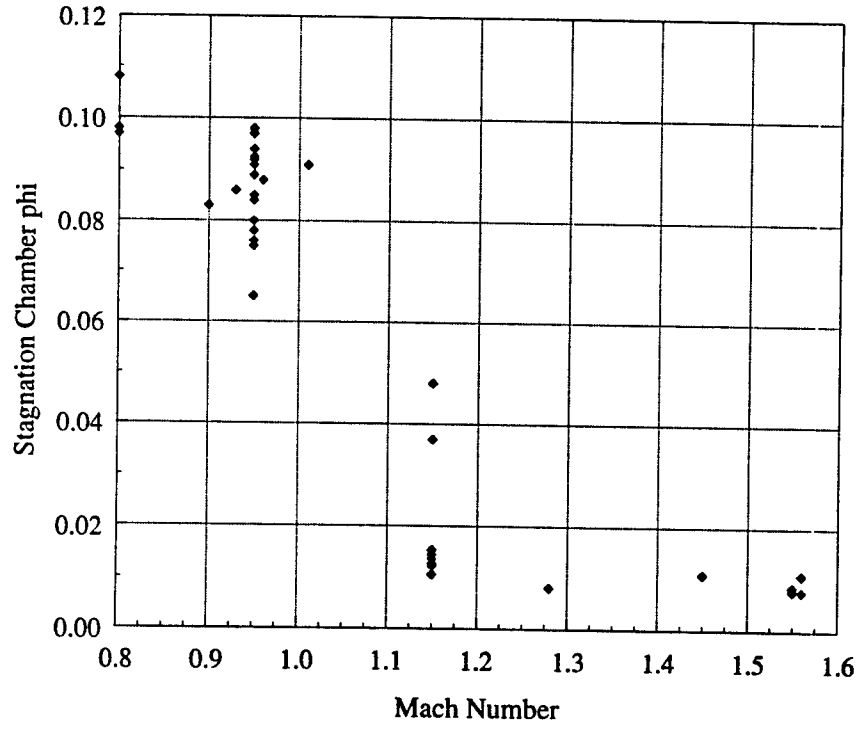

Figure 12. Stilling chamber relative humidity for missile tests.

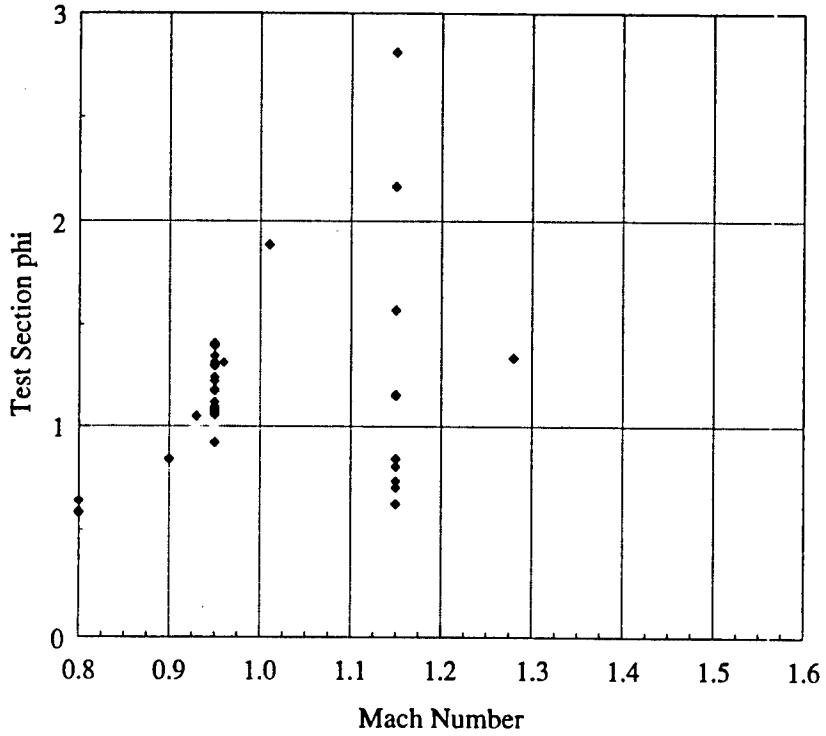

Figure 13. Test section relative humidity for missile tests.

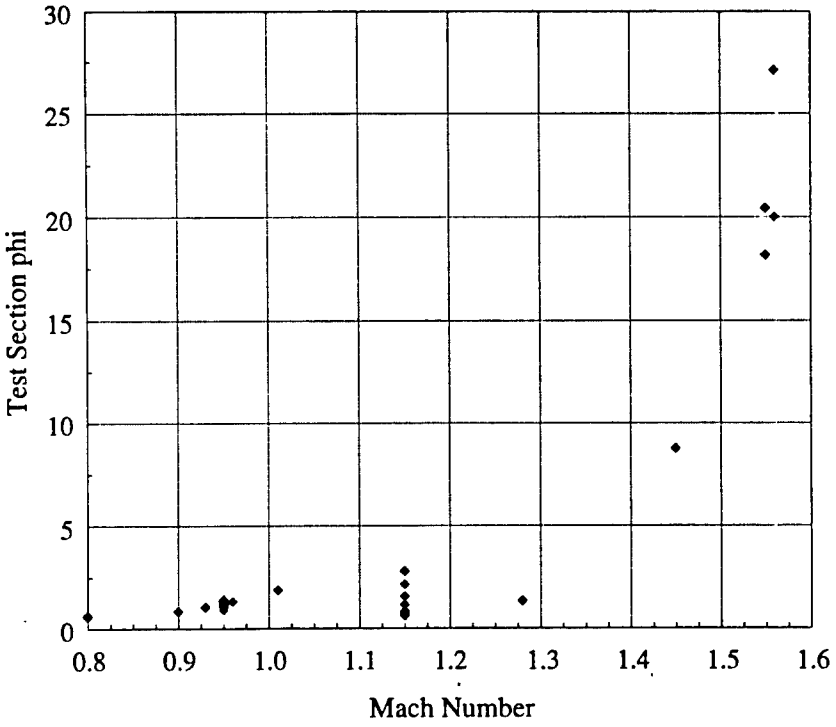

Figure 14. Test section relative humidity for missile tests.

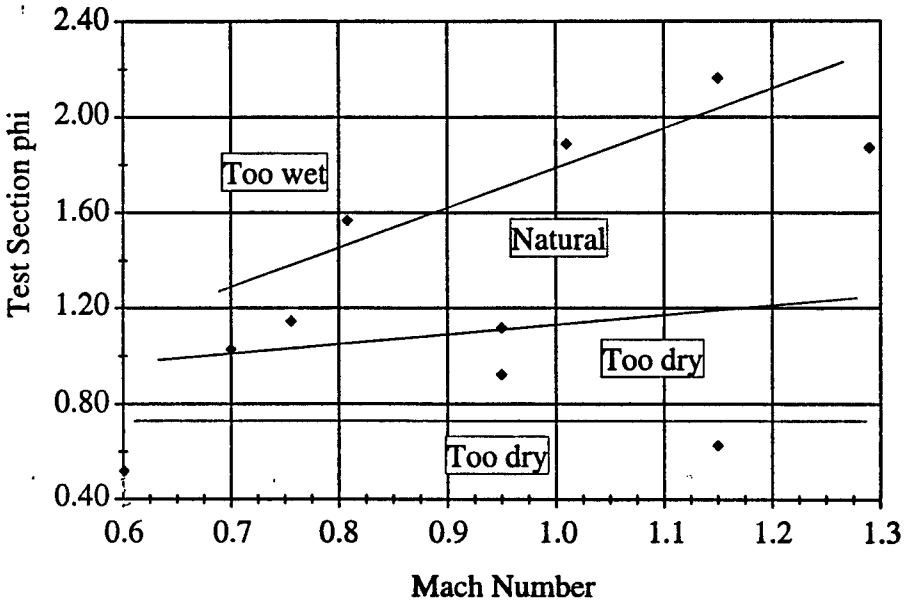

Figure 15. Regions of application of laser vapor screen flow visualization in 16T wind tunnel.

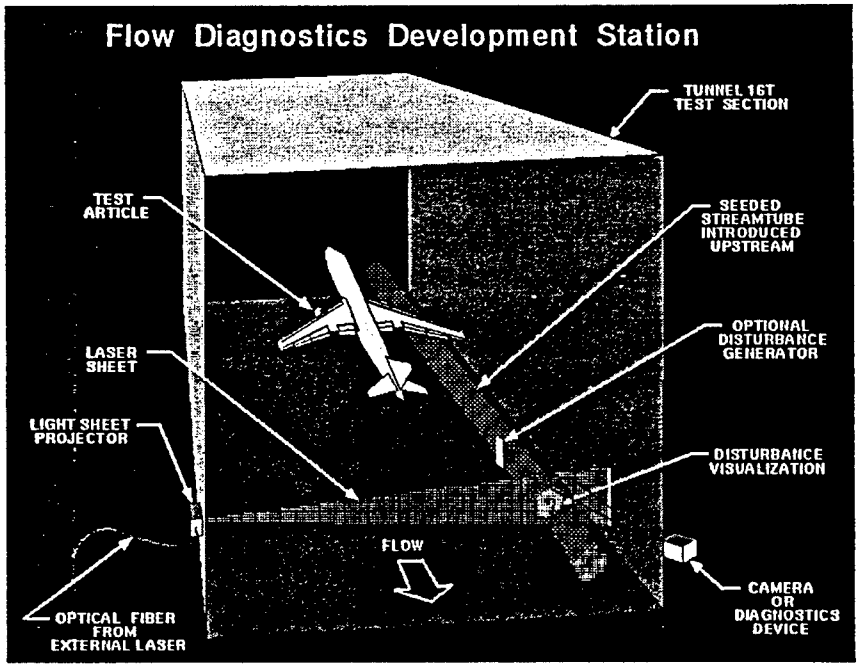

Figure 16. Proposed Flow Diagnostics Development Center for 16T wind tunnel.

Appendix A TST Test Data

Number	Run No.	Mach No.	p_o	ω	ϕ_o	ϕ_{TS}
1	940	0	1529	.0187	.787	.787
2	940	.035	1529	.0187	.787	.790
3	940	.068	1503	.0188	.805	.816
4	940	.105	1498	.0188	.802	.829
5	940	.125	1483	.0187	.794	.831
6	940	.082	1498	.0188	.806	.822
7	940	.095	1498	.0189	.811	.833
8 (4)	940	.105	1490	.0188	.804	.830
9	940	.116	1486	.0188	.803	.836
10 (5)	940	.125	1483	.0187	.799	.836
11	940	.133	1483	.0187	.800	.842
12	940	.141	1476	.0186	.793	.840
13	940	.149	1473	.0185	.789	.842
14	940	.156	1473	.0185	.790	.848
15	940	.163	1464	.0184	.782	.846
16	940	.170	1464	.0184	.783	.853
17	940	.177	1455	.0184	.780	.855
18	940	.186	1455	.0184	.782	.865
19	940	.196	1445	.0184	.778	.871
20	940	.209	1407	.0184	.761	.805
21	127/1	.600	1000	.0193	.249	.686
22	127/1	.600	1000	..0196	..253	.697
23	127/1	.599	1000	.0208	.252	.688
24	127/1	.600	1000	.0197	.254	.700
25	127/1	.599	1000	.0223	.253	.688
26	127/1	.476	987	.0234	.254	.476
27	127/1	.390	992	.0234	.271	.415

28	127/1	.600	1000	.0198	.256	.704
29	127/1	.600	1000	.0201	.251	.690
30	127/1	.059	999	.0238	.315	.318
31	273/4	0	1791	.0167	.652	.652
32	273/4	0	1687	.0172	.632	.632
33	273/4	.03	1615	.0186	.698	.700
34	273/4	.041	1603	.0173	.646	.649
35	273/4	.066	1603	.0184	.709	.718
36	273/4	.156	1613	.0164	.638	.685
37	273/4	.306	1621	.0174	.679	.892
38	273/4	.341	1612	.0162	.609	.854
39	294/1	.835	1237	.0042	.057	.401
40	294/1	.835	1237	.0046	.059	.409
41	297/1	.599	1487	.0124	.206	.559
42	297/1	.599	1487	.0125	.207	.564
43	297/1	.600	1487	.0128	.212	.577
44	297/1	.600	1487	.0131	.224	.612
45	297/1	.600	1487	.0132	.226	.617
46	297/1	.599	1487	.0143	.237	.643
47	297/1	.600	1494	.0149	.248	.675
48	297/1	.600	1488	.0151	.250	.681
49	297/1	.5995	1487	.0155	.256	.697
50	297/1	.601	1487	.0158	.269	.738
51	460	.598	1464	.0166	.261	.706
52	460	.654	1425	.0172	.263	.866
53	460	.673	1415	.0173	.263	.928
54	460	.691	1413	.0174	.264	.998
55	460	.700	1407	.0174	.263	1.029
56	460	.727	1403	.0173	.261	1.137

57	460	.755	1400	.0174	.262	1.283
58	460	.77	1395	.0175	.262	1.415
59	460	.808	1392	.0175	.254	1.568
60	460	.838	1347	.0177	.233	1.646
61	460	.840	1274	.0181	.225	1.606
62	460	.848	1210	.0178	.231	1.745
63	460	.827	1181	.0178	.206	1.378
64	460	.796	1163	.0180	.232	1.366
65	460	.756	1124	.0180	.231	1.146
66	460	.730	1108	.0180	.235	1.047
67	460	.699	1073	.0180	.235	.926
68	460	.615	988	.0182	.232	.674
69	460	.569	975	.0183	.238	.593
70	460	.426	951	.0179	.243	.405
71	460	.273	931	.0186	.263	.325
72	460	.059	966	.0179	.280	.283
73	460	0	997	.0174	.291	.291
74	459/1	.601	1470	.0137	.224	.519

Appendix B Missile Data

Number	Run No.	Mach No.	p_{ts}	ω	ϕ_o	ϕ_{TS}
1	3374/4	.95	278	.0146	.085	1.221
2	3375/2	.95	278	.0116	.065	.923
3	3375/3	.95	278	.0128	.076	1.096
4	3375/4	.95	278	.0131	.076	1.093
5	3375/5	.95	278	.0136	.076	1.074
6	3375/6	.95	278	.0138	.076	1.067
7	3375/7	.95	278	.0141	.076	1.058
8	3375/8	.95	278	.0143	.076	1.055
9	3375/9	.95	278	.0144	.076	1.063
10	3375/9	.95	278	.0145	.078	1.083
11	3378/10	.95	278	.0146	.080	10118
12	3375/11	.95	278	.0146	.080	1.118
13	3375/16	.95	278	.0153	.091	1.310
14	3375/20	.95	278	.0158	.084	1.173
15	3376/1	.95	278	.0159	.085	1.180
16	3376/6	.95	278	.0160	.094	1.346
17	3376/16	.95	278	.0164	.092	1.300
18	3376/20	.95	278	.0166	.098	1.407
19	3377/1	.95	278	.0166	.097	1.395
20	3377/6	.95	278	.0166	.089	1.241
21	3377/12	.95	278	.0165	.092	1.302
22	3377/16	.95	278	.0166	.0971	1.395
23	3377/20	.95	278	.0164	.0915	1.295
24	3378/1	.96	276	.0164	.088	1.313
25	3378/1	.90	276	.0166	.083	.842
26	3378/1	.93	276	.0166	.086	1.049
27	3378/1	.80	325	.0189	.108	.640

28	3378	.80	325	.0166	.097	.590
29	3378/8	.80	325	.0185	.098	.580
30	3378/10	.80	325	.0187	.098	.586
31	3379/1	1.01	258	.0169	.091	1.888
32	3379/1	1.15	217	.0065	.037	2.163
33	3379/1	1.15	218	.0087	.048	2.809
33A	3379/1	1.15	219	.0033	.0184	1.070
34	3382/1	1.15	218	.0023	.0127	.737
35	3383/2	1.15	218	.0024	.0128	1.150
36	3384/1	1.15	218	.0026	.0145	.844
37	3384/3	1.15	218	.0024	.0137	.807
38	3384/7	1.15	218	.0026	.0154	.915
39	3384/12	1.15	218	.0023	.0123	.705
40	3385/2	1.15	218	.0019	.0107	.626
41	3385/5	1.15	218	.0020	.0106	1.155
42	3386/1	1.28	218	.0013	.0081	1.337
43	3386/1	1.45	229	.0013	.0109	8.778
44	3386/1	1.56	194	.0013	.0109	27.11
45	3386/1	1.55	190	.0010	.0086	20.43
46	3387/1	1.55	190	.0009	.0078	18.16
47	3387/1	1.56	186	.0009	.0077	20.01
48	3386/1	1.29	276	.0013	.0103	1.872

EXPERIMENTAL INVESTIGATION OF LIQUID CRYSTAL APPLICATIONS FOR BOUNDARY LAYER CHARACTERIZATION

Derek E. Lang
Graduate Student
A. Tom Mattick
Associate Professor
Department of Aeronautics and Astronautics

University of Washington
Aerospace and Energetics Research Building
Seattle, WA 98195

Final Report for:
Summer Research Extension Program
U.S. Air Force Academy/Aeronautics Research Center

Sponsored by:
Air Force Office of Scientific Research
Bolling Air Force Base, DC

And

U.S. Air Force Academy/Aeronautics Research Center

December 1997

EXPERIMENTAL INVESTIGATION OF LIQUID CRYSTAL APPLICATIONS FOR BOUNDARY LAYER CHARACTERIZATION

Derek E. Lang
Graduate Student
A. Tom Mattick
Associate Professor
Department of Aeronautics and Astronautics

Abstract

Heat transfer measurements in supersonic flow are a critical part of the design and analysis of high-speed vehicles and missiles. The U.S. Air Force Academy/Aeronautical Research Center is developing measurement techniques based on liquid crystal thermography to provide global heat transfer data. This research complements the research by focusing on problems associated with the application of narrow-bandwidth liquid crystals in low enthalpy wind tunnels. The ability to achieve quality colorplay appears to be strongly dependent on the initial temperature conditions and heat flux. Even with poor quality colorplay, useful heat transfer data can be obtained. In combination with thermocouple data, liquid crystals provide an effective technique for global flow visualization and heat transfer measurement.

EXPERIMENTAL INVESTIGATION OF LIQUID CRYSTAL APPLICATIONS FOR BOUNDARY LAYER CHARACTERIZATION

Derek E. Lang
A. Tom Mattick

Introduction

The U.S. Air Force Academy Aeronautical Research Center (ARC) is developing heat transfer measurement capabilities for application in Trisonic Wind Tunnel (TWT). As part of the Air Force Office of Scientific Research (AFOSR) 1996 summer research program, an initial capability was developed using surface mounted thermocouples that provide heat transfer at specific points on the model (Ref 1). Subsequent research focused on developing a liquid crystal measurement capability that provides global surface heat transfer data. ARC has applied the liquid crystal technique to a variety of geometries in the TWT with wide-band crystals (Ref 2). This research provides additional insight into the sensitivities of liquid crystals in supersonic heat transfer measurements so that ARC can determine the optimum experiment design for its research applications.

This research focuses on two areas: 1) developing data on the use of narrow band liquid crystals and 2) analysis of heat transfer measurements in flow conditions similar to the TWT. The first part involves transient calibration of the crystals and study of influences affecting monitoring of the liquid crystals for measurements. The second part involves lessons learned from practical conduct of heat transfer measurements in a low enthalpy flow.

Methodology

Background. The rate of heat transfer is dependent on the characteristics of the boundary layer formed at the model surface and the temperature differences driving the heat transfer. The heat flux equation below illustrates the dependence on the heat transfer coefficient, h, the adiabatic wall temperature, T_{aw}, (assumed equal to recovery temperature) and the wall temperature, T_w.

$$q = h\,(T_{aw}-T_w)$$

The experimentalist determines heat transfer by measuring surface temperature(s) at given locations over time. Lang (Ref. 1) describes several methods for reducing this temperature data to heat transfer. The complementary error function and Cook-Felderman approaches are used here.

Ireland, et. al., (Ref. 3) describe the liquid crystal measurement techniques used to accurately provide a single temperature measurement or continuous temperature data depending on the data reduction method used. As the temperature changes, the liquid crystal displays "colorplay", i.e., the visual color changes between red, yellow, green, and blue. For narrow-band crystals, the colorplay occurs over a short range of temperatures. For example, a 17C crystal with a 1C bandwidth may display visual colors for temperatures between 17-18C. The complementary error function equation for heat transfer shown below is commonly used with narrow-band crystals to determine the heat transfer coefficient, h, over the model surface.

$$\frac{T_w - T_{aw}}{T_{w,0} - T_{aw}} = \exp(\beta^2) erfc(\beta)$$

$$\text{where, } h = \frac{\beta\sqrt{\rho ck}}{\sqrt{t}}$$

The experimenter selects a distinguishable color, e.g., yellow, to correlate with a specific temperature, T_w, and records the time, t, during the test at which the color becomes visible. The density, ρ, specific heat, c, and thermal conductivity, k, which together are defined as the thermal product, are properties of the model material. This approach uses semi-infinite slab assumptions and assumes a constant heat transfer coefficient.

Another approach useful in this research was to use the Cook-Felderman formulation of the heat transfer equation. This approach also uses the semi-infinite slab assumptions, but makes no assumptions for boundary conditions. This approach is well suited for the transient wind tunnel environment where heat flux, heat transfer coefficient, and total temperature may vary. By using continuous temperature data for the duration of the test (e.g., using a thermocouple), a solution is computed by numeric integration:

$$q(t_n) = \frac{2\sqrt{\rho ck}}{\sqrt{\pi}} \sum_{i=1}^{n} \frac{T_{w,i} - T_{w,i-1}}{\sqrt{t_n - t_i} + \sqrt{t_n - t_{i-1}}}$$

Static Calibrations. The first phase of the research was the calibration of the liquid crystals. The ARC provided Hallcrest BM/R17C1W/C17-10, BM/R14.5C1W/C17-10, and

BM/R12.5C1W/C17-10 liquid crystals for evaluation. The crystals were calibrated using a transient technique shown in Figure 1. The crystals were applied to a flat plate with a surface mounted thermocouple and then cooled until colorplay was exhibited at the location of the thermocouple. The temperature and associated colorplay was recorded with one of two types of video cameras (a Sony SVHS or Hi-8) in NTSC format as the temperature at the thermocouple location passed through the liquid crystal bandwidth. Viewing angle, illumination, and illumination angle were varied to assess their effects.

Wind Tunnel Tests. The next phase of the research used the UW Cold Flow Facility shown in Figure 2 to examine the performance of the liquid crystals in supersonic flow conditions. The Cold Flow Facility is a supersonic blowdown facility with the capability for interchanging nozzle sections. The Cold Flow Facility was operated at total temperatures of 18-20°C with stilling chamber pressures about 5.8×10^5 Pa. The model surface temperature decreased to temperatures of -5°C once supersonic flow was established. Figure 3 shows the flat plate model configuration. The flat plate is held vertically on the floor of the tunnel channel by an aluminum baseplate with a piece of heavy stock paper between the two to provide insulation. Table 1 lists the model material properties for Plexiglas and Ertalyte as well as their respective thermal products and thermal diffusivities, $k/\rho c$. Omega "Cement-On" type-K thermocouples were attached to the model surfaces to verify temperature readings. The liquid crystal was applied using airbrush with a minimum number of passes over the surfaces to ensure a thin coating.

The specific tests analyzed are listed in Table 2. In the first test, the tunnel was started gradually by opening the regulator. The tunnel achieved supersonic speeds within four seconds before reaching its operating pressure. The remaining tests were started using the main valve. The flow

stabilized at a supersonic speed in less than a second. Tests were conducted with various initial model wall and stilling chamber temperatures.

Uncertainty Analysis. An uncertainty analysis was performed for both thermocouple and liquid crystal (BM/R12.5C1W/C17-10) heat transfer measurements based on ASME standard uncertainty methods and 95 percent confidence levels. For each measurement parameter, χ, Table 3a and 3b provide typical test conditions, the standard error for the measurement, $\delta\chi$, the contribution to uncertainty, and the total uncertainty values as a percentage of the computed heat transfer coefficient and heat flux. Uncertainty for the computed heat transfer value, V, was computed as:

$$(\delta V / V)^2 = \sum \left(\frac{1}{V} \frac{\partial V}{\partial \chi} \delta \chi \right)^2$$

The total uncertainty for heat transfer coefficient and heat flux was 9.4 and 8.6 percent, respectively, for the thermocouple-based measurements; and 7.1 and 7.8 percent for the liquid crystal-based measurements. While the uncertainty in time measurement for the liquid crystals (dependent on camera speed) was worse than the thermocouple, the Cook-Felderman data reduction technique used for the thermocouples amplified the effect of the uncertainty contribution. The numerical integration also resulted in greater uncertainties due to the material thermal product. Determination of the adiabatic wall temperature was a significant effect on the complementary error function approach. This has particular significance for the wind tunnel tests where determining the flow state and recovery factor were problematic.

Results

Calibration. An analog video recording system was selected in lieu of digital recording directly to computer. This type of system was later used for the wind tunnel tests. Images were recorded for the entire test at the standard 30 frames per second, and post-processed by viewing the videotape. Comparison of images from the Sony SVHS video camera to those of the Hi-8 video camera also showed the latter to have higher resolution. However, significant loss of resolution generally resulted when data was transferred from videotape to computer using a Snappy Video Card or Truevision Targa2000 Video Card/Adobe Premiere framegrabbing software. For comparison, ARC used a Matrox Meteor framegrabbing system that stored images on computer (Ref. 2). Automated post-processing of the resulting data was conducted with subroutines created in Matlab. While the system with an RGB camera provides higher resolution, the system was limited in the amount of data that can be stored on RAM and a frame schedule had to focus the recordings around the critical events during the test. Note also that the time counter was read directly for manual post-processing. Additional effort is required to automate processing of the RGB image at ARC; thus a simple light source was recorded in the images to indicate the initiation of data collection as an interim solution.

Factors affecting the accuracy of the calibration included thermocouple accuracy, video camera speed, and image resolution. In determining the level of accuracy sought for the narrow-band crystals, particular attention was paid to the limitations of the calibration technique. For example, the uncertainty of the thermocouples was minimized to $\pm$ 0.02C (3σ) compared to the 0.6-0.8C bandwidth for the yellow colors of the liquid crystals. Isolating the thermocouple electronics from electromagnetic pickup (e.g., computer, and power sources, counter) and

minimizing the distance between the thermocouple and the thermocouple electronics reduced the major source of uncertainty, noise.

The thermal mass of thermocouple and attachment of the thermocouples to the test article posed additional problems. The plate was cooled from behind to avoid damaging the liquid crystals (the coolant would cause condensation on the plate and dilute or "wash" off the crystals). As the front of the plate cooled, the colorplay front moved radially away from the coolant application toward the thermocouple. Figure 4 shows the colorplay front lagging in the region of the thermocouple when cooling was applied opposite the thermocouple leads. Cooling the plate behind the leads so that the leads were cooled with the wall reduced this effect. Figure 4 also shows the low viscosity glue to inhibit the colorplay likely due to contamination of the crystals when the thermocouples were applied over the liquid crystals. For the wind tunnel models, the liquid crystals were applied after attachment of the thermocouples

The calibration focused on three points: green-yellow transition; yellow; and yellow-red transition. The color transitions were sharp for large heat fluxes and diffuse for small fluxes. When the color transitions were sharp, the color bands were so narrow that the camera resolution limited the ability to spatially identify the transition points. The diffuse transitions had wider color-bands, but the transition was progression of hues. Thus, it was difficult to visually determine when one "color" started and finished. While attaining the precise transition points proved difficult, the level of uncertainty was still less than that associated generally with a wide-band crystal which contains a range of hues for a "color."

In Ref. 3, Ireland, et. al., discussed the dependence of the crystal colorplay (and corresponding temperature) as a function of viewing and illumination angles. Because color is a function of hue, saturation, and intensity, the direction of the light path relative to the crystal orientation will affect the color indication. Figures 5a, 5b, and 5c, however, show a relative insensitivity of the narrow-band crystals to viewing angle. Table 2a and 2b show the position of a lamp not to be a significant effect either. The temperature range of the narrow-band crystal was so small that the width of the colorplay region (i.e., those crystals that had any coloration) was also relatively narrow. In the transient calibration, spatial resolution was probably a more critical factor. In other words, the colorplay temperatures were less sensitive to angles, because determining whether any colorplay was occurring near the thermocouple was more distinct than identifying the specific hue. As viewing angle increased away from the normal to the plate surface, the intensity of the colors did decrease.

Potential effects of glare due to the reflection of light on the model surface were not apparent during calibrations. In the wind tunnel, the plate rested behind the viewing window, and glare did affect the intensity of the colors by washing out any colors otherwise visible. Locating the angle of the light source did not appear to affect the colorplay on the model surface in the presence of the glass.

Figure 5b suggests that the liquid crystals had higher colorplay temperatures when heated than cooled. A number of factors may have been the cause. The speed of image capturing may have been too slow compared to the colorplay speeds; thus the variance in temperature would be associated with the change in temperature between image frames. The rate of temperature

change was also different for cooling which occurred passively versus heating done actively. Heating was applied on the front of the plate versus cooling that occurred from the rear. Another possibility might be a hysterisis effect since cooling was sometimes followed by an immediate burst of heat.

Wind Tunnel Tests. Figure 6 shows the complexities of the flow passing over the plate. At the height of the thermocouple, the colorplay front moved aft from the leading edge until it reached the thermocouple. By the next frame, the entire plate has changed color. The movement of the front indicated high heat transfer at the leading edge with decreasing heat transfer aft. The thinner plate thickness at the leading edge that has less thermal mass was one factor causing this heat transfer profile. The heat transfer profile was also characteristic of a laminar boundary layer. If the boundary layer was laminar, transition started somewhere aft of thermocouple tip, but ahead of the turbulent spot.

The speed of the colorplay front at the thermocouple level was faster than the colorplay front on the left of the dark triangular region, and suggested a different flowfield. The colorplay front in the triangular region moved aft, again indicating laminar flow. Meanwhile, the right apex of the triangle moved forward over time, but then stopped about an inch behind the leading edge where it met the rearward moving laminar front indicating the beginning of transition (i.e., the point of lowest heat transfer). Transition is promoted (i.e., the flow is tripped) by an impinging shock coming from the leading edge of the baseplate. Alternatively, the aluminum baseplate behind the plate with its higher thermal conductivity may have been responsible for some of these heat transfer effects.

The flow appears to be tripped by the screw head and influenced by channel wall boundary layer. It transitioned through colorplay quickly indicating high heat transfer. In this frame, colorplay had not reached the end of the plate; thus the beginning of fully turbulent flow was likely just aft of the forward screw head. The bright line down the center of the plate was due to a protrusion along the plate surface exposed to higher heat transfer.

While several qualitative flow-features were discernible from images like Figure 6, it was more difficult to develop quantitative data from the images. Only one or two of these images were attained per run, and the opaque regions were captured rather than well-defined narrow bands of color. The colorplay front itself was re-defined by the contrast between light and dark areas.

Table 5 summarizes the quality of the colorplay for each test. Run 1 was the only test with good colorplay in which clear colorbands marched along the plate. The start-up procedure using the regulator was primary difference between this run and the others.

Colorplay began in Run 1 about the same time as supersonic flow was established, but the test conditions may have been significantly altered by the preceding subsonic flow. Run 1 was at the low end of the heat transfer spectrum compared to the other runs, but not the least nor significantly different from other runs.

The opaque regions were similar to the washed-out colors found with the runs in the TWT (Ref. 2). In the previous study, the washout was attributed to the steep slope of the surface temperature-time profiles associated with high heat transfer coefficient. It was concluded that the change in temperature with time through the liquid crystal temperature band occurred so

quickly that only a blur of color could be seen given the speed limitations of the framegrabber. However, Run 4 and 7 have comparable rates of surface temperature change, dT/dt, and heat transfer coefficients to Run 1 with much lower colorplay quality (See Table 5). The only consistent parameter between the all the runs with any visible colorplay is the small difference between initial stilling chamber and wall temperatures. This might infer a lower heat flux at the time of colorplay - which is marginally true in Table 5 - but this should still impact the rate of surface temperature change.

The opaque coloration raised several questions about the behavior of the crystals. The opaque color regions were initially believed to be an extreme of the diffuse colorplay front where all the colors mix with one another. If the entire plate were undergoing rapid temperature changes, one would expect to see large regions of the same color. However, the coloration remained well after the surface passed through the crystal bandwidth, and even beyond the end of the test. Thus, it was not clear whether this phenomenon was normal crystal behavior.

Using the runs with some level of colorplay, it was possible to examine some aspects of the quantitative heat transfer results. Thermocouple data provide baseline information on the heat transfer coefficient and heat flux that should be seen with the liquid crystals. Figures 7a and 7b show good agreement between all of the runs for these measurements with Eckert's empirical correlation for laminar flow (Ref. 4).

Figure 8 compares heat transfer coefficients based on liquid crystal measurements to Eckert's empirical curve. At the leading edge, the comparison shows the experimental measurements

substantially lower than the empirical curve (though within the same order of magnitude) between the two. A disparity was expected since the semi-infinite assumptions used for the complementary error function approach are not as appropriate for thin bodies. Probably an equally, if not more, significant factor is that colorplay occurs so near the start-up, that the accuracy of time measurement is becomes highly critical. Note also, heat transfer coefficient is generally not constant for the transient start-up phase. Agreement between the two appears more promising further aft.

Generally, more accurate heat transfer measurements can be achieved if the temperature driving potential, T_w-T_{aw}, is large relative to the uncertainty of the temperature measurement, δT, and the time lapse, t_n-t_0, is large relative to the uncertainty in time. Usually, the model surface is initially the same as room temperature. In the case of the low enthalpy TWT, the temperature range is governed whether or not a heater is used, resulting in temperatures of 80-110F. The Cold Flow Facility, however, is able to achieve significantly lower total temperatures due to the expansion of the gas from 2,500 psia in the storage tanks to 85 psia in the stilling chamber. But with only a passive cooling system, it was difficult to maintain a constant stilling chamber temperature, even with heat-sink rods placed in the stilling chamber as shown in Figure 2.

The increased temperature driving potential achieved by lowering the adiabatic wall temperature may not, however, provide the optimum heat transfer conditions. In absence of a model shroud, subsonic flow precedes the supersonic flow driving the wall temperature to the adiabatic wall temperature. Moreover, the larger temperature driving potential will also increase the heat flux that may be associated with the washout problem, and definitely the difference between wall

temperature and stilling chamber temperature that does appear to play a role in colorplay quality. For similar reasons, pre-heating the model surface may not be advantageous. Pre-heating also introduces uncertainties in surface temperature uniformity.

Heat flux can also be controlled without adversely impacting measurement of heat transfer coefficient through the selection of model materials. Ideally, one desires heat transfer from the flow to be isolated at the surface of the model. However, heat is conducted from the surface into the model. From a semi-infinite slab assumption for heat transfer, the key parameter influencing the conduction of heat from the surface into the wall is the thermal product and thermal diffusivity. Lang in Ref. 2 found that material properties were the most significant factor for hue quality in wide-band crystals.

In reality, the heat transfer is not one-dimensional. Rather, heat dissipation and penetration affect the heat transfer away from the surface. In Figure 9, the combination of heat transfer and thermal diffusivity to be a critical combination influencing the quality of the colorplay (Ref. 2). As time progresses, the surface temperature changes from its initial value, T_{w0}, to the adiabatic wall temperature (at large times), giving a total change $\Delta T^* = T_{aw}-T_{w0}$. For an intermediate time, the *fractional* temperature change, $f = (T_w-T_{w0})/\Delta T^*$, depends on slab thickness, L, film heat transfer coefficient, h, and thermal conductivity, k, via the Biot number, here defined as $Bi = hL/2K$. Figure 10 plots curves of fractional change for several Biot values, as a function of the fractional temperature change that would apply for an infinite slab exposed for the same duration to the same flow. Where a given curve coincides with that for $Bi = \infty$, the infinite-slab approximation is accurate. As an example, consider turbulent airflow at Mach=3, stagnation

temperature 300K (so that T_{aw}=278.4K), over a slab having an initial temperature T_{w0}=295K. In this case, $\Delta T^* = -21.6K$. It is desired that the infinite-slab approximation be valid over surface temperatures ranging from T_{w0} down to the colorplay temperature of a certain liquid crystal, e.g., T_w=288K. For this case, the fractional temperature change would be $f = (288-295)/\Delta T^* = 0.56$. Figure 10 shows that the infinite-slab approximation will be accurate for $Bi \geq 2$. If for example, the thermal conductivity, k = 1 W/m.K, and the estimated film coefficient, h = 200 $W/m^2.K$, a thickness $L \geq .02$ m (2 cm) is required for the infinite-slab approximation to be accurate.

Generally, heat transfer in this transient environment is a challenging parameter to determine. In the first place, the adiabatic wall temperature is a function of recovery factor, which assumes apriori knowledge of whether the flow is laminar or turbulent. Alternate definitions of Stanton Number, C_h, have been used for high enthalpy supersonic flow in which the total temperature replaces adiabatic wall temperature such that:

$$C_h = \frac{q}{\rho_\infty U_\infty C_p (T_{tot} - T_w)}$$

However, in a low enthalpy tunnel where the total temperature is higher than the initial wall temperature, the recovery temperature may be lower than wall temperature depending on the recovery factor. In such cases, the direction of heat transfer may be in reverse. Alternative methods of using the liquid crystals can be used to solve for recovery factor simultaneously with heat transfer, such as using the hue method in continuous data collection or applying more than one liquid crystal to the model. Other issues affecting determination of heat transfer include:

- Unsteady total temperature by using thermocouple data in approaches similar to that used by Babinsky for determining global heat transfer (Ref. 5).
- Non-uniform boundary conditions influencing heat transfer as the air travels downstream the surface and exchanges heat along the way (Ref. 6).
- Assumption of a constant heat-transfer coefficient for the complementary error function approach, whereas the environment in the TWT and Cold Flow Facility are generally transient (Ref. 1).
- The thermal spike observed during tunnel start-up.

Conclusions

The purpose of this research was to gain insight into the application of liquid crystals for heat transfer measurements in the low-enthalpy TWT. The narrow-band crystal work compliments the experiential database being developed by ARC on wide-band crystals. Similar problems, such as colorplay washout, arose between the narrow-band and wide-band crystals. It appears that heat transfer coefficient is less effect on colorplay quality than anticipated from earlier work. The relative magnitudes of initial surface temperature and total temperature have some relation to this problem as might heat flux. Examination of the surface temperature rate of change did not prove conclusive as an explanation for the poor colorplay. Thus, additional research is necessary to understand the washout problem.

Based on thermocouple data and sample liquid crystal data, even poor colorplay quality from liquid crystals can provide some useful heat transfer data. Increasing framegrabbing speeds and

developing more accurate heat transfer data reduction techniques will enhance the accuracy of the heat transfer results. Materials selection remains a critical factor in planning liquid crystal heat transfer experiments. The relation of Biot number to fractional change in temperature based on infinite slab assumptions provides a guide for designing the required thickness of the models. And finally, additional consideration should be given to analyzing heat transfer given recovery temperature as an unknown.

References

1. Lang, Derek E., "USAFA Trisonic Wind Tunnel Analysis for Heat Transfer Measurements," USAFA DFAN Report 96-02, August 1996.

2. Lang, Derek E., "Hue Analysis Factors for Liquid Crystal Transient Heat Transfer Measurements," Graduate Student Research Program Report, Air Force Office of Scientific Research, September 1997.

3. Ireland, P.T., Wang, Z., and Jones, T.V., "Liquid Crystal Heat Transfer Measurements," Measurement Techniques, Lecture Series 1995-01, von Karman Institute for Fluid Dynamics, January 30-February 3, 1995.

4. Eckert, E. RG, "Engineering Relations for Friction and Heat Transfer to Surface in High Velocity Flow," *Journal of the Aeronautical Sciences*, Vol. 22, No. 8, pp. 585-587.

5. Babinsky, H. and Edwards, J.A., "Automatic Liquid Crystal Thermography for Transient Heat Transfer Measurements in Hypersonic Flow," *Experiments in Fluids*, Vol. 21, 1996, pp. 227-236.

6. Butler, R.J. and Baughn, J.W., "The Effect of the Thermal Boundary Condition on Transient Method Heat Transfer Measurements on a Flat Plate with a Laminar Boundary Layer," *ASME: Journal of Heat Transfer*, Vol. 118, For Publication August 1996.

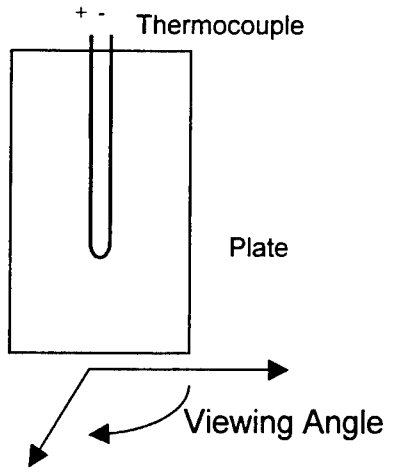

Figure 1: Transient Calibration Rig

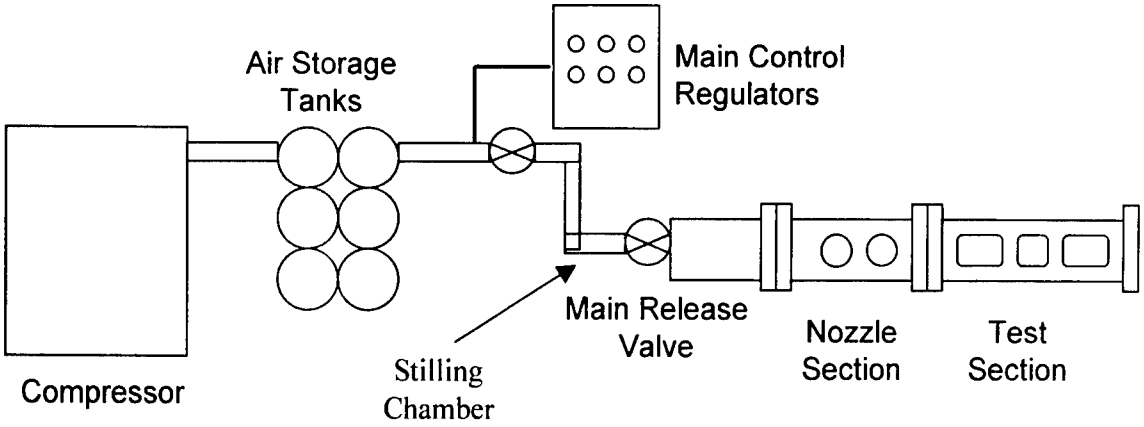

Figure 2: UW Cold Flow Facility

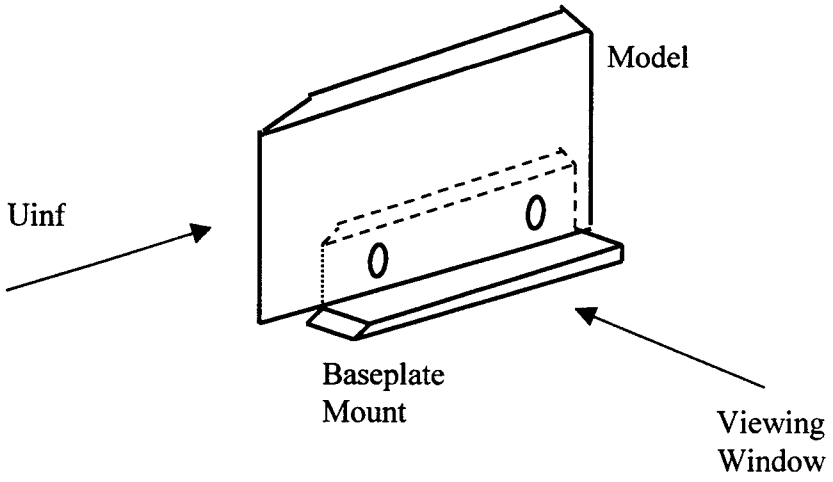

Figure 3: Flat Plate Model Configuration

Table 1: Material Properties

Material Property	Plexiglas	Ertyalyte
Density kg/m^3	1190	1201
Specific Heat, J/kg.K	1462	1075
Thermal Conductivity, W/m.K	0.19	1.26
$\sqrt{\rho c k}$, $W.s^{1/2}/m^2.K$	571	501
$k/\rho c$, $1/m^2 s$	6.90e-08	1.5e-07

Table 2: Test Cases

Run	Startup	T_{tot}(C)	$T_{w,0}$(C)	P_{tot}(Psia)	Material
1	Regulator	19.1	19.7	92	Plexiglas
2	Valve	15.6	18.3	85	Plexiglas
3	Valve	19.1	19.3	84	Ertalyte
4	Valve	15.3	22.3	86	Ertalyte
5	Valve	13.6	21.2	85	Ertalyte
6	Valve	12.5	15.6	84	Ertalyte
7	Valve	18.5	19.2	87	Ertalyte

Table 3a: Heat Transfer Uncertainty for Thermocouple Measurement

Measured Parameter (χ)	Typical Value	$\delta\chi$ (±)	q-Uncertainty (%)	h-Uncertainty (%)
T_{wi}-T_{wi-1} (C)	3.5	0.02	1.1	1.1
t_n-t_i (s)	0.4	0.01	7.1	7.4
$\sqrt{\rho ck}$ (W.s$^{1/2}$/K.m^2)	501	25	5.2	5.7
T_{aw}-T_w (C)	-30.3	0.02	--	0.1
Total			8.6	9.4

Table 3b: Heat Transfer Uncertainty for Liquid Crystal Measurement

Measured Parameter (χ)	Typical Value	$\delta\chi$ (±)	q-Uncertainty (%)	h-Uncertainty (%)
T_w-T_{aw} (C)	21.9	0.3	6.1	4.7
t_n-t_0 (s)	1.5	0.03	1.0	1.0
$\sqrt{\rho ck}$ ($W.s^{1/2}/K.m^2$)	501	25	4.8	5.3
$T_{w,0}$-T_{aw} (C)	30.3	0.02	0.2	0.2
Total			7.8	7.1

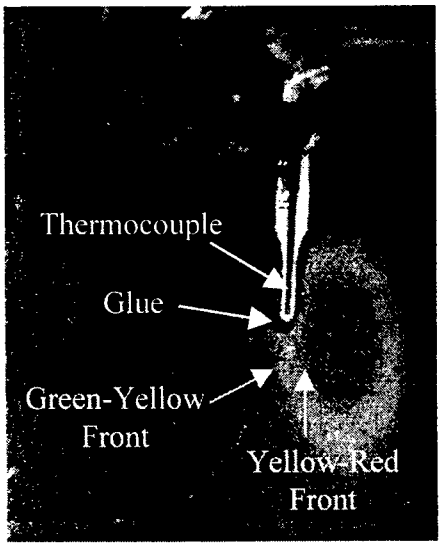

Figure 4: Effect of Thermocouple on Calibration Heat Transfer

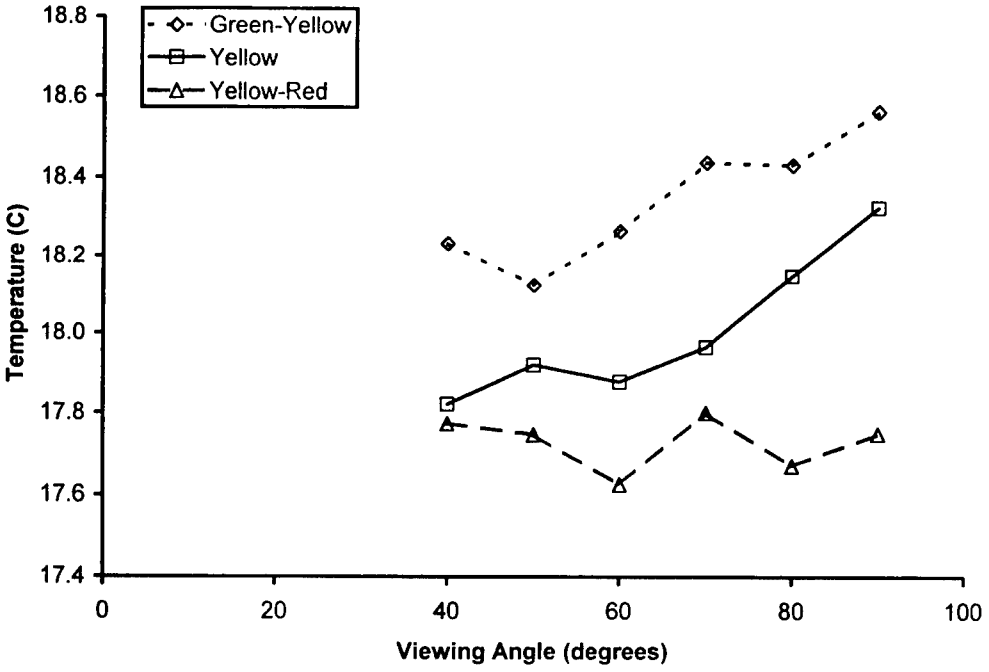

Figure 5a: Viewing Angle Sensitivity - BM/R17C1W/C17-10

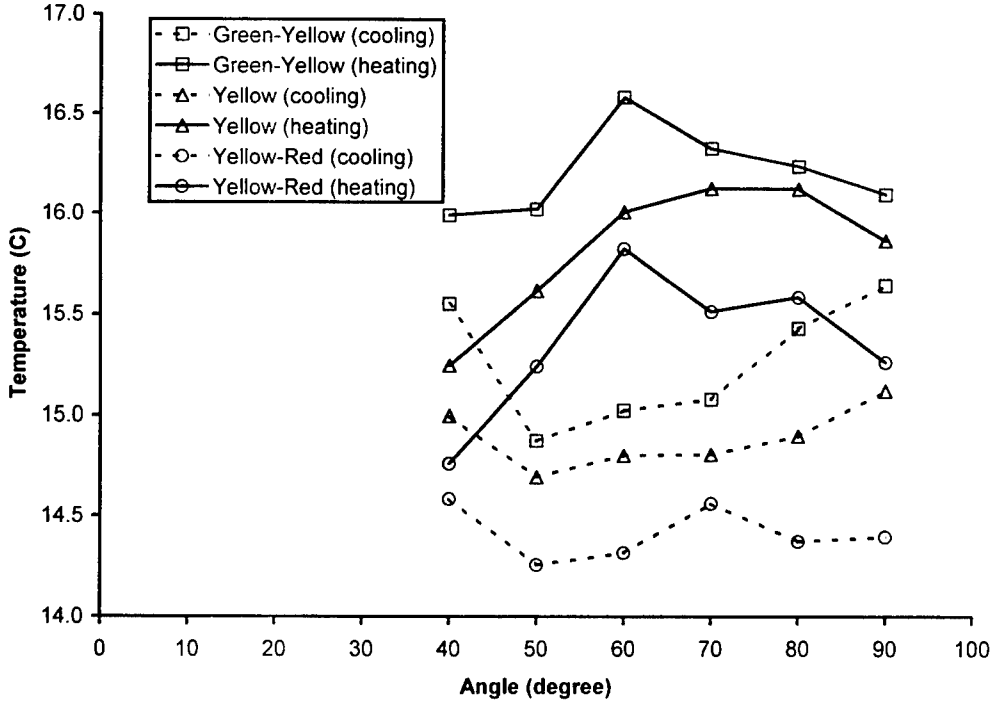

Figure 5b: Viewing Angle Sensitivity - BM/R14.5C1W/C17-10

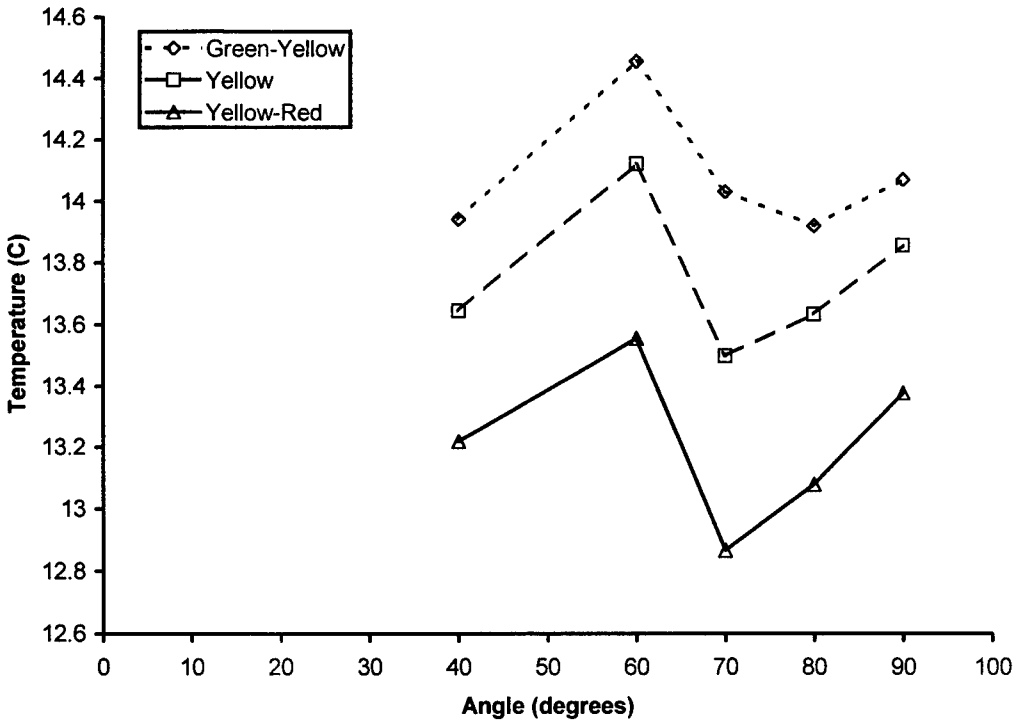

Figure 5c: Viewing Angle Sensitivity - BM/R12.5C1W/C17-10

Table 4a: Illumination Sensitivities - BM/R17C1W/C17-10

Light Source	Viewing Angle (degrees)	Green-Yellow (C)	Yellow (C)	Yellow-Red (C)
Ceiling	90	17.8	17.6	17.1
Lamp - 90°	90	17.7	17.5	17.0
Lamp - 45°	90	17.8	17.2	16.8

Table 4b: Illumination Sensitivities - BM/R14.5C1W/C17-10

Light Source	Viewing Angle (degrees)	Green-Yellow (C)	Yellow (C)	Yellow-Red (C)
Ceiling	90	15.6	15.4	15
Lamp - 90°	90	15.2	14.7	14.3
Lamp - 90°	45	15.4	15.0	14.4
Lamp - 45°	90	15.4	14.9	14.4

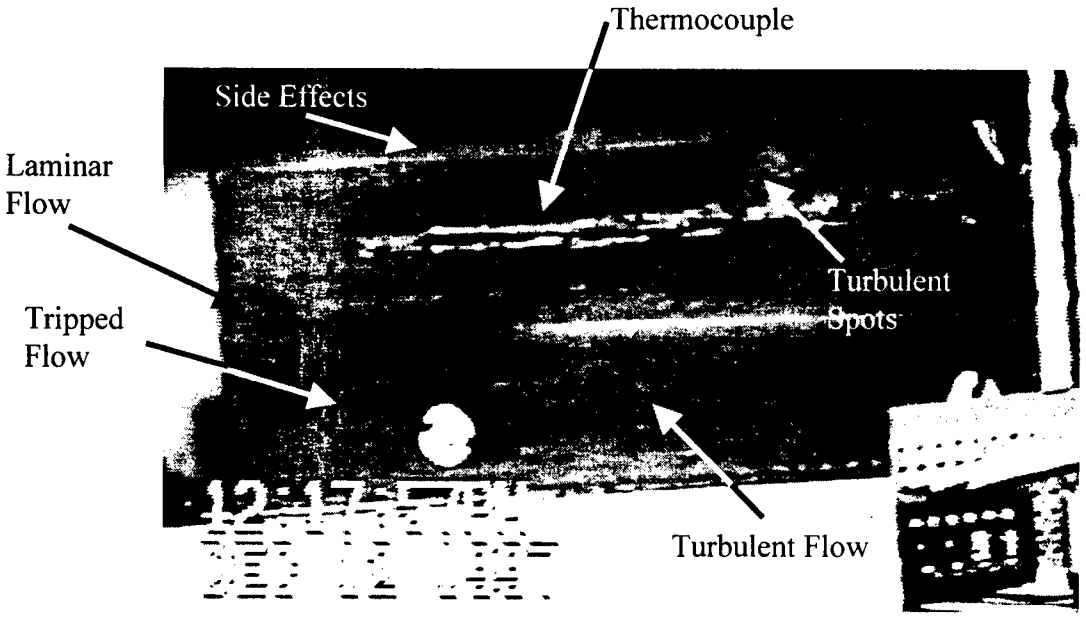

Figure 6: Colorplay over Flat Plate in Run 7

Table 3: Potential Factors Affecting Colorplay

Run	T_{tot}-T_{w0} (C)	DT/dt (C/s)	h(T_w=13.5) (W/m^2.K)	q(T_w=13.5) (W/m^2)	Colorplay Quality
16	-0.6	-5	170	-3600	Good
17	-2.7	-28	200	-4900	None
18*	-0.2	na	na	na	Poor
19	-7.0	-8	190	-5500	None
20	-7.6	-20	165	-5600	None
21	-3.1	-17	70	-1600	Poor
22	-0.7	-5	195	-4400	Poor

* - surface thermocouple non-responsive

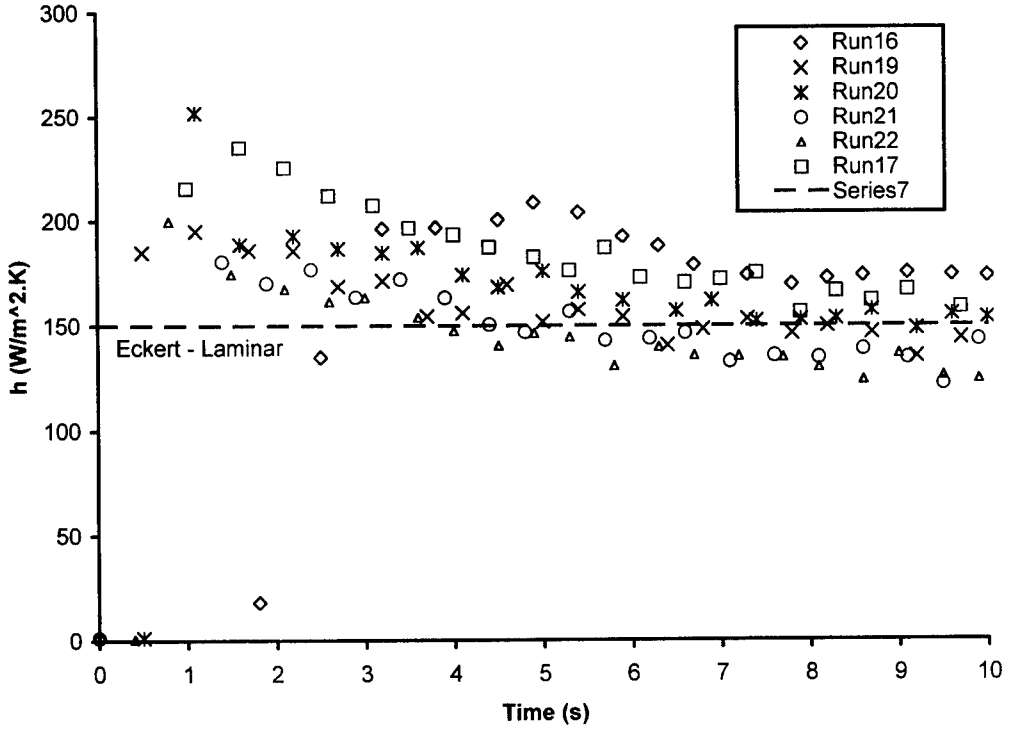

Figure 7a: Heat Transfer Coefficients Profiles

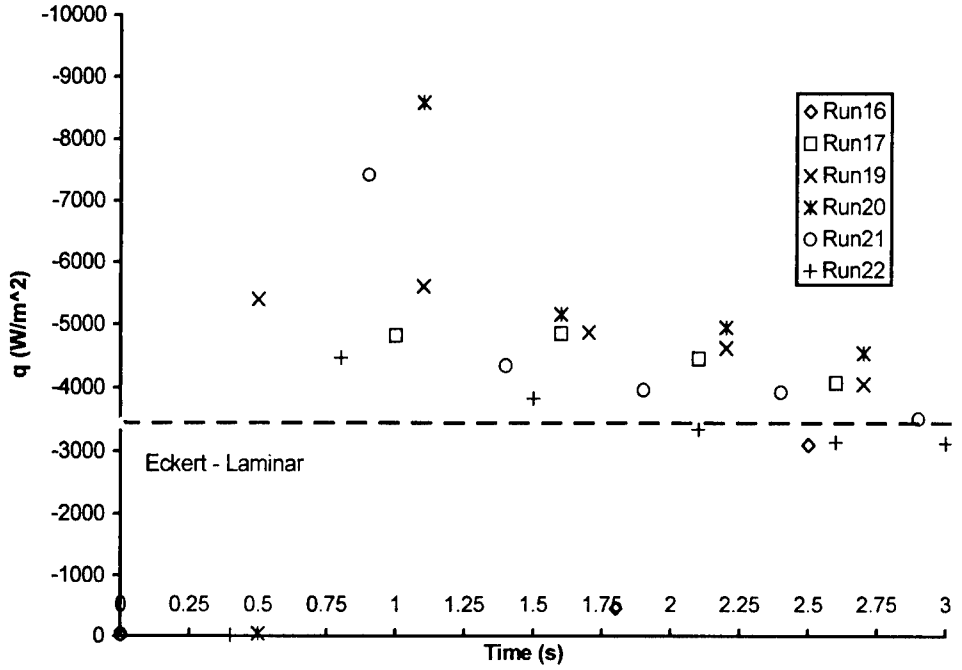

Figure 7b: Heat Flux Profiles

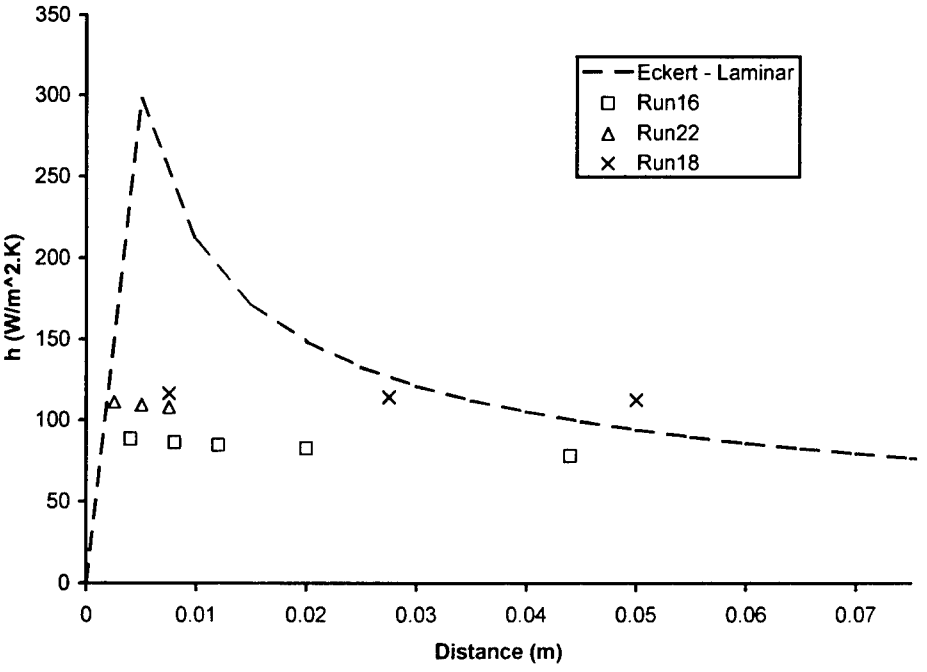

Figure 8: Comparison of Liquid Crystal Heat Transfer

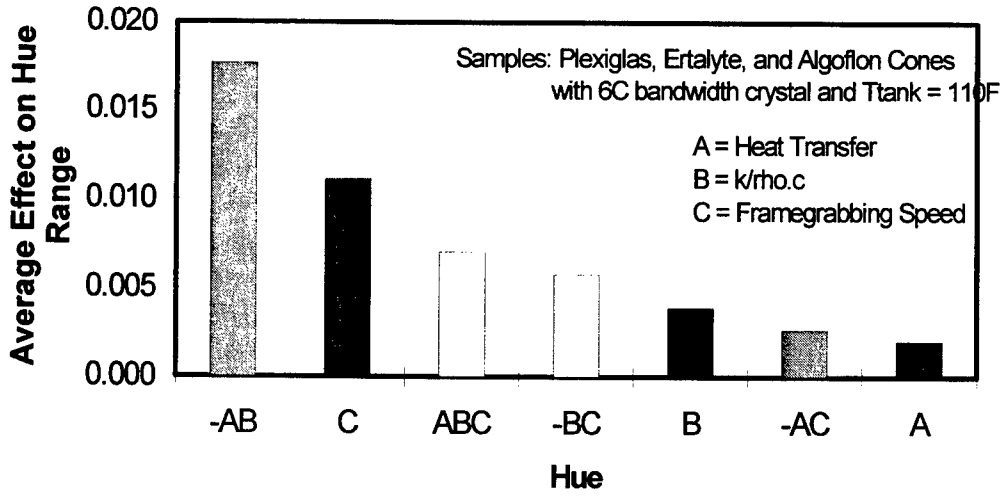

Figure 9: Relative Significance of Thermal Diffusivity and Heat Transfer (Ref. 2)

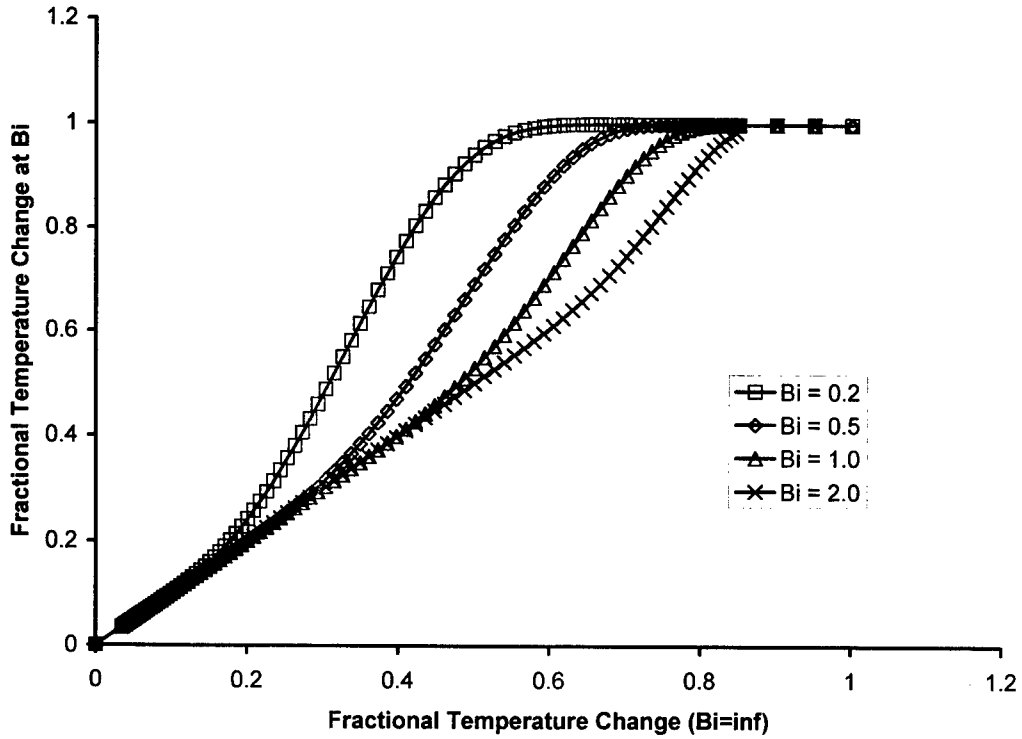

Figure 10: Accuracy of Infinite-Slab Approximation vs Biot Number

DEVELOPMENT OF JET ENGINE TEST FACILITY VIBRATION SIGNATURE AND DIAGNOSTIC SYSTEM

Sandra A. Ashford
Assistant Professor of Mechanical
Department of Mechanical Engineering

University of Detroit Mercy
4001 W. McNicholes Blvd.
P.O. Box 19900
Detroit, MI

Final Report for:
Summer Faculty Research Program
Tinker Air Force Base

Sponsored by:
Air Force Office of Scientific Research
Bolling Air Force Base, DC

and

Air Force Air Logistic Center
Tinker Air Force Base

August 1998

DEVELOPMENT OF JET ENGINE TEST FACILITY VIBRATION SIGNATURE AND DIAGNOSTIC SYSTEM

Sandra A. Ashford
Assistant Professor
Department of Mechanical Engineering
University of Detroit Mercy

Abstract

This report studies the applicability of using a personal computer to acquire vibration data during a jet engine test at the test cells of Tinker Air Force Base, and perform vibration signature analysis on that data. This study required that computer programs be written to perform both the data acquisition and the data analysis. The data acquisition was successfully completed, and the vibration analysis resulted in graphical output of vibration signatures produced by the vibration signature analysis package. The results proved that a personal computer can be used to both acquired and analyze jet engine vibration data.

DEVELOPMENT OF JET ENGINE TEST FACILITY

VIBRATION SIGNATURE AND DIAGNOSTIC SYSTEM

Sandra A. Ashford

Introduction

The Test Cells at the Oklahoma City Air Logistics Center of Tinker Air Force Base have been using the same vibration analysis system since 1980. This system produces vibration signatures which are used to the determine the type of maintenance needed before an engine such that it can be returned to service. The maintenance needed can range from a full overhaul, to a partial overhaul, to a trim balance. Knowledge that the vibration can be reduced by a trim balance rather than a full overhaul can produce a significant cost savings[1]. When an engine's vibration level excess the acceptable limits, a total rebuild occurs at a cost in excess of $10,000 per engine, unless it is determined that a partial rebuild or trim balance will eliminate the problem. Vibration signatures provide levels and trends at all rotor speeds, giving much more complete information than simply the maximum vibration level. Therefore, vibration signatures can isolate the vibration problem such that only the problem portion of an engine needs to be rebuilt.

The current vibration signature system was put in place in 1980 at a cost in excess of 10 million dollars.. The system has worked for nearly two decades, producing plots such as those shown in Appendix B, and reducing the maintenance costs of the TF30 and TF33 jet aircraft engines it analyzes. However, there are several problems with the current system. First, it can only perform vibration signatures on TF30 and TF33 engines, leaving no vibration signature analysis for the F101, F108 and F110 engines being overhauled at the Air Logistic Center. Second, this software can only be run on the system it was originally installed on, and cannot be downloaded to any other system or produce a hardcopy output of the software program. This system currently has an annual maintenance cost of over $7500 and requires over 500 sq. ft. of climate-controlled floor spaces. Additionally, maintenance of the system requires 3 to 4 hours of a test cell engineer's time per week. This computer system which was installed in the late 1970's

has capabilities less than that of a 386 Personal Computer. The computer system is difficult to run, and requires an additional test cell technician to run the vibration system. There is no long term computerized storage of the vibration signature data from the tested engines. This makes it impossible to analyze vibration trends for a particular engine throughout its service life.

Methodology

Vibration analysis systems have been successfully used to analyze jet engines and turbo machinery problems[2-6]. The recommendation was made to perform the vibration signature analysis on a personal computer. To accomplish this, all new computer software had to be written. This was a formidable task in that there was no written documentation about the underlying mathematical and relational equations used in the original software, and there was no way to access the original software code.

It was decided to write the new software using LABVIEW as the platform. LABVIEW, created by National Instruments, provides a graphic programming platform, and provides excellent compatibility with DAQ (Data Acquisition) cards which can be used to acquire the rotor speed and vibration probe data. LABVIEW has prewritten software to perform Fast Fourier Transforms (FFT) on the data and software to perform filtering on the data.

For this study, a "Bare Bones" vibration analysis package was written to determine the feasibility of this type of vibration data acquisition and analysis. Even a "Bare Bones" acquisition and analysis system required a substantial software development effort to acquire data, run signature analysis, produce output, and produce plots. The computer programs (called VI's referring to the LABVIEW Virtual Instrument platform they were created on) are listed in Appendix A. This includes programs to acquire steady-state data which continually update the graphic output of the voltage data being received by the data acquisition card inside the PC. The voltage data, acquired by the DAQ (Data Acquisition) card, consists of the measurement of the two rotor speeds and the three vibration probe measurements. The

frequency of data acquisition and number of data points to be acquired is an input to the VI, and can be changed by pushing the virtual buttons on the PC computer screen. A virtual button push starts the data acquisition which continues until all the required data is taken. Subsequent button pushes will continue to acquire additional steady state vibration data sets.

At the conclusion of the test, the raw voltage data is stored in files to be analyzed post-test. The post-test analysis is done with the same computer and takes no more than one to two minutes. Graphic output of the vibration data is viewed on-screen and also can be imported into excel files for hard copy graphic output. The graphic output produced from the results of this analysis is shown in Figures 1-3.

The acceleration and deceleration acquisition and analysis programs are completely separate programs from the steady state acquisition programs. The frequency and number of data points per data set is input into the VI with button clicks, as with the steady-state acquisition program. Once the virtual "Start Test" button has been pushed, the program continues to acquire data sets during the acceleration run until the "Stop Test" virtual button has been pushed. The graphics window continually shows the voltage data being recorded by the data acquisition system. Once again, the raw voltage data is stored and analyzed post test with an additional analysis program. The acceleration data analysis package produces on-screen graphic output of Max. Peak-to-Peak, Max. FFT, Composite FFT, and Synchronous Vibration at each rotor speed. The post-test acceleration analysis program produced output required for the plots shown in Figures 4-24. The 3-D vibration plots shown in Figures 18-24 give the engineer a better feel for the frequency of the problem vibration and how these vibration problems change with wheel speed. This type of output was not available with the previous system

Conclusions and Recommendations

The objective of this work was to determine the suitability of using a personal computer to perform vibration data acquisition and analysis for test engine tests performed in the test cells of Tinker Air Force Base. This has been accomplished, and it was determined that a PC can be used to adequately

acquire and analyze vibration signature data. However, this work has just begun, and the programs written for this project are in further need of development. The accuracy of the analysis needs further development, as well as the implementation of filtering and anti-alising to the system. More automation of the system is necessary to make the system easier to use. A method needs to be put into place to store the signature data as well as the results of the maintenance performed. Additionally, a method needs to be put in place to interpret the vibration signature data to determine the specific type of problem found during an overhaul, or the specific type of trim balance performed in an automated fashion. This way, for example, if during an overhaul a rotor was found to be cracked, the vibration signature produced by this problem would be known, and future engines having the same problem would be known before the overhaul takes place. This type of analysis is currently done exclusively from the experience of an engineer working in the test cells for well over a decade.

References:

1) Walker, G., "Slow-Speed Balancing of a 310 MW LP Turbine Saves $250,000," *Shock and Vibration Digest*, Vol. 28, No. 6, PP. 8-10, Nov. 1996

2) Hanna, R.L., *Introduction of Spectral Analysis Techniques into a Turbomachinery Vibration Troubleshooting System*, Thesis, North Carolina State University, 1996

3) Allwood, R.J., and Christy, P.I. "Vibration Analysis of Gas Turbines by an Intelligent Knowledge-Based System," *Journal of Aerospace Engineering*, 1991

4) Segal, A., and Bogorad, E. "Gas Turbine Diagnosis by Means of Noise and Vibration Measurement and Analysis," Proceedings of Inter-Noise, Newport Beach, CA, July 10-12, 1995

5) Schuster, S.A., and Jurgeleit, W., "Real-Time Signal Processing for a Jet Engine Vibration Test System," Journal of Sound and Vibration, Vol. 28, No. 1, Jan. 1994

6) Hayashida, R.D., Motter, J., and McDole, K., " Turbomachinery Monitoring Systems Capture and Analyze Vibration Data," IEEE Computer Applications in Power, July, 1991

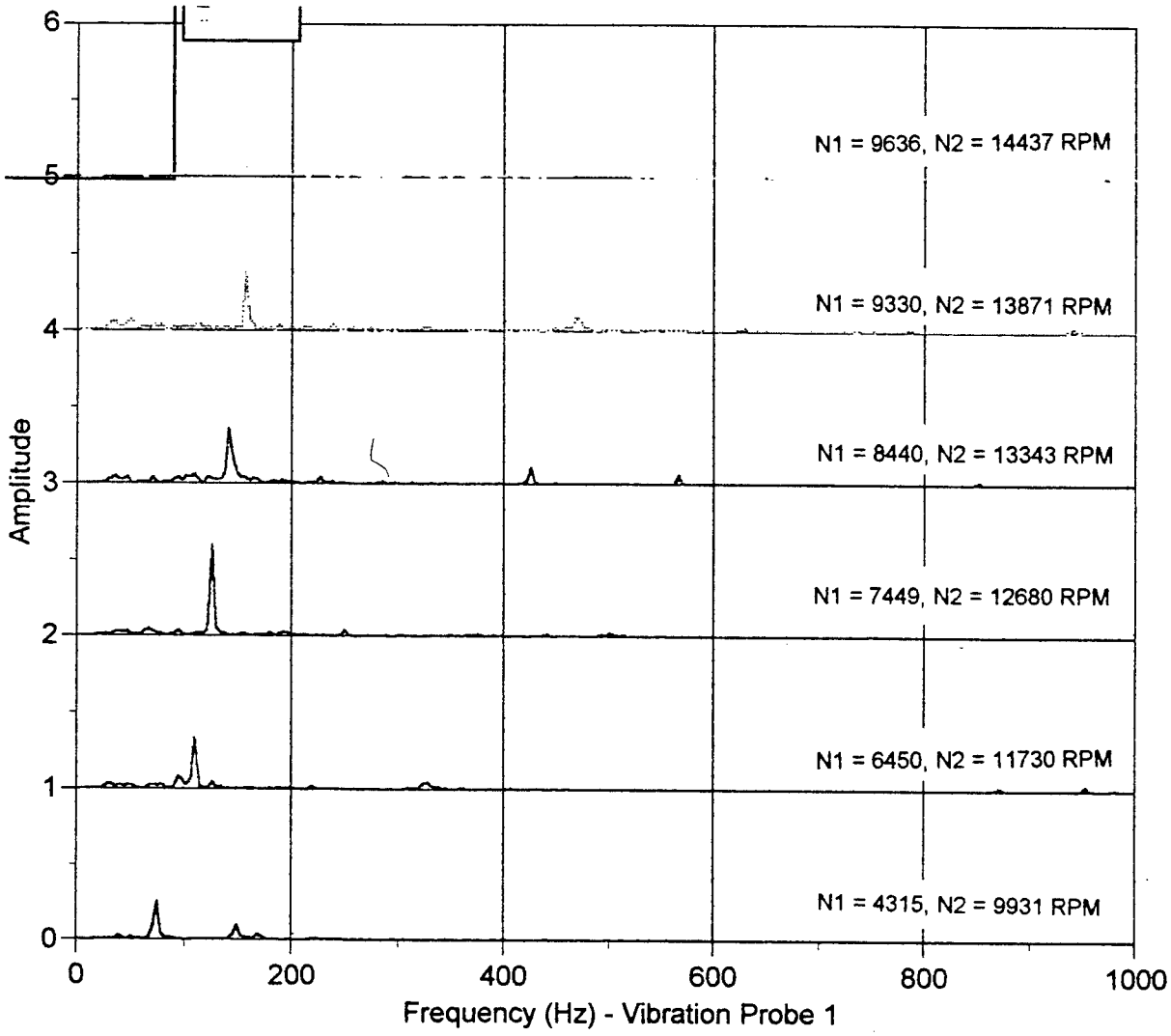
N1 = 9636, N2 = 14437 RPM
N1 = 9330, N2 = 13871 RPM
N1 = 8440, N2 = 13343 RPM
N1 = 7449, N2 = 12680 RPM
N1 = 6450, N2 = 11730 RPM
N1 = 4315, N2 = 9931 RPM
Amplitude
0
1
2
3
4
5
6
0
200
400
600
800
1000
Frequency (Hz) - Vibration Probe 1

Figure 1.

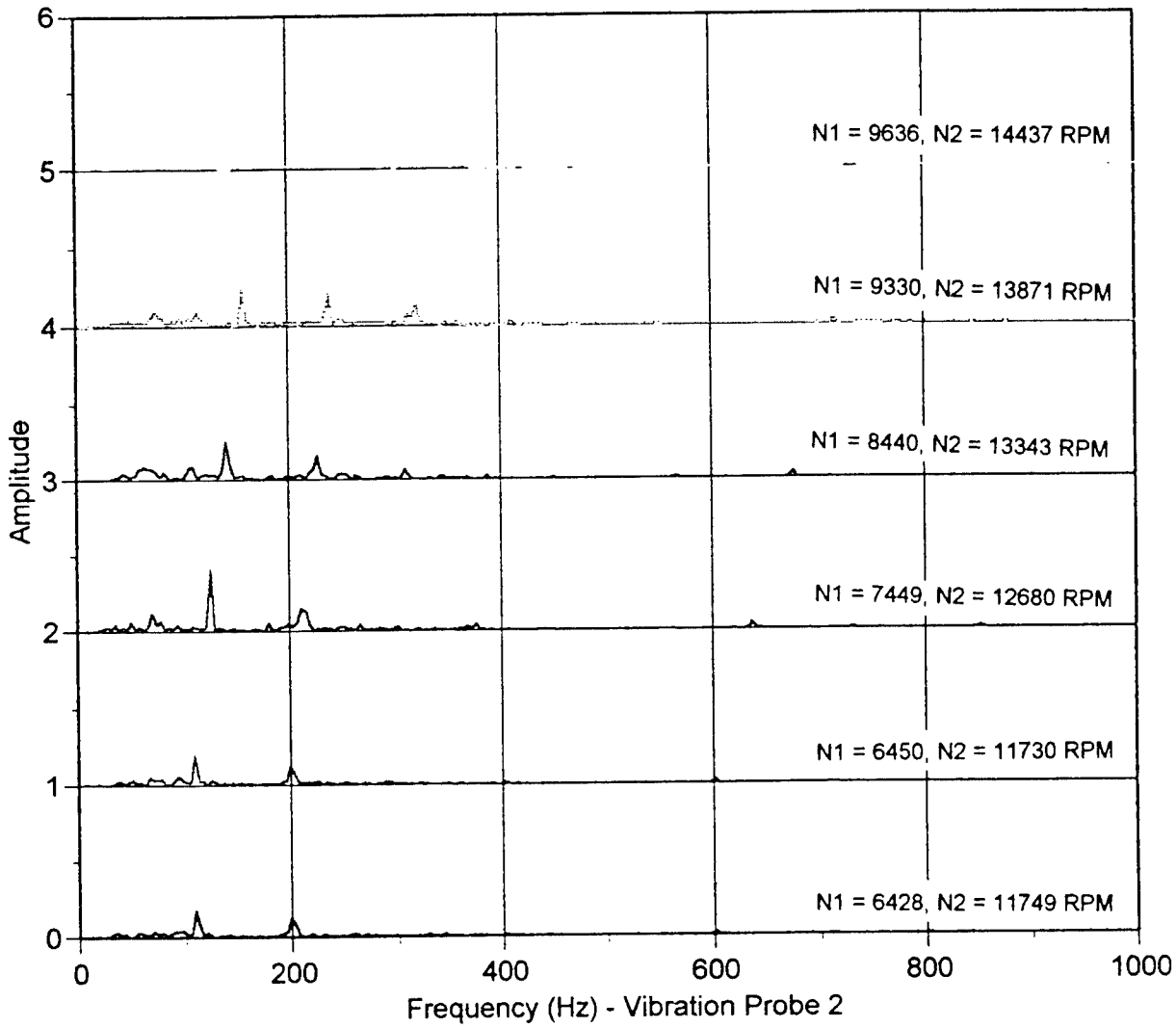
6
5
4
3
2
1
0
Amplitude
N1 = 9636, N2 = 14437 RPM
N1 = 9330, N2 = 13871 RPM
N1 = 8440, N2 = 13343 RPM
N1 = 7449, N2 = 12680 RPM
N1 = 6450, N2 = 11730 RPM
N1 = 6428, N2 = 11749 RPM
0
200
400
600
800
1000
Frequency (Hz) - Vibration Probe 2

Figure 2.

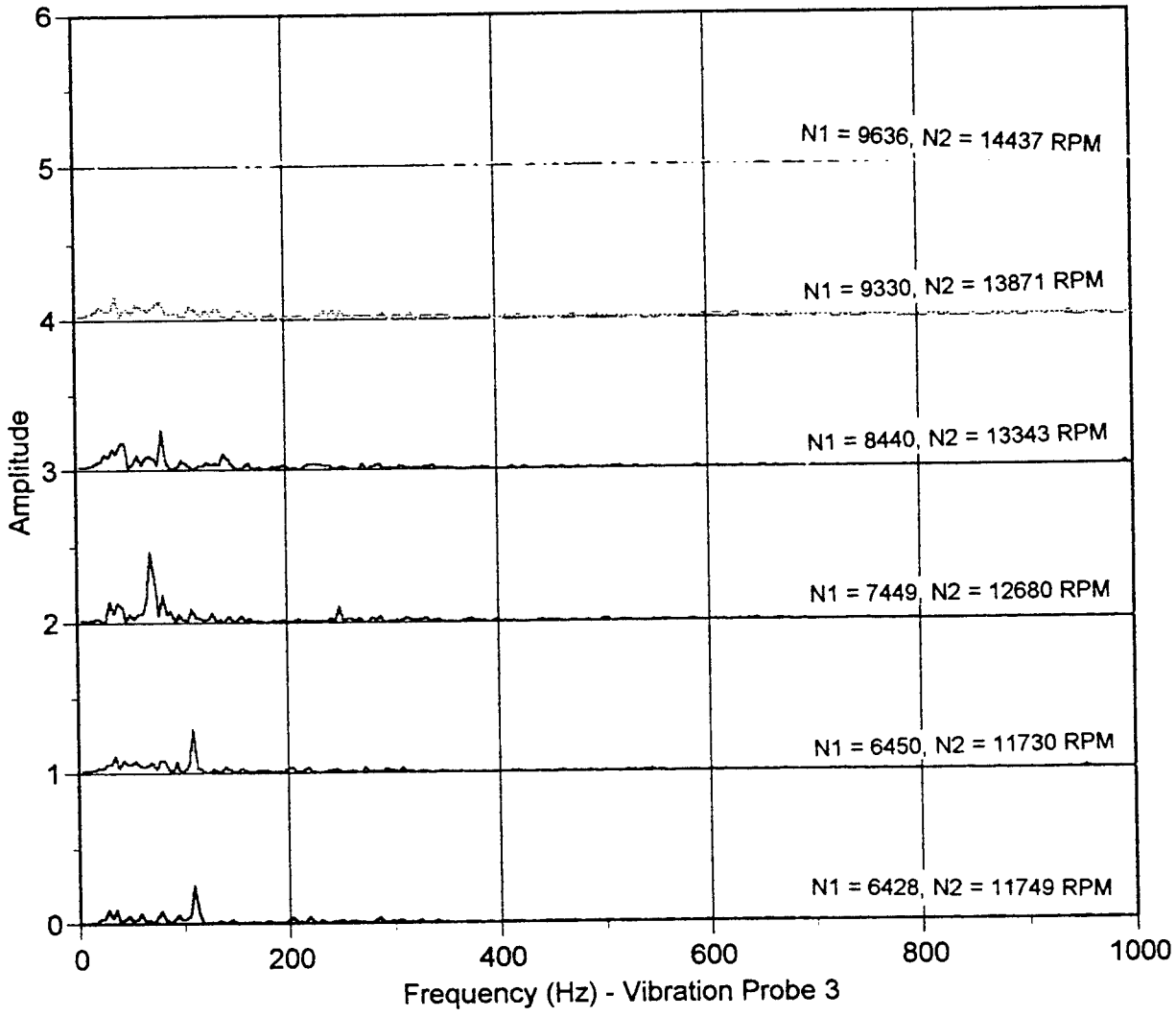
N1 = 9636, N2 = 14437 RPM
N1 = 9330, N2 = 13871 RPM
N1 = 8440, N2 = 13343 RPM
N1 = 7449, N2 = 12680 RPM
N1 = 6450, N2 = 11730 RPM
N1 = 6428, N2 = 11749 RPM
Amplitude
0
1
2
3
4
5
6
0
200
400
600
800
1000
Frequency (Hz) - Vibration Probe 3

Figure 3.

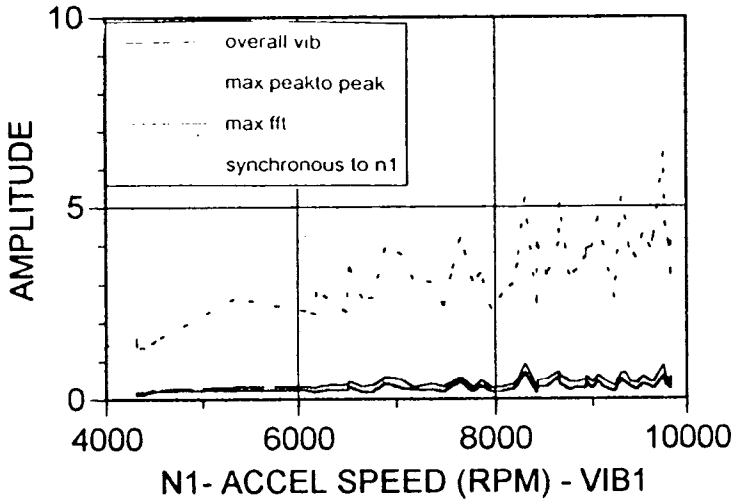

Figure 4.

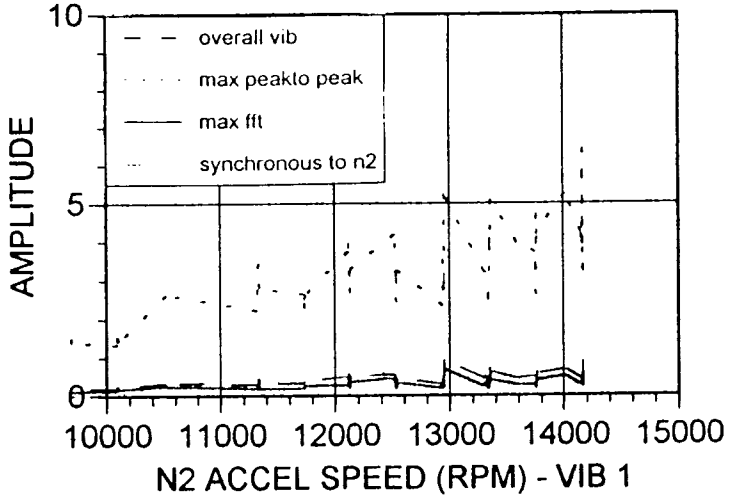

Figure 5.

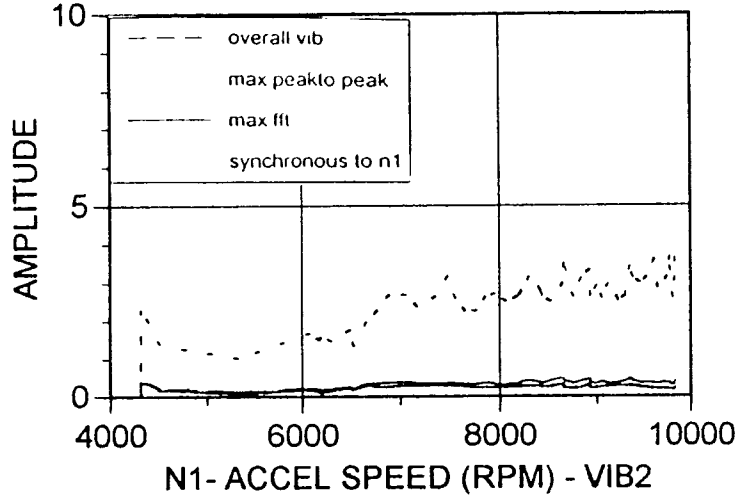

Figure 6.

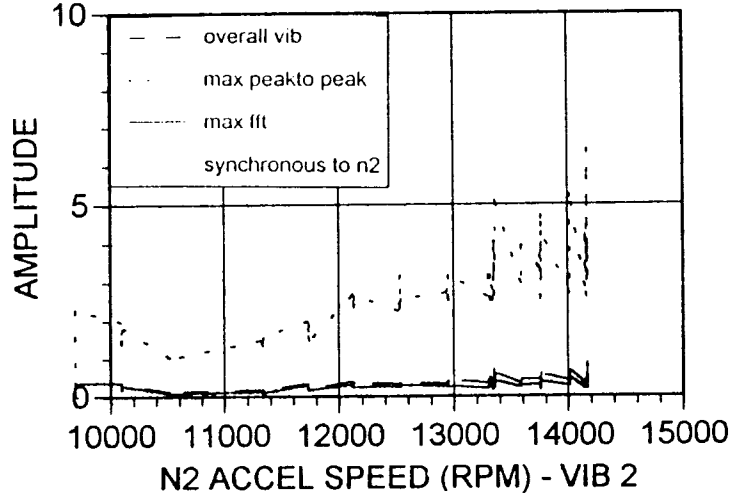

Figure 7.

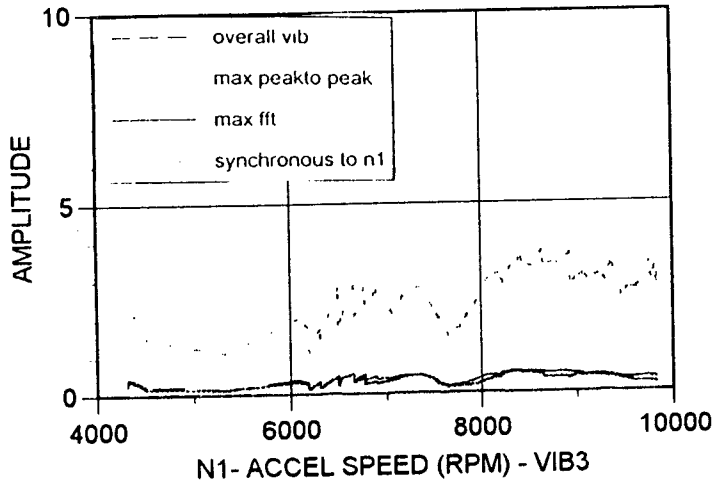

Figure 8

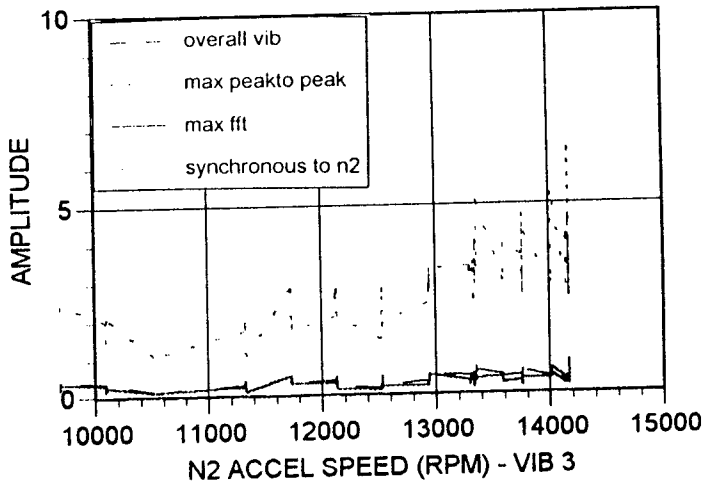

Figure 9

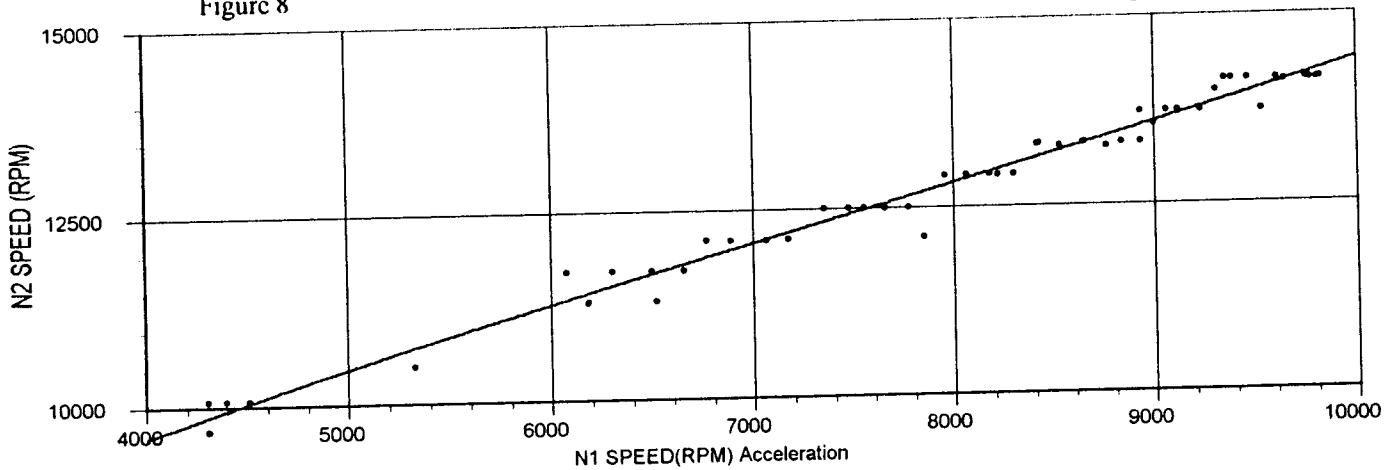

Figure 10

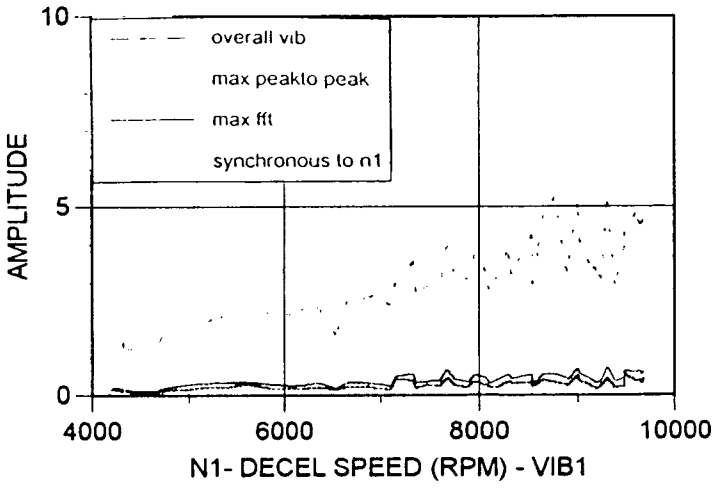

Figure 11

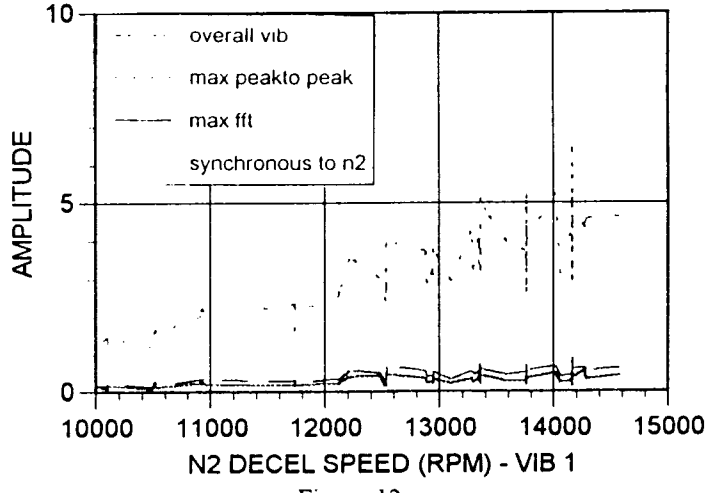

Figure 12

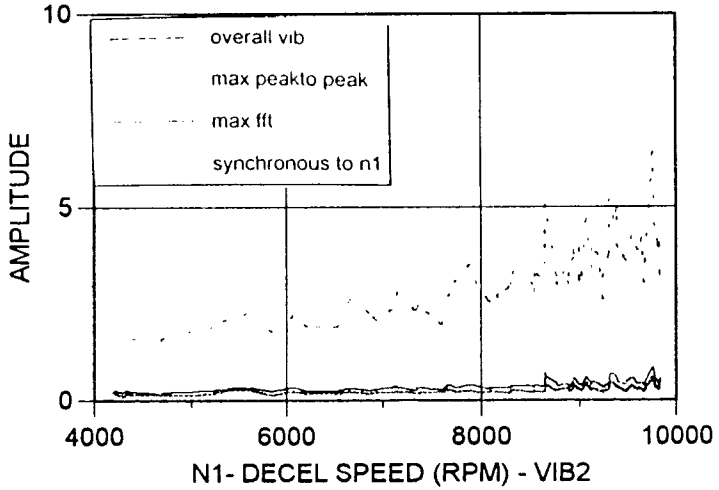

Figure 13

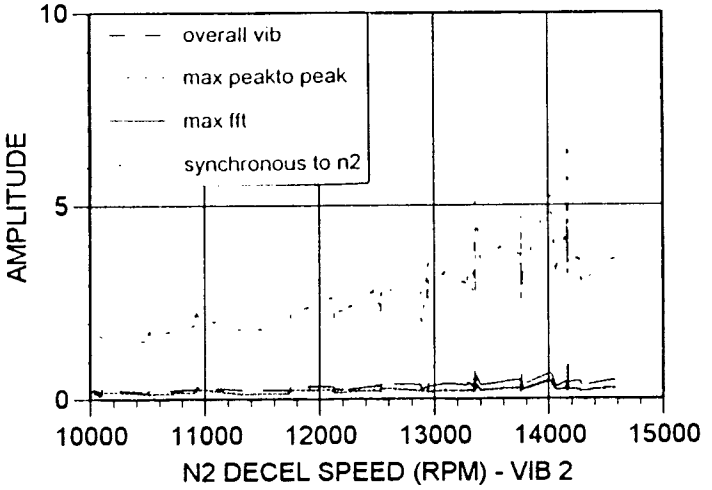

Figure 14

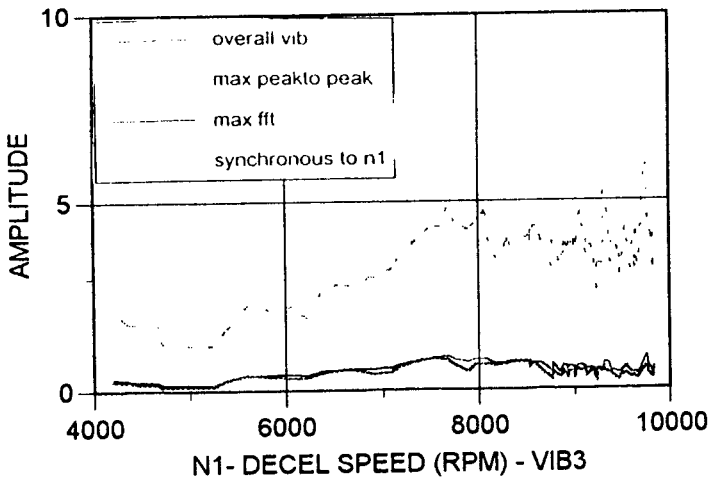

Figure 15

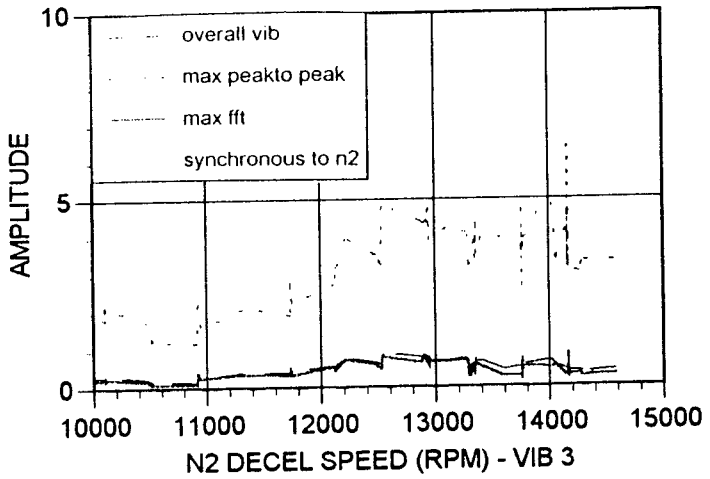

Figure 16

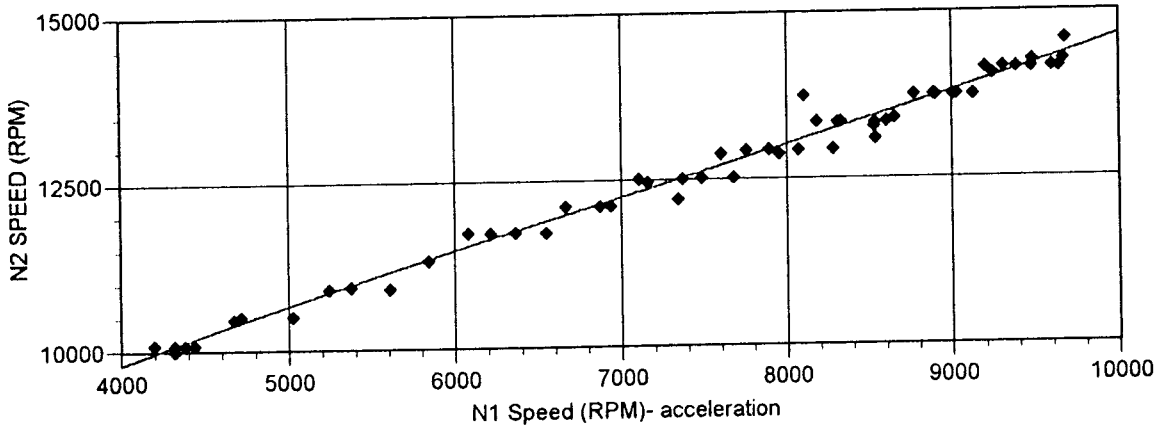

Figure17

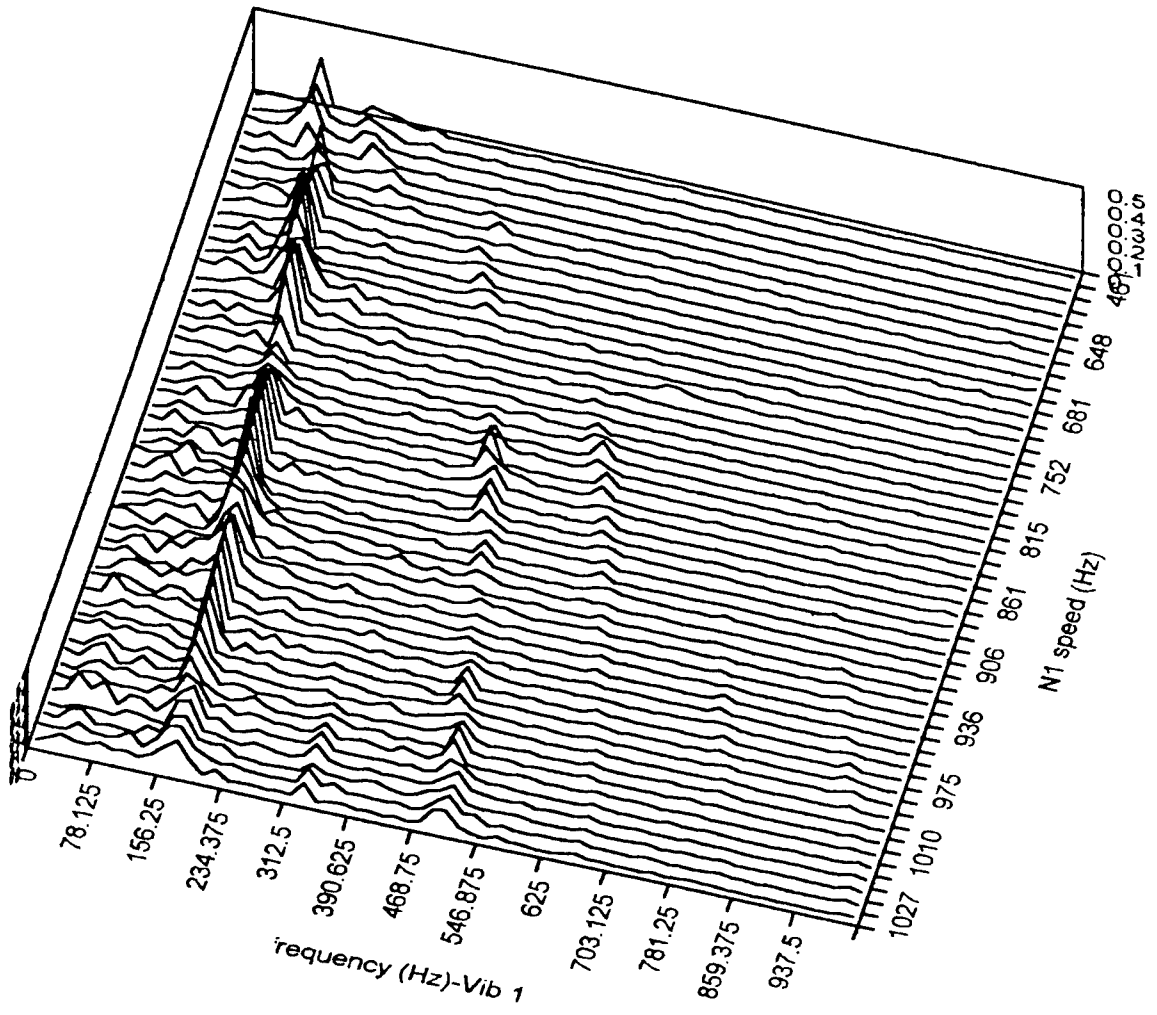

Vibration Probe No. 1 Amplitude During Acceleration
Figure 18.

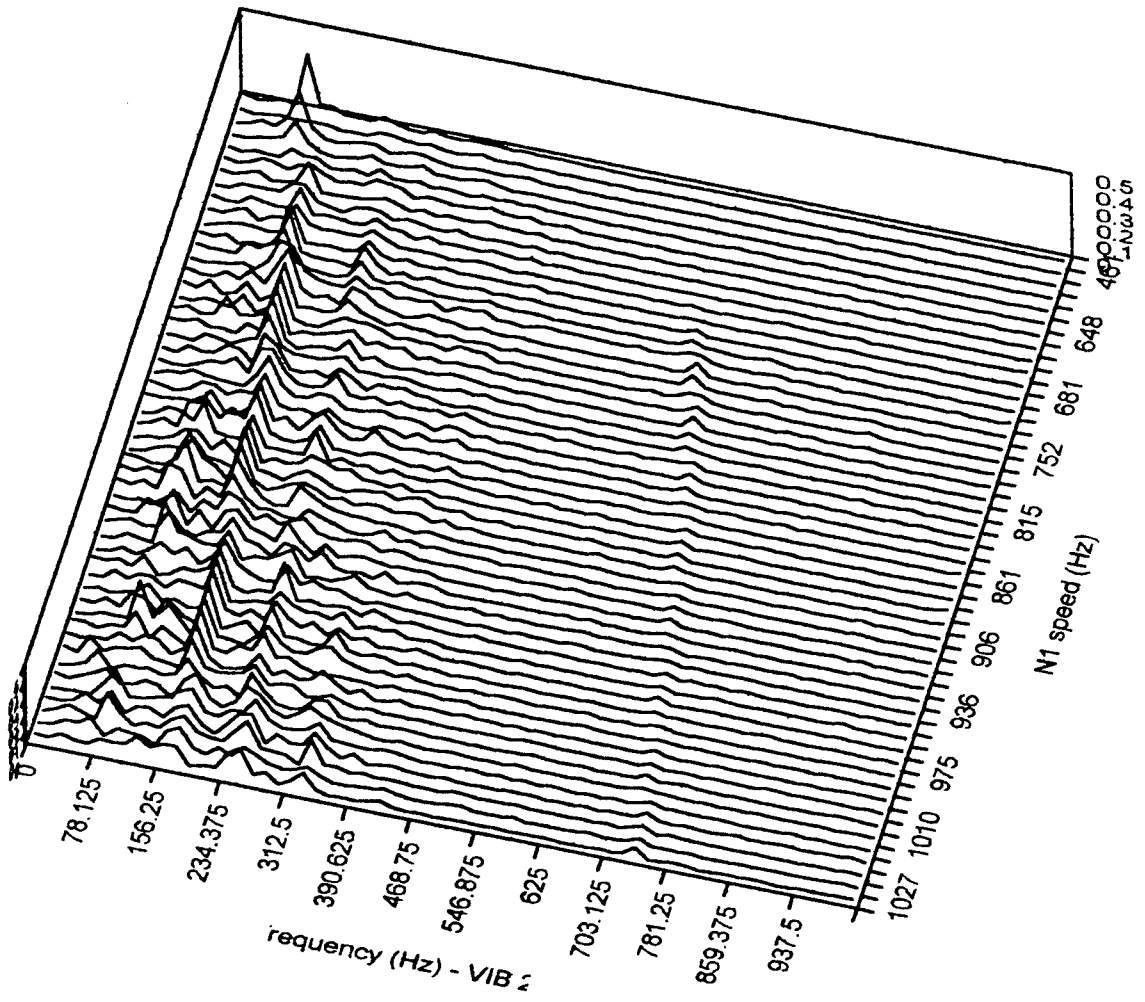

Vibration Probe No. 2 Amplitude During Acceleration
Figure 19.

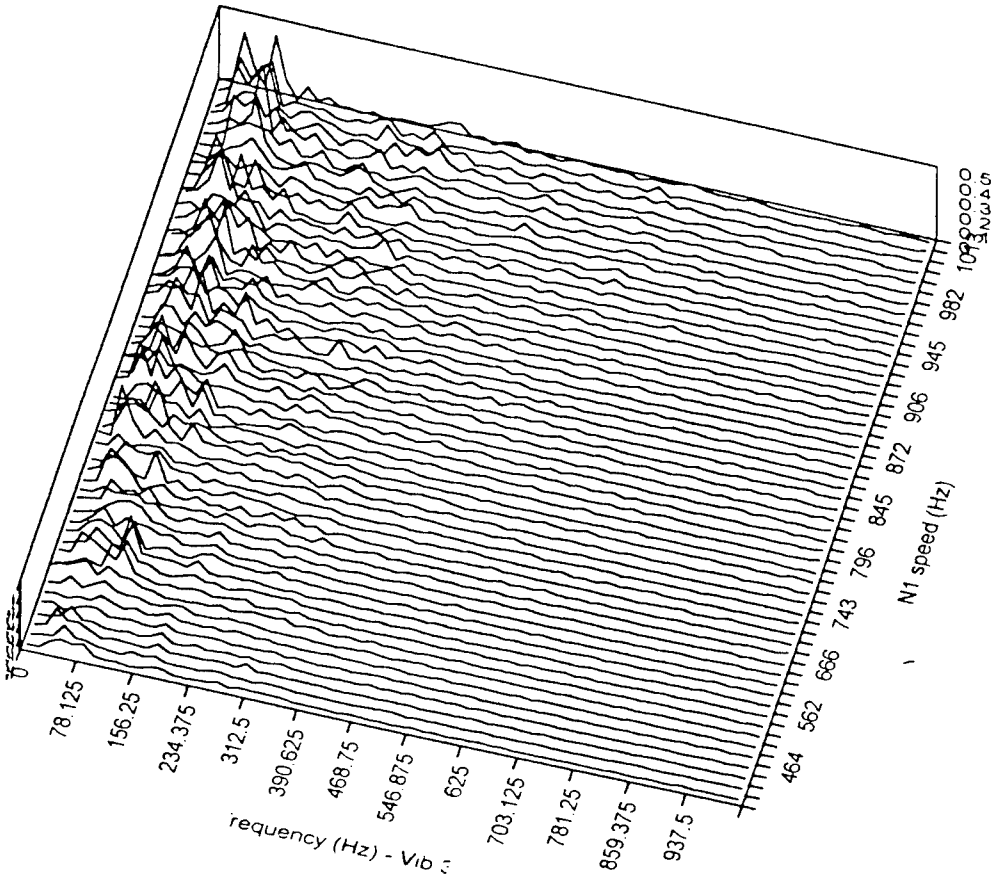

Vibration Probe No. 3 Amplitude During Acceleration
Figure 20.

Appendix A
Software Descriptions

Programs to analyze Acceleration and Deceleration Data:

The VI "**Acquire Acceleration Data**" will acquire acceleration data continuously until the "test complete" button is pushed. The rate at which data is acquired, and number of data points per each acceleration speed is input. The program records the voltage for both wheel speeds, and the vibration probes number one, two, and three.

The VI "**Get Accel From Disk And Put Back To Excel**" - this programs takes the acceleration or deceleration data which was stored to excel after running the test and performs an fft on the data, creates charts of max peak-to-peak for each engine speed and max. fft at each engine speed, and plots this data for each of the vibration probes. It also plots out the n1 vs. n2 engine speed. The plots can be viewed within labview, or the data will be sent back to excel such that hard copies of the data can be made.

The excel files which are produced and put into directory **c:/testdata/output/** are:

ACFFTV1- the data scan index, n1 speed, n2 speed, frequency, and fft for each frequency of vibration probe number 1. This data can be used to create a 3-D Zmod plot of fft vs. n1 and frequency.

ACFFTV2- the data scan index, n1 speed, n2 speed, frequency, and fft for each frequency of vibration probe number 2. This data can be used to create a 3-D Zmod plot of fft vs. n1 and frequency.

ACFFTV3- the data scan index, n1 speed, n2 speed, frequency, and fft for each frequency of vibration probe number 3. This data can be used to create a 3-D Zmod plot of fft vs. n1 and frequency.

ACMAXV1- gives n1, n2, overall vibration, max fft, max amplitude, and synchronous vibration for vibration probe number one. These can be used to produce the 2-D plots currently given by AVID.

ACMAXV2- gives n1, n2, overall vibration, max fft, max amplitude, and synchronous vibration for vibration probe number two. These can be used to produce the 2-D plots currently given by AVID.

ACMAXV3- gives n1, n2, overall vibration, max fft, max amplitude, and synchronous vibration for vibration probe number three. These can be used to produce the 2-D plots currently given by AVID.

note: these files should be deleted before running the program again, as new data will be continually put into the same files.

The program "**Create 3d accel plots**" can be run after the program "**Get Accel From Disk And Put Back To Excel**" to create the excel files necessary for the 3-D acceleration and decelleration plots. The excel plot files produced are put into the directory **c:\testdata\output\accel**

v1_fft.xls - produces a table of fft values for vibration probe 1. The first row of data contains the n1 speeds (in Hz), and the first colum of data contains the vibration frequency. The data in the table is the fft amplitude data for vibration probe 1 corresponding to the vibration frequency listed in colum 1 and the n1 speed (Hz) listed in row 1.

v2_fft.xls - produces a table of fft values for vibration probe 2. The first row of data contains the n1 speeds (in Hz), and the first colum of data contains the vibration frequency. The data in the table is the fft amplitude data for vibration probe 2 corresponding to the vibration frequency listed in colum 1 and the n1 speed (Hz) listed in row 1.

v3_fft.xls - produces a table of fft values for vibration probe 3. The first row of data contains the n1 speeds (in Hz), and the first colum of data contains the vibration frequency. The data in the table is the fft amplitude data for vibration probe 3 corresponding to the vibration frequency listed in colum 1 and the n1 speed (Hz) listed in row 1.

v1n2fft.xls - produces a table of fft values for vibration probe 1. The first row of data contains the n2 speeds (in Hz), and the first colum of data contains the vibration frequency. The data in the table is the fft amplitude data for vibration probe 1 corresponding to the vibration frequency listed in colum 1 and the n1 speed (Hz) listed in row 1.

v2n2fft.xls - produces a table of fft values for vibration probe 2. The first row of data contains the n2 speeds (in Hz), and the first colum of data contains the vibration frequency. The data in the table is the fft amplitude data for vibration probe 2 corresponding to the vibration frequency listed in colum 1 and the n1 speed (Hz) listed in row 1.

v3n2fft.xls - produces a table of fft values for vibration probe 3. The first row of data contains the n2 speeds (in Hz), and the first colum of data contains the vibration frequency. The data in the table is the fft amplitude data for vibration probe 3 corresponding to the vibration frequency listed in colum 1 and the n1 speed (Hz) listed in row 1.

Programs which analyze steady-state data:

The vi **New Aquire Steady State** aquires the steady-state data. This vi will aquire as many steady state signatures as necessary. At the start of each steady state signature, push the "Aquire 1" button. The vi will then aquire the the specified number of data points as the specified rate and input them into the file c:\testdata\output\ss#.xls, where # stands for the index of the steady state scan. (Note, these specifications are to be input on the form before the test begins). An output of the n1 and n2 speeds, in volts, as well the the vibration probes are shown as output while the test is running. Each steady state speed data will be put in a different file, numbered from 1 to 9. At the end of the test, the "stop, test over" button pushed will end the vi from waiting for the next test data.

The vi **Put all ss data into one excel file** gets the steady-state data from all steady state speeds and calculates the fft and the max fft and sends it to an excel file for plotting.

The excel files which are produced and put into directory **c:/testdata/output/** are:

fftv1.xls - prints out frequency, speed index, fft, n1 and n2 for vibration probe number 1.

fftv2.xls - prints out frequency, speed index, fft, n1 and n2 for vibration probe number 2.

fftv3.xls - prints out frequency, speed index, fft, n1 and n2 for vibration probe number 3.

v1fft.xls - prints out frequency in the first row, then on the following rows it prints the ftt's for vibration probe number 1 at these frequencies for each of the speeds at which steady-state data was taken.

v2fft.xls - prints out frequency in the first row, then on the following rows it prints the ftt's for vibration probe number 2 at these frequencies for each of the speeds at which steady-state data was taken

v3fft.xls - prints out frequency in the first row, then on the following rows it prints the ftt's for vibration probe number 3 at these frequencies for each of the speeds at which steady-state data was taken

The vi **Get ss from disk** gets the steady-state data for all speeds taken, and plots the fft's graphically on the screen for four steady-state speeds at all 3 vibration probes.

The vi **Get ss from disk for one speed** calculates and plots the fft for one speed, and the fft and frequency at the 6 highest fft's.

Appendix B
AVID Output

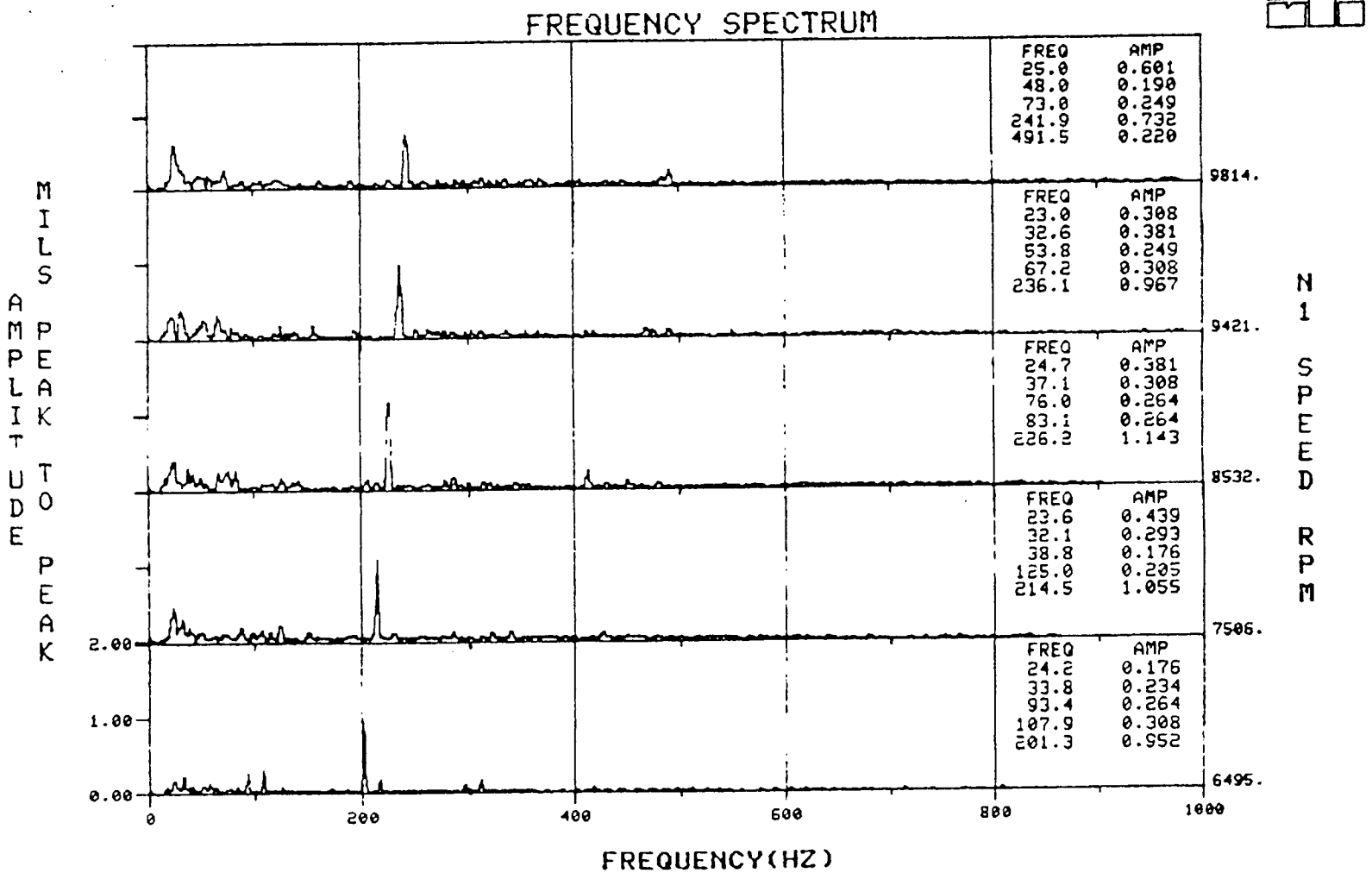

PROBE NUMBER	U3	DATE/TIME	260397 0917
ENGINE TYPE	TF30P9	N2 SPEED RPM	12123. 12813.
ENG SERIAL NO	676618		13510. 14139.
TEST CELL	01		14527. 0.

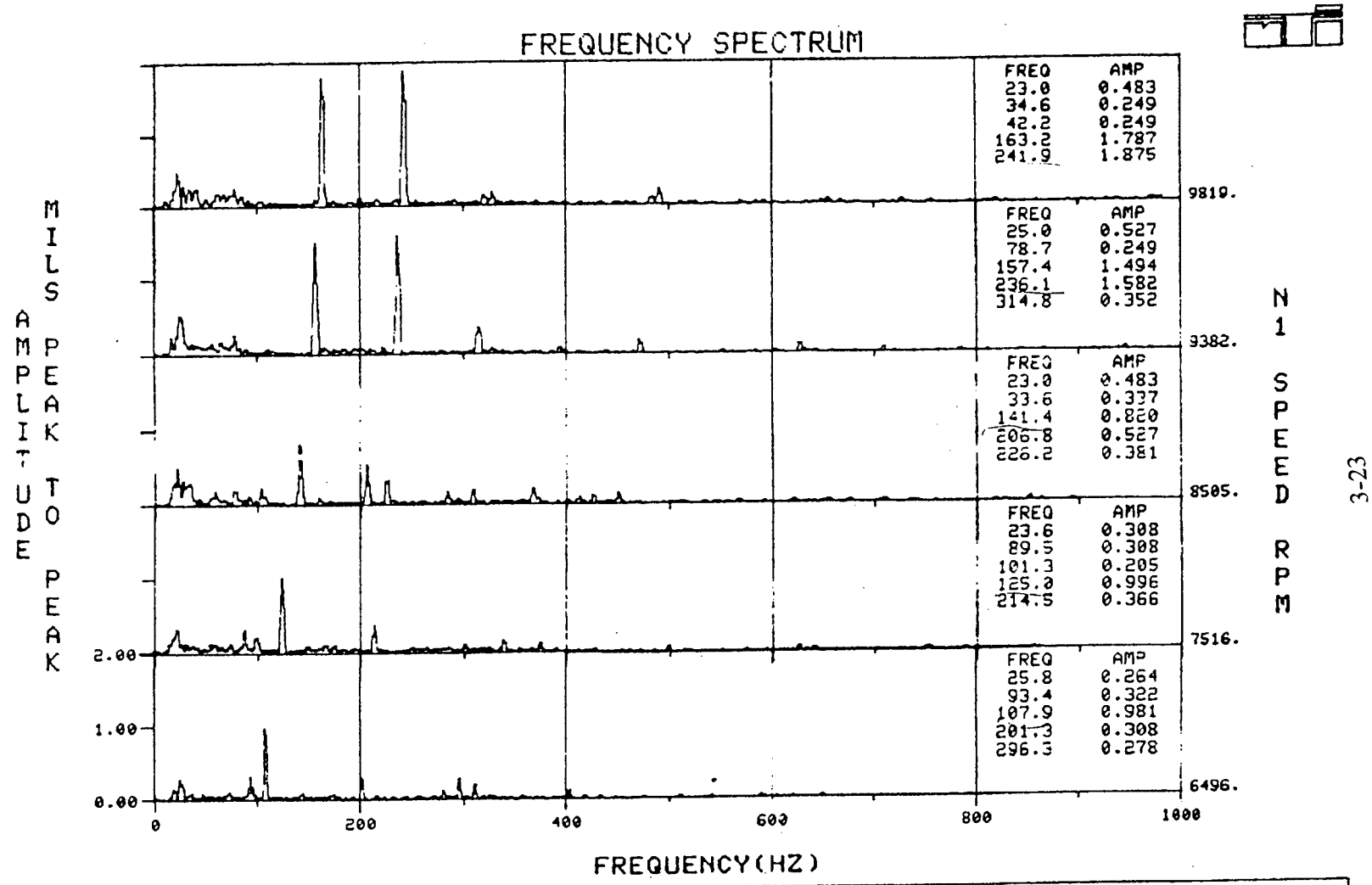

PROBE NUMBER	01	DATE/TIME	260397 0917
ENGINE TYPE	TF30P9	N2 SPEED RPM	12078. 12817.
ENG SERIAL NO	676618		13460. 14145.
TEST CELL	01		14518. 0.

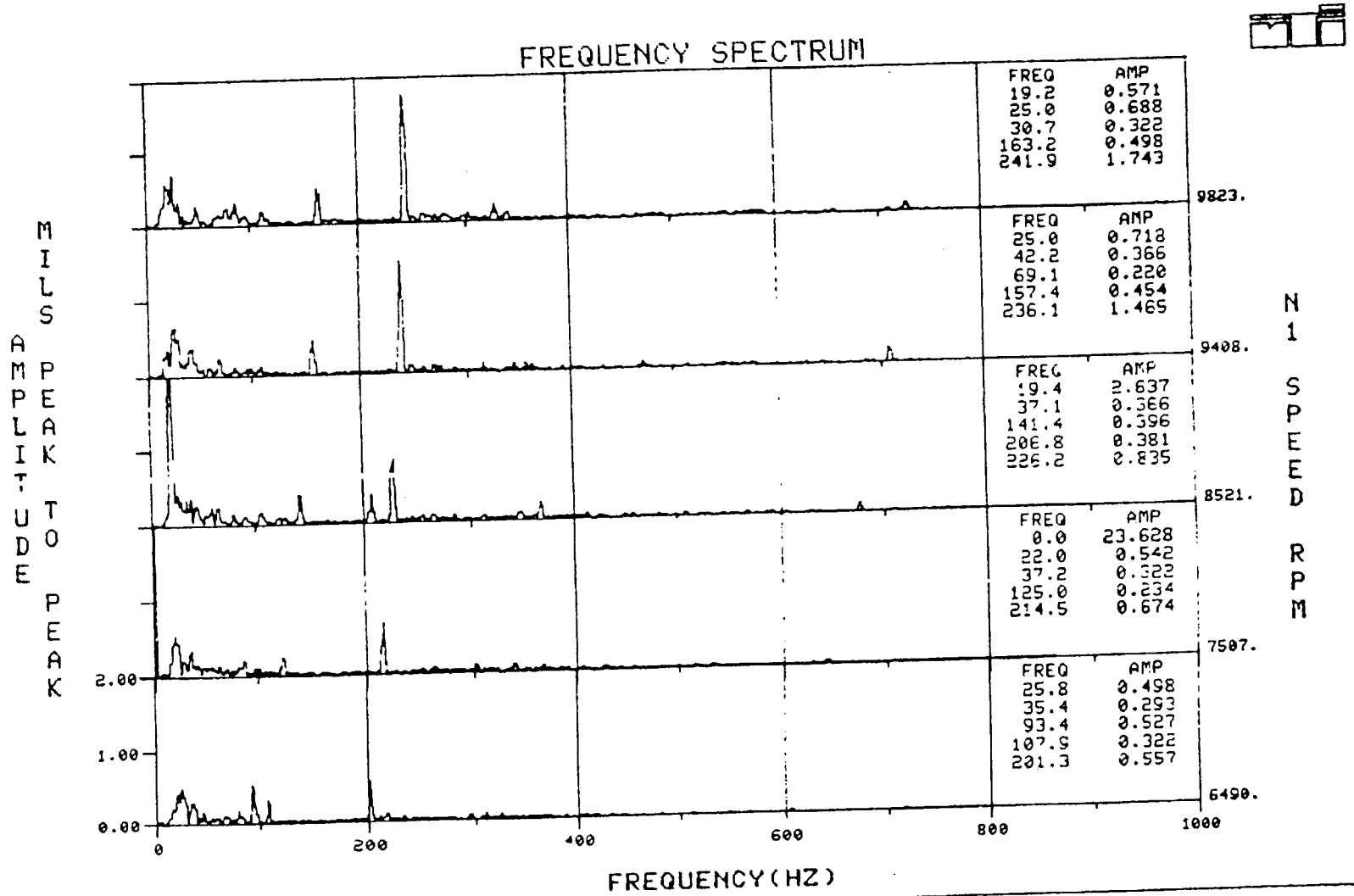

PROBE NUMBER	U2	DATE/TIME	260397 0917
ENGINE TYPE	TF30P9	N2 SPEED RPM	12057. 12851.
ENG SERIAL NO	676618		13494. 14147.
TEST CELL	01		14516. 0.

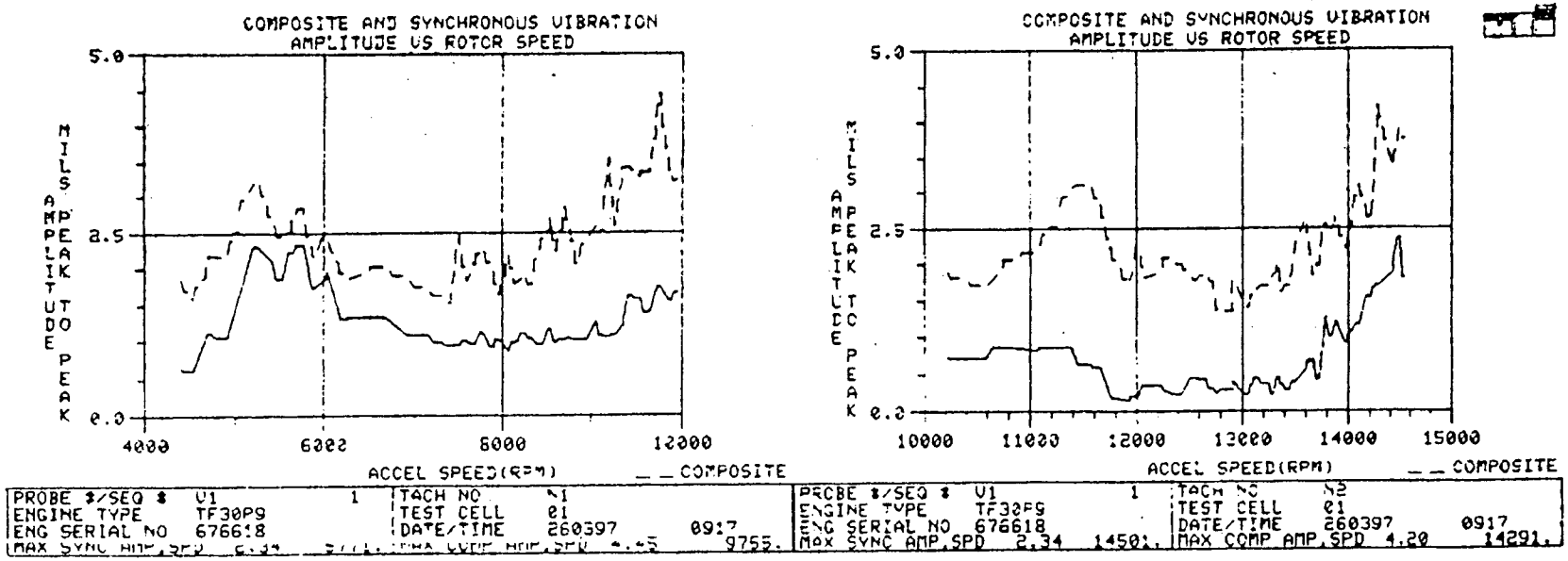
COMPOSITE AND SYNCHRONOUS VIBRATION
AMPLITUDE VS ROTOR SPEED
MILS PEAK AMPLITUDE
5.0
2.5
0.0
4000
6000
8000
10000
ACCEL SPEED(RPM)
COMPOSITE
PROBE #/SEQ # V1 1
ENGINE TYPE TF30P9
ENG SERIAL NO 676618
TACH NO N1
TEST CELL 01
DATE/TIME 260397 0917
MAX SYNC AMP,SPD 2.34 1450.
MAX COMP AMP,SPD 4.20 9755.
COMPOSITE AND SYNCHRONOUS VIBRATION
AMPLITUDE VS ROTOR SPEED
MILS PEAK AMPLITUDE
5.0
2.5
0.0
10000
11000
12000
13000
14000
15000
ACCEL SPEED(RPM)
COMPOSITE
PROBE #/SEQ # V1 1
ENGINE TYPE TF30P9
ENG SERIAL NO 676618
TACH NO N2
TEST CELL 01
DATE/TIME 260397 0917
MAX SYNC AMP,SPD 2.34 14501.
MAX COMP AMP,SPD 4.20 14291.

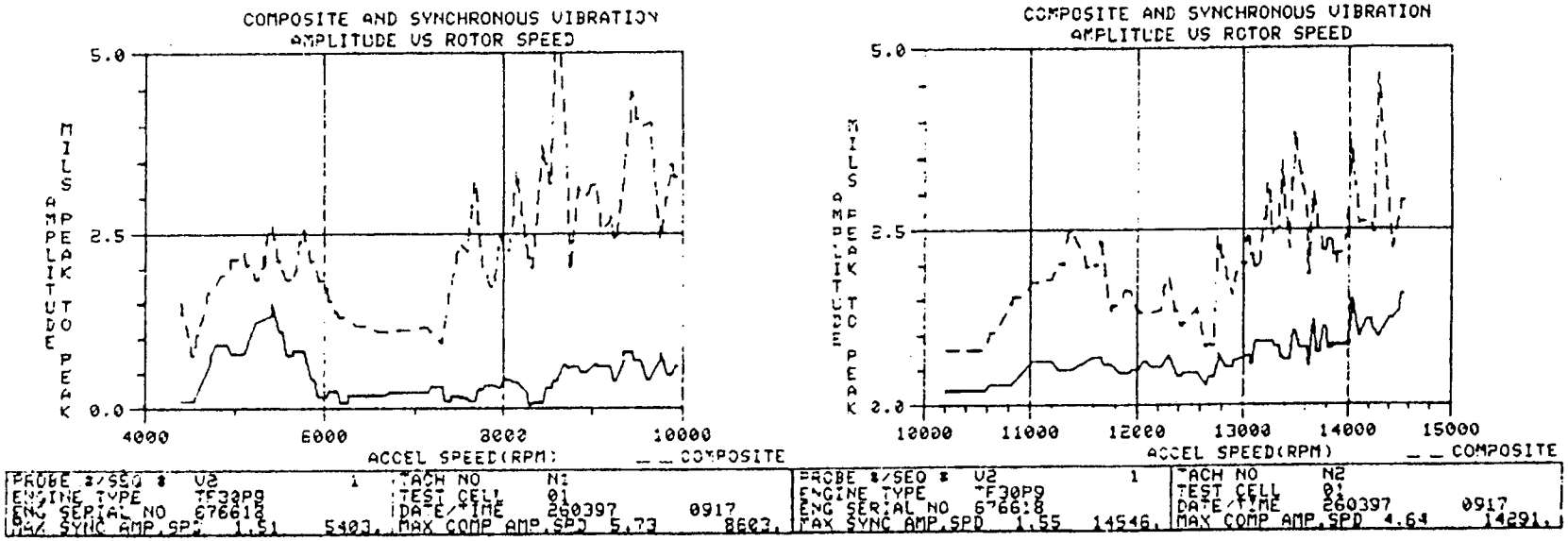
COMPOSITE AND SYNCHRONOUS VIBRATION
AMPLITUDE VS ROTOR SPEED
MILS PEAK AMPLITUDE
5.0
2.5
0.0
4000
6000
8000
10000
ACCEL SPEED(RPM)
COMPOSITE
PROBE #/SEQ # V2 1
ENGINE TYPE TF30P9
ENG SERIAL NO 676618
TACH NO N1
TEST CELL 01
DATE/TIME 260397 0917
MAX SYNC AMP,SPD 1.51 5403.
MAX COMP AMP,SPD 5.73 8603.
COMPOSITE AND SYNCHRONOUS VIBRATION
AMPLITUDE VS ROTOR SPEED
MILS PEAK AMPLITUDE
5.0
2.5
0.0
10000
11000
12000
13000
14000
15000
ACCEL SPEED(RPM)
COMPOSITE
PROBE #/SEQ # V2 1
ENGINE TYPE TF30P9
ENG SERIAL NO 676618
TACH NO N2
TEST CELL 01
DATE/TIME 260397 0917
MAX SYNC AMP,SPD 1.55 14546.
MAX COMP AMP,SPD 4.64 14291.

TACHOMETER
N1 SPEED(RPM)
N2 SPEED(RPM)
PROBE NUMBER
ENG SERIAL NO
SEQUENCE NO
TEST CELL
DATA TYPE
DATE/TIME
ACCELERATION
COMPOSITE AND SYNCHRONOUS VIBRATION
AMPLITUDE VS ROTOR SPEED
ACCEL SPEED(RPM)
COMPOSITE

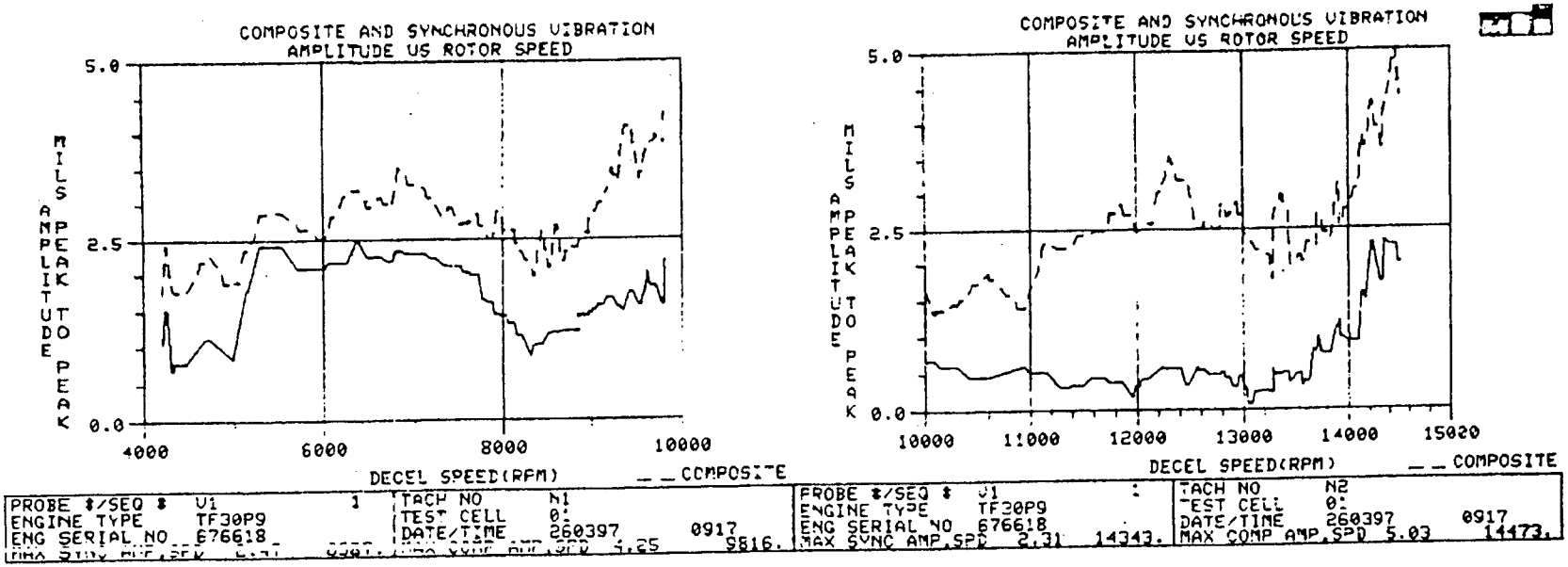
COMPOSITE AND SYNCHRONOUS VIBRATION
AMPLITUDE VS ROTOR SPEED
MILS AMPLITUDE PEAK
5.0
2.5
0.0
4000
6000
8000
10000
DECEL SPEED(RPM)
COMPOSITE
PROBE #/SEQ # V1 1
ENGINE TYPE TF30P9
ENG SERIAL NO 676618
TACH NO N1
TEST CELL 0
DATE/TIME 260397 0917
MAX SYNC AMP,SPD 2.25 9816.
COMPOSITE AND SYNCHRONOUS VIBRATION
AMPLITUDE VS ROTOR SPEED
MILS AMPLITUDE PEAK
5.0
2.5
0.0
10000
11000
12000
13000
14000
15000
DECEL SPEED(RPM)
COMPOSITE
PROBE #/SEQ # V1
ENGINE TYPE TF30P9
ENG SERIAL NO 676618
MAX SYNC AMP,SPD 2.31 14343.
TACH NO N2
TEST CELL 0
DATE/TIME 260397 0917
MAX COMP AMP,SPD 5.03 14473.

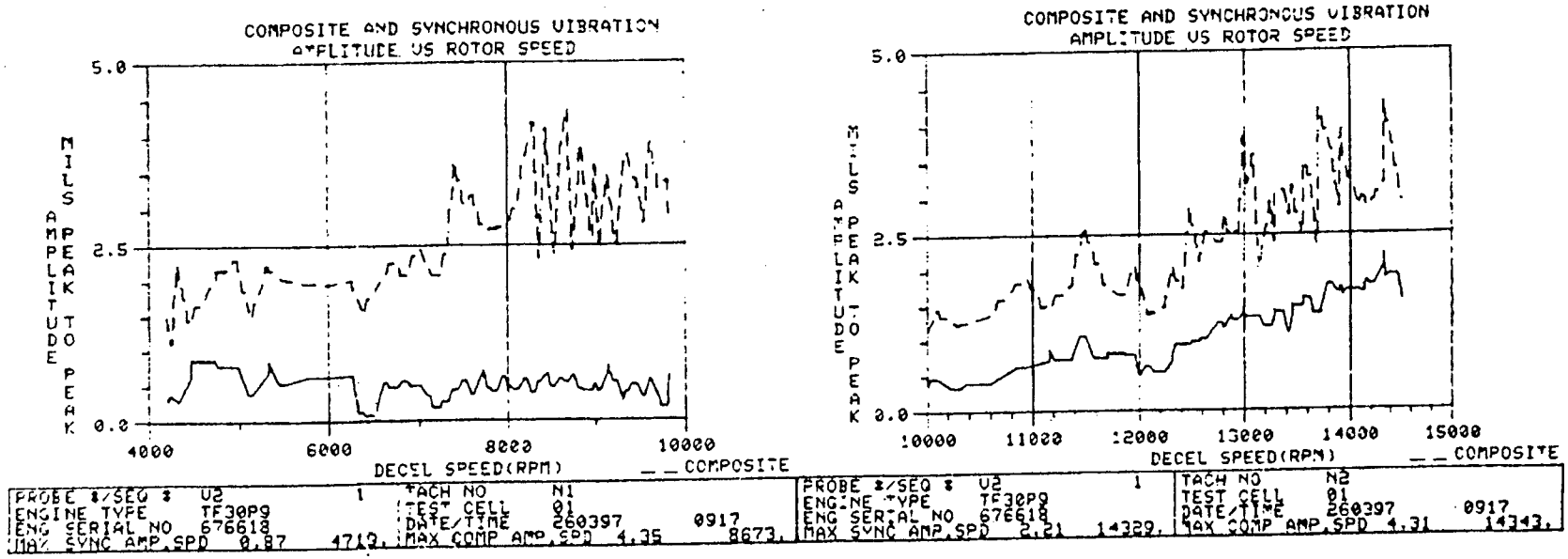
COMPOSITE AND SYNCHRONOUS VIBRATION
AMPLITUDE VS ROTOR SPEED
MILS AMPLITUDE PEAK
5.0
2.5
0.0
4000
6000
8000
10000
DECEL SPEED(RPM)
COMPOSITE
PROBE #/SEQ # V2 1
ENGINE TYPE TF30P9
ENG SERIAL NO 676618
MAX SYNC AMP,SPD 0.87 4713.
TACH NO N1
TEST CELL 01
DATE/TIME 260397 0917
MAX COMP AMP,SPD 4.35 8673.
COMPOSITE AND SYNCHRONOUS VIBRATION
AMPLITUDE VS ROTOR SPEED
MILS AMPLITUDE PEAK
5.0
2.5
0.0
10000
11000
12000
13000
14000
15000
DECEL SPEED(RPM)
COMPOSITE
PROBE #/SEQ # V2 1
ENGINE TYPE TF30P9
ENG SERIAL NO 676618
MAX SYNC AMP,SPD 2.21 14329.
TACH NO N2
TEST CELL 01
DATE/TIME 260397 0917
MAX COMP AMP,SPD 4.31 14343.

TACHOMETER

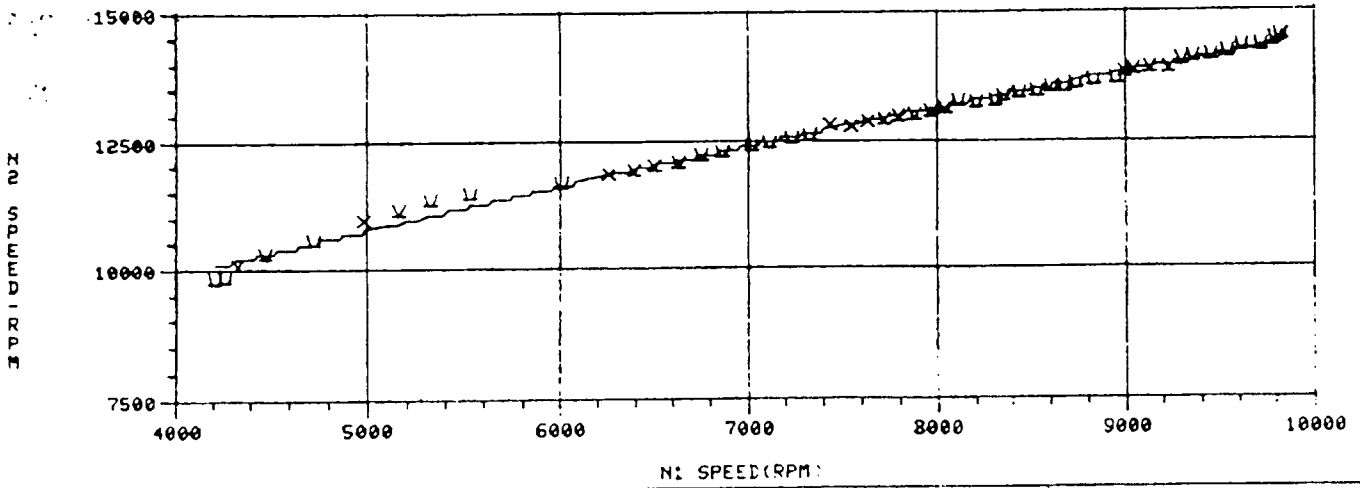

PROBE NUMBER	01	TEST CELL	01
ENGINE TYPE	TF30P9	DATA TYPE	DECELERATION
ENG SERIAL NO	676618	DATE/TIME	260397 0917
SEQUENCE NO	1		

COMPOSITE AND SYNCHRONOUS VIBRATION AMPLITUDE VS ROTOR SPEED

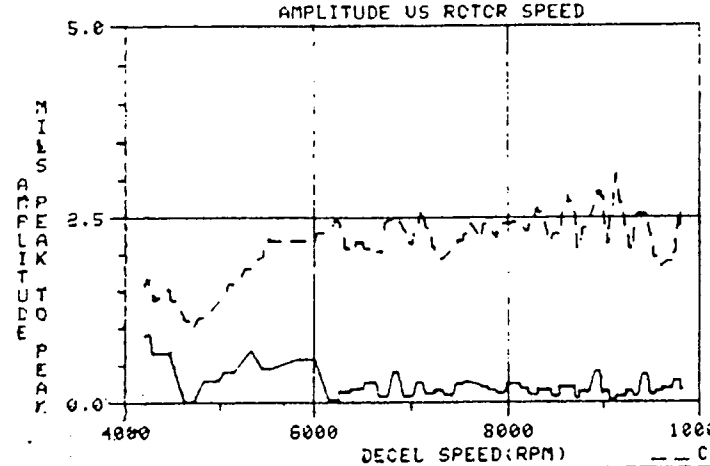

PROBE #/SEQ #	03 1	TACH NO	N1
ENGINE TYPE	TF30P9	TEST CELL	01
ENG SERIAL NO	676618	DATE/TIME	260397 09:?
MAX SYNC AMP,SPD	0.91 4256.	MAX COMP AMP,SPD	3.06 9125.

COMPOSITE AND SYNCHRONOUS VIBRATION AMPLITUDE VS ROTOR SPEED

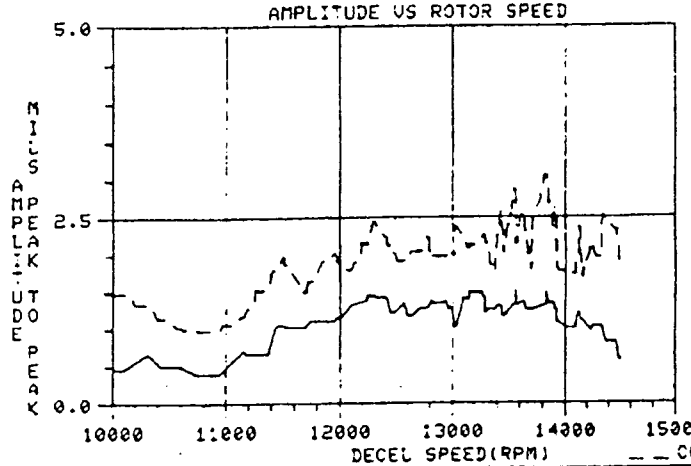

PROBE #/SEQ #	03 1	TACH NO	N2
ENGINE TYPE	TF30P9	TEST CELL	01
ENG SERIAL NO	676618	DATE/TIME	260397 0917
MAX SYNC AMP,SPD	1.50 13564.	MAX COMP AMP,SPD	1.07 13824.

USE OF STATISTICAL PROCESS CONTROL IN A REPAIR/REFURBISH/REMANUFACTURE ENVIRONMENT

Roger G. Ford, Ph.D., P.E.
Associate Professor of Engineering
Engineering Department

St. Mary's University
One Camino Santa Maria
San Antonio, Texas 78228-8534

Final Report for:
Summer Faculty Research Program
San Antonio Air Logistics Center
Kelly Air Force Base
San Antonio, Texas
Contract Number: F49620-93-C-0063

Sponsored by:
Air Force Office of Scientific Research
Bolling Air Force Base, DC

and

San Antonio Air Logistics Center
Kelly Air Force Base
San Antonio, Texas

December 1997

USE OF STATISTICAL PROCESS CONTROL IN A REPAIR/REFURBISH/REMANUFACTURE ENVIRONMENT

Roger G. Ford, Ph.D., P.E.
Associate Professor of Engineering
Department of Engineering
St. Mary's University

Abstract

The San Antonio Air Logistics Center at Kelly Air Force Base is a repair/refurbish/remanufacture facility for the Air Force. As such, a traditional manufacturing environment is not prevalent due to the fact that aircraft and aircraft parts are sent to the center for rebuilding and recertifying before being placed back on full active duty. During previous summers, an on-going effort to determine if the industrial engineering technique known as statistical process control has been or should be utilized at the center has been conducted. This contract covers the calendar year of 1997 and is a continuation of the same effort. This report details the efforts, findings, results, and conclusions of two graduate students and their professor aided by a Kelly coordinator in several areas of the center's operations. The areas investigated include the T38/F5 Gear Box End Item, the F15 Central Gear Box (CGB) area, the F16 Power Take-off (PTO) Shafts, an Automated Precision Inspection System (APIS) area investigation, the F-15 Aircraft Mounted Accessory Drive (AMAD) area, misidentified parts from the Defense Logistic Agency, the fuel controls area, the Gas Turbine Engine (GTE) area, load valves area, and the Electronic Engine Controls (EEC) area. Results of the study are given as well as conclusions for each of the areas. Statistical Process Control (SPC) was actually implemented in the CGB and PTO areas.

USE OF STATISTICAL PROCESS CONTROL IN A REPAIR/REFURBISH/REMANUFACTURE ENVIRONMENT

Roger G. Ford, Ph.D., P.E.

Introduction

The project team made up of Dr. Roger G. Ford, St. Mary's graduate students Kelly Jackson and Slimane Rechoum, and Kelly Air Force Base and project contact Dr. Mark Smith was given the task to evaluate areas within the LD Directorate at the San Antonio Air Logistics Center for application of the technique of Statistical Process Control (SPC). The aim of the project was to see if SPC was being used, where it could be used, and to determine areas of inefficiency that could be assisted by the project team.

Discussion of Problem

Various areas within the LD Directorate were investigated. The following report lists each area investigated along with problems found, actions taken, conclusions, and reports including SPC use in two of the areas.

Methodology

The methodology used in the project was to find areas where the Directorate itself desired the project team's help, spend considerable time in investigation of the area to determine if there were indeed problems present, determine what the project team could do to assist the area in solving the problems, and to evaluate the use of SPC in the area in question.

I. CGB Reject Team Activity

Introduction:

A large number of parts were found in a room in building 331. The lot was a mix of good and bad parts from F-15 and F-16 CGB, AMAD, JFS, Starters, and ADG. Some supervisors decided to stock mis-routed, bad, or extra parts in that 'back room' in lieu of taking appropriate actions like rerouting or condemning them. Most of them were F-15 CGB parts.

Actions Taken:

A reject analysis team was formed to look into the process of the F-15 CGB. The meetings were held once a week. The section chief LDT Adalberto Martinez, as a response to Colonel LDP C. Holsen's orders, in the reject meeting on 25 September 97, had urged the team to show more efficiency and solve the problems at the source and not to cure only their symptoms. He assigned Lieutenant LDPA David Meadows to be the team leader and supervise the meetings.

At the end of every month, the following documents were made:

- The Reject Analysis Sheet: It shows in a table format the rejected parts with their recurrence frequency, the types of rejects with their percentages, and the reject rate per kit.
- The Reject CGB Reject Type Distribution Chart: A pie chart displaying the reject type distribution.
- The Monthly Reject Rate Chart: It shows the reject rate for every month.
- The Standardized Control Chart: This chart indicates for every week whether the process is in control.

The branch chief A. Martinez urged the team members to take the necessary actions to solve problems as soon as possible. He made sure that all parties involved in putting together part kits be represented at the meetings. Those include: disassembly, cleaning, parts pool, inspection, assembly, scheduling, planning, and quality control.

After Lt. David Meadows took over the meetings, the team went on in the same rhythm. Most of the time, all team members were present. Presumably, he is the kind of person who can make intelligent use of the charts and data. A copy of relevant documents were given to Lt. Meadows and the meaning of each chart was explained to him by the project graduate student. He handed them out to the section chief. Lt. Meadows' feedback from A. Martinez was : He liked the charts, they look nice meaning that neither he nor the section chief did tried to use the information or understand it. The documents were still produced for the record.

In the meeting of November 5th, Lieutenant David Meadows informed us that he was leaving for a TDY until February 98. He designated LDPAE Louis Quintanilla to be leading the team in the mean time.

Results:

The main results of this operation are:

- Uncovered the bad practice of stocking unwanted parts in the 'back room'. Now supervisors know that this is not a solution. Instead, it becomes a larger problem.
- Save and reroute those parts to where they belong immediately. Releasing those parts actually reduced part shortages in the assembly shops.
- Make employees from different levels work in a team. In the beginning, the meetings almost turned into fights. Everybody felt offended, thinking that this was some kind of a prosecution.

Over time, they understood that rejected parts are everybody's problem, and that communication is necessary to solve it.

- Make the employees measure the quality of their production. The employees started moving a step forward, recognizing the need for numbers and statistics.

Conclusion:

Lt. A. Martinez mentioned that meetings where rejected parts are gathered and redistributed is not a solution and should not exist. He understands that SPC is the best way to solve problems with rejected parts. However, neither he nor anyone else has ever been interested in using the statistics and SPC charts that were generated.

The situation improved during the months of November and December. Team members are being more comprehensive, and communicate better. This is very important in solving the problems. It is only in the last three weeks that some team members felt the need for some statistics.

Most mechanics, especially Mike Dupree, Tina Angel (F-15 CGB),and Marty Martinez (F-16 JFS), were always helpful, cooperative, and concerned about quality and efficiency. Some of the supervisors, however, were usually accusing and defensive.

F-15 CGB Monthly Average Reject Rate Per Kit

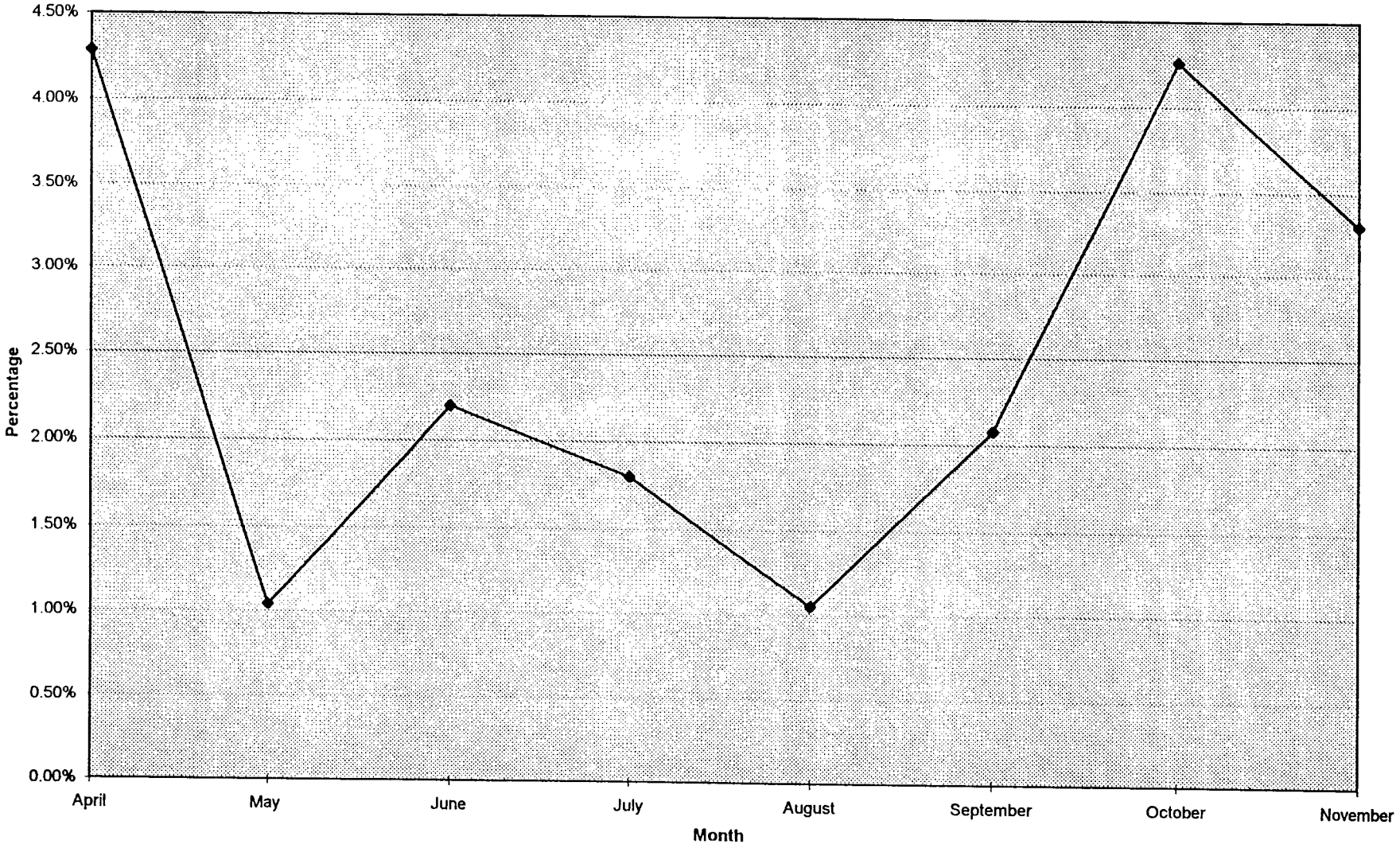

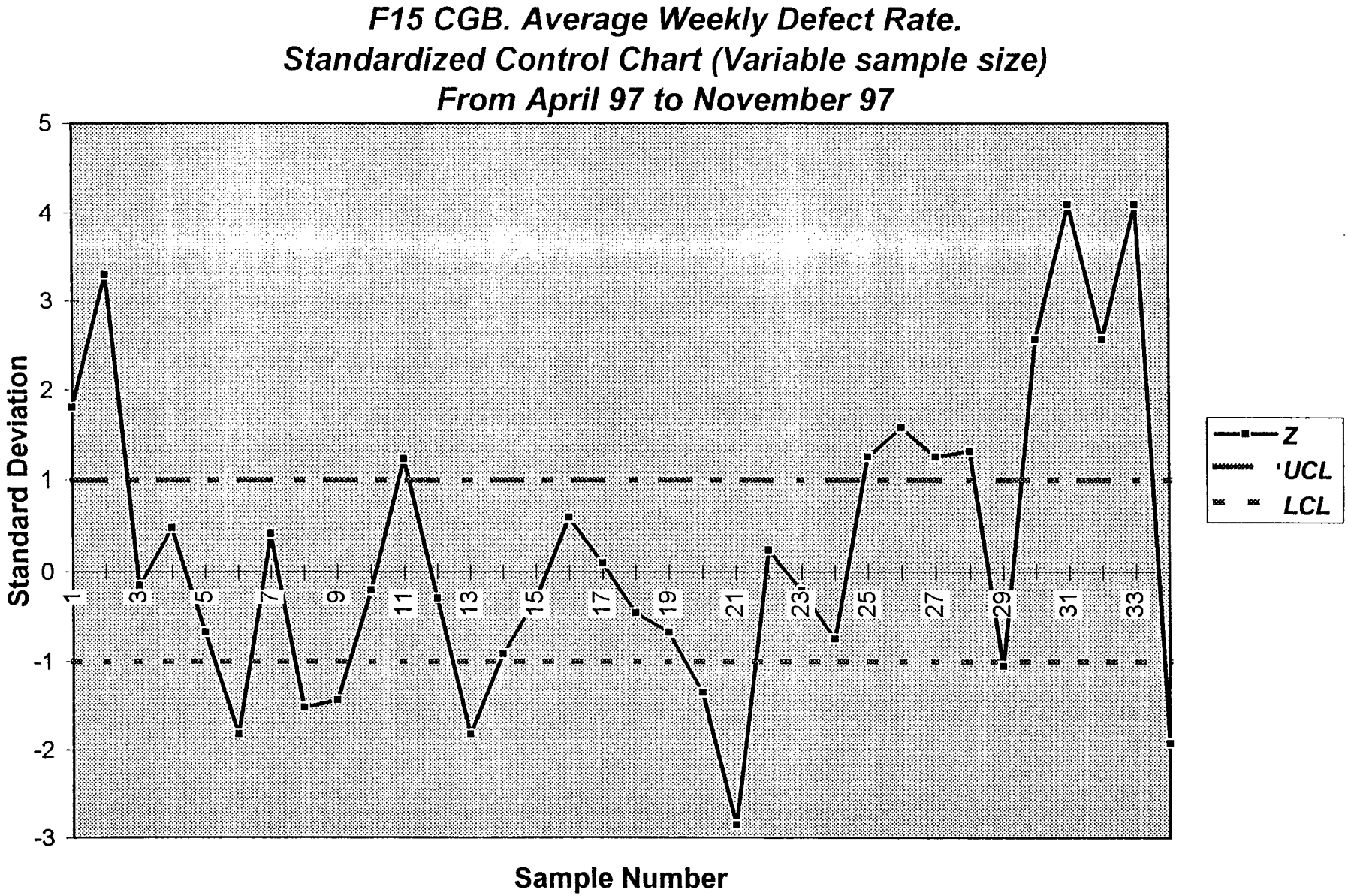
F15 CGB. Average Weekly Defect Rate.
Standardized Control Chart (Variable sample size)
From April 97 to November 97
Standard Deviation
5
4
3
2
1
0
-1
-2
-3
1
3
5
7
9
11
13
15
17
19
21
23
25
27
29
31
33
Sample Number
Z
UCL
LCL

II. Fuel Controls:

In February 97, Bill Navarijo LDCQ called us (the project team) to look at the situation in the F-16 fuel control C/N 13518A. He noticed it had too many end item failures, but, he did not have the figures to show that. The logbook was used to figure out the exact reject rate. Tracking of the data began from the month of October 96 to February 97. The reject rate for that period of time astounding:

Month	Items Tested	Items Sold	Items Rejected	Reject Rate
October 96	16	6	10	62.5%
November 96	13	7	6	46.2%
December 96	42	24	18	42.9%
January 97	40	20	20	50.0%
February 97	23	9	14	60.9%
Total	134	66	68	
	Average Reject Rate			***50.7%***

An average reject rate of 50.7% is definitely too high. The quality assurance personnel realized the shop cannot live with that kind of reject rate.

After presenting the situation to supervision, the project team formed the F-16 Fuel Team. The following charter was put together:

The F-16 Fuel Control Team Charter:

Purpose: Work on reducing end item rejects for the F-16 fuel control and make recommendations for improvements to LDPF and LDP.

Responsibilities: The quality assurance specialist is the team leader and is responsible for briefing LDP and LDPF managers on a monthly basis. Testers and mechanics will provide data and work on recommendations. The research assistant will gather data and put together charts for the team. The LD quality advisor will facilitate the team. The team leader will follow up to make sure the approved recommendations are followed through, and that members are participating in the meetings.

Authority: The team leader can make recommendations and improvements with proper documentation to LDP and LDPF.

Feedback: The team communicates recommendations to LDPBC and LDP and management recommendations to the team members. LDP will be briefed on status of the team. Minutes will be provided after every meeting.

Composition: The quality assurance specialists, testing section, overhaul section, engineering, planner, the equipment specialist, and the research assistant. LDPBC branch chief is an invited guest.

Voting: Decisions are made by consensus. Absent members will abide by the team's recommendations.

Meeting frequency: Initially meet once a week, but at least once a month. Meet on Tuesdays at 0930.

It is worth mentioning a few facts about the logbook. It includes data about the following:

1- the control number: in this case it is **13518A**

2- the serial number: of the fuel control.

3- the date: when the item was tested.

4- the status of the item: Sold or Rejected, and the defect type if rejected.

5- the mechanic number: a four digit number designating the tester.

6- whether the item is overhauled: O/H for overhaul, and OCM for on condition maintenance. Most of these items are overhauled.

7- Some comments: to help the mechanic in repairing the rejected item.

Most of these data are explicit, except for the status of the item. The status indicates whether an item is sold or rejected. If the item is rejected, the mechanic should mention the reject reason. Mechanics are not consistent when writing down the defect types. Since there is no standard defect terminology or coding, defects can have different names every time they come up. This makes it difficult to track. Moreover, the project team did not have the authority to make the mechanics use a standard code for each kind of defect.

A list of all the defect types was collected that were used in the logbook . The mechanic LDPPC Raymond Leija helped put them in groups of phrases with similar meanings. This was necessary before doing any analysis.

The data was placed into a spreadsheet, and a Pareto chart was built with the following results:

F-16 Fuel Control Defect Pareto Chart

Data From October 96 To February 97

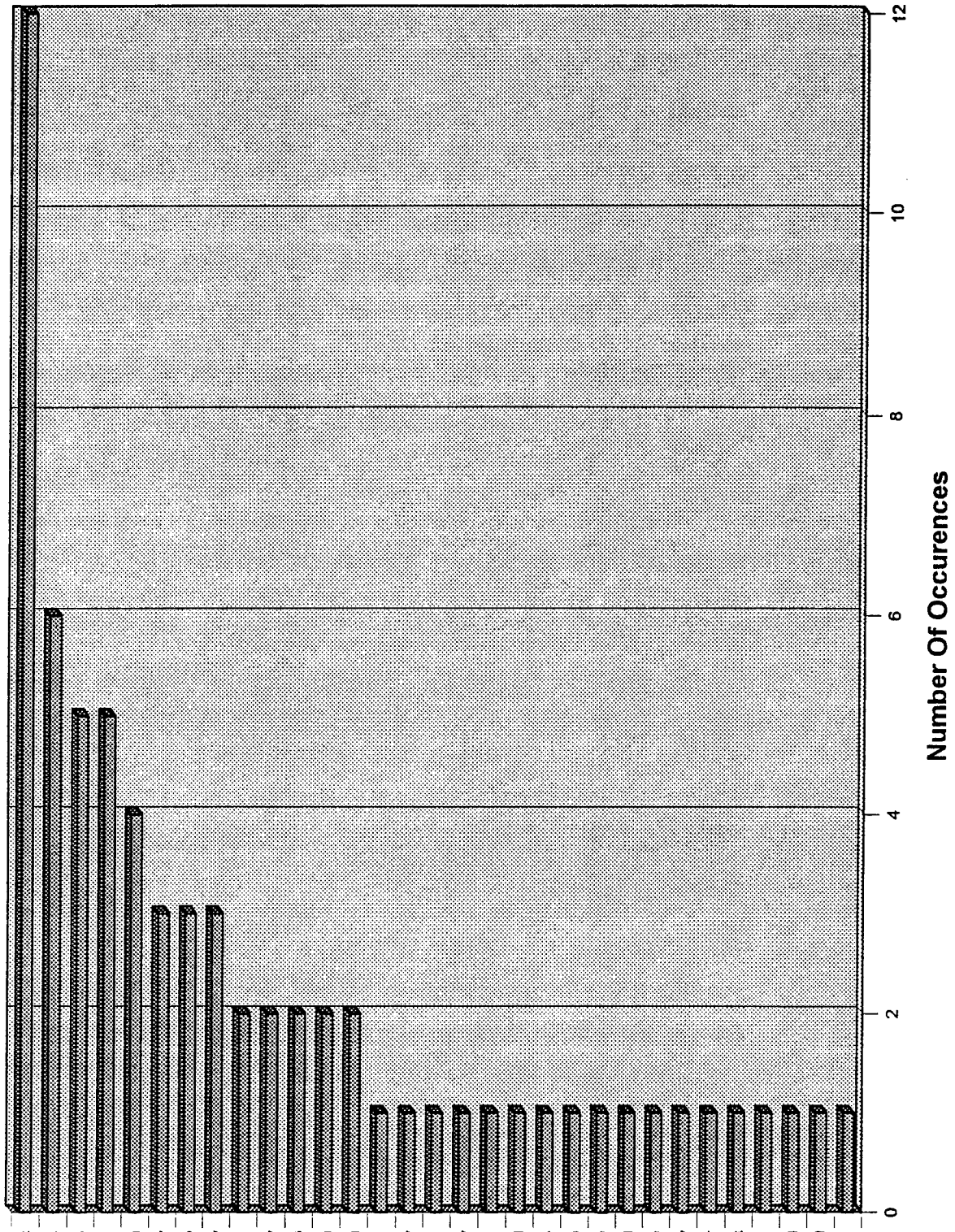

After examining the data, the mechanics said that the defects related droop can usually be cured only by adjusting screw #8. In this case there are two such defects: -droop fast (12 occurrences) and -droop slow (3 occurrences), a total of 15 out of 69 detects. That is 21.7% of defects caused by only 2 out of 32 (6%) of the defect types.

In the meeting of 20 March 97, engineer Kevin Schabaker pointed out that this kind of procedure may have secondary effects, and that he needs to carry on a study to clarify this matter. The following are the minutes for that meeting:

From: SLIMANE Rechoum
Sent: Thursday, March 20, 1997 8:10 AM
To: NAVARIJO Bill; CROOM PAUL M; MITCHELL HAROLD G; ALONZO YVONNE M; MENDOZA Art; SCHABACKER KEVIN
Subject: F-16 FCP Team Meeting

The following are the minutes for the F-16 fuel control team:

1) Attendees:

Bill Navarrijo	LDCQ
Paul Croom	LDPPC
Brett Drutar	LDPPC
Jimmy Trevino	LDPPC
Raymond V. Leija	LDPPC
Harold Mitchell	LDPPC
Hyuk Beom Kwon	LDPP
Rudy Loza	LDPPC
Yvonne Alonzo	LDPPE
Art C.Mendoza	LDPPC
Kevin Schabacker	LDPE

2) The team reviewed the charts for the Thursday briefing with Mr. Stallings. The end items reject rate for the month of March was 14.3% which well below the previous six month average of 48.9 %.

Action Items:
1) The planner will submit a 202 to make changes in the T.O.

2) The Engineer Kevin Schabacker will conduct a study to ensure the turning of the #8 screw won't create any problems.

3) Next meeting is in 2 weeks.

The team decided that the testers would do the adjustments with the help of the mechanic, and see the impact on the reject rate. Following are the minutes that were sent out after the meeting.

From: SLIMANE Rechoum
Sent: Tuesday, April 08, 1997 10:58 AM
To: NAVARIJO Bill; MEDINA NARDELIO; MENDOZA Art; SLIMANE Rechoum; SMITH Mark; ALONZO YVONNE M; PEREZ ANTONIO F; SCHABACKER KEVIN; ROMO ED; SANCHEZ HERMAN D; BALLARD Tom
Subject: Minutes for the F-16 Fuel Controls team meeting (04/08/97)

The following are the minutes for the F-16 Fuel Controls team meeting:

1)The attendees :

Bill Navarijo	LDCQ
Nardello Medina	LDPPC
Raymond V. Leija	LDPPC
Art C.Mendoza	LDCQ
Slimane Rechoum	LDCS
Mark Smith	LDCS
Yvonne Alonzo	LDPPE
Antonio F.Perez	LDPPC
Rudy Loza	LDPPC
Kevin Schabacker	LDPS
Ed Romo	LDPS

2) Kevin Schabacker gave the team members copies of the AFMC from 202 to adjust the test procedures for the #8 screw. He also provided the list of steps for the new testing procedure.

3) Mark Smith and Slimane Rechoum brought reject data to the meeting. The reject rate for March was 30.1% down from 60.9% in February. The bad servo is now the most frequent problem that is caused by a material problem with the drive leaks. Engineering is working on fixing the problem.

4) Action Items:

A) Tester will implement new testing procedures, will collect data and bring them to the next team meeting.

B) Next meeting is scheduled for 22 April at 0930.

The mechanics explained the procedures of adjusting item #8 and helped the mechanics implement them.

The following results were obtained for the following months of March, April and May:

Month	Items Tested	Items Sold	Percentage	Items Rejected	Percentage
January 97	40	20	50.0%	20	50.0%
February 97	23	9	39.1%	14	60.9%
March 97	33	23	69.7%	10	30.3%
April 97.	11	8	72.7%	3	27.3%

The reject rate has dropped from 60.9% in February to 30.3% during March and further down to 27.3% in April. The new procedures implemented are definitely working well and giving a good response. In the meeting of 08 April 97 it was decided that the next step is to make the change part of the Technical Order. The following were the minutes for that meeting.

From: SLIMANE Rechoum
Sent: Tuesday, April 08, 1997 10:58 AM
To: NAVARIJO Bill; MEDINA NARDELIO; MENDOZA Art; SLIMANE Rechoum; SMITH Mark; ALONZO YVONNE M; PEREZ ANTONIO F; SCHABACKER KEVIN; ROMO ED; SANCHEZ HERMAN D; BALLARD Tom
Subject: Minutes for the F-16 Fuel Controls team meeting (04/08/97)

The following are the minutes for the F-16 Fuel Controls team meeting:

1)The attendees :

Bill Navarijo	LDCQ
Nardello Medina	LDPPC
Raymond V. Leija	LDPPC
Art C.Mendoza	LDCQ
Slimane Rechoum	LDCS
Mark Smith	LDCS
Yvonne Alonzo	LDPPE
Antonio F.Perez	LDPPC
Rudy Loza	LDPPC
Kevin Schabacker	LDPS
Ed Romo	LDPS

2) Kevin Schabacker gave the team members copies of the AFMC from 202 to adjust the test procedures for the #8 screw. He also provided the list of steps for the new testing procedure.

3) Mark Smith and Slimane Rechoum brought reject data to the meeting. The reject rate for March was 30.1% down from 60.9% in February. The bad servo is now the most frequent problem that is caused by a material problem with the drive leaks. Engineering is working on fixing the problem.

4) Action Items:

A) Tester will implement new testing procedures, will collect data and bring them to the next team meeting.

B) Next meeting is scheduled for 22 April at 0930.

The Pareto chart shown above indicates that the defects *Shaft seal leak, Bad servo* represent the second most important types of defects. The mechanics identified that they are both caused by the Servo-mechanism unit. The shop had run out of new servos and started using old ones, while waiting for the new ones to be shipped in. This problem has been corrected by the end of the month of April.

In the meeting of 05 June 97, it was reported, for the first time, the monthly reject rate of 0.0% for May 97. 25 fuel controls that were tested and sold. The meetings became shorter and shorter as time went

along. It was decided that the meeting be on a monthly basis. The following are the minutes for the 5 June meeting.

F-16 Fuel Controls SPC-Team Meeting Minutes (05 June 97 0930-1015):

1) Attendees:

Art Mendoza	LDCQ
Rudy Loza	LDPPC
Kevin Schbacker	LDPS
Brett Drutar	LDPPT
Slimane Rechoum	LDCS
Mark Smith	LDCS

2) Mark Smith covered reject rate for the month of May which was 0.0%. 25 items were tested and were all sold. A total of 33 items in a row have passed test (April through June).

3) Actions that led to team's success:

- Mechanic has adjusted screw and corrected leakage.
- The problems with the driveshaft and servo parts have been corrected.
- Mechanics got certification to use ultrasonic tank cleaning.
- The mechanic has made fewer visits to the test stand indicating a better fuel control is being produced.

4) Next meeting is on 10 July 0930 in LDPP conference room B345. Kevin Schabacker will cover data gathering procedures with the testers.

It was expected that the production was going to stop during the month of June 97. However, the issue of the T.O. change was still pending.

In the meeting of 14 July 97, the engineer Kevin Schabaker, who is taking in charge the change in the T.O., raised a number of important issues concerning the new procedures:

- How to prove that the reject rate drop is a direct consequence of the new procedure, and not just pure coincidence.

- In case the change takes place, the T.O. must provide precise instructions indicating how much and in which direction screw #8 needs to be turned. This requires the mechanic to record the adjustments performed on item #8.

The data from the month of April-97 up to August-97 was analyzed with the following conclusive results:

Month	*Items Sold*	*#8 Adj. on Sold Items*	*Ratio*
Apr-97	15	3	20%
May-97	25	(No Data Reported)	?
Jun-97	1	1	100%
Jul-97	7	4	57%
Aug-97	6	3	50%
Average			38%

For some unknown reason, the mechanics did not report in the logbook whether screw #8 was being adjusted in the month of May. However, the data show the new procedure has saved 38% of the fuel controls. Those would, otherwise, have been failed and sent back to the mechanics.

During the months of July, August, and September, the reject rate suddenly increased up to 45.5% in August. The portion of the logbook corresponding to that time period is shown in the next page.

Month	S/N	Status
Jul-97	6-82-03	sold
Jul-97	08-92-77	sold
Jul-97	3-82-53	bad servo
Jul-97	2-83-40	sold
Jul-97	3-82-53	sold
Jul-97	4-85-82	sold
Jul-97	11-85-270	sold
Jul-97	4-88-81	No flow
Jul-97	4-88-81	#8 will not adjust
Jul-97	88-91-143	sold
Jul-97	4-88-81	#8 frozen
Aug-97	67	helicoil came out on screw #8
Aug-97	4-88-81	screw #8 rouded out
Aug-97	4-88-81	unable to control (high end)
Aug-97	67	too much flow, unable to control
Aug-97	4-88-81	sold
Aug-97	67	sold
Aug-97	02-93-02	sold
Aug-97	01-92-299	sold
Aug-97	1-86-07	sold
Aug-97	7-89-116	droop too low
Aug-97	7-89-116	sold
Sep-97	7-82-24	bad servo valve
Sep-97	7-82-24	very erratic
Sep-97	6-84-92	control low flow
Sep-97	7-82-24	failed sea level cal (high)
Sep-97	6-84-92	sold
Sep-97	9-82-107	sold
Sep-97	3-86-84	sold
Sep-97	7-84-102	sold
Sep-97	6-90-99	sold
Sep-97	7-82-24	will not repeat
Sep-97	10-91-212	sold
Sep-97	7-82-24	sold

It can be seen that there are three fuel controls that repeatedly fail tests :

* The fuel control S/N 4-88-81 was tested 6 times before it sells,
* The fuel control S/N 67 was tested 3 times before it sells,
* The fuel control S/N 7-82-24 was tested 5 times before it sells.

These items incur considerable overhead on production. The mechanics keep overhauling and testing the same items over and over again while delaying other healthier items. This kind of problems should be avoided by condemning weak items.

For the sake of comparison, the following chart shows the actual reject rate versus the reject rate without the three ill items. The chart shows that the reject rate should not be larger than 20%.

The reject rate went back to zero in the month of October.

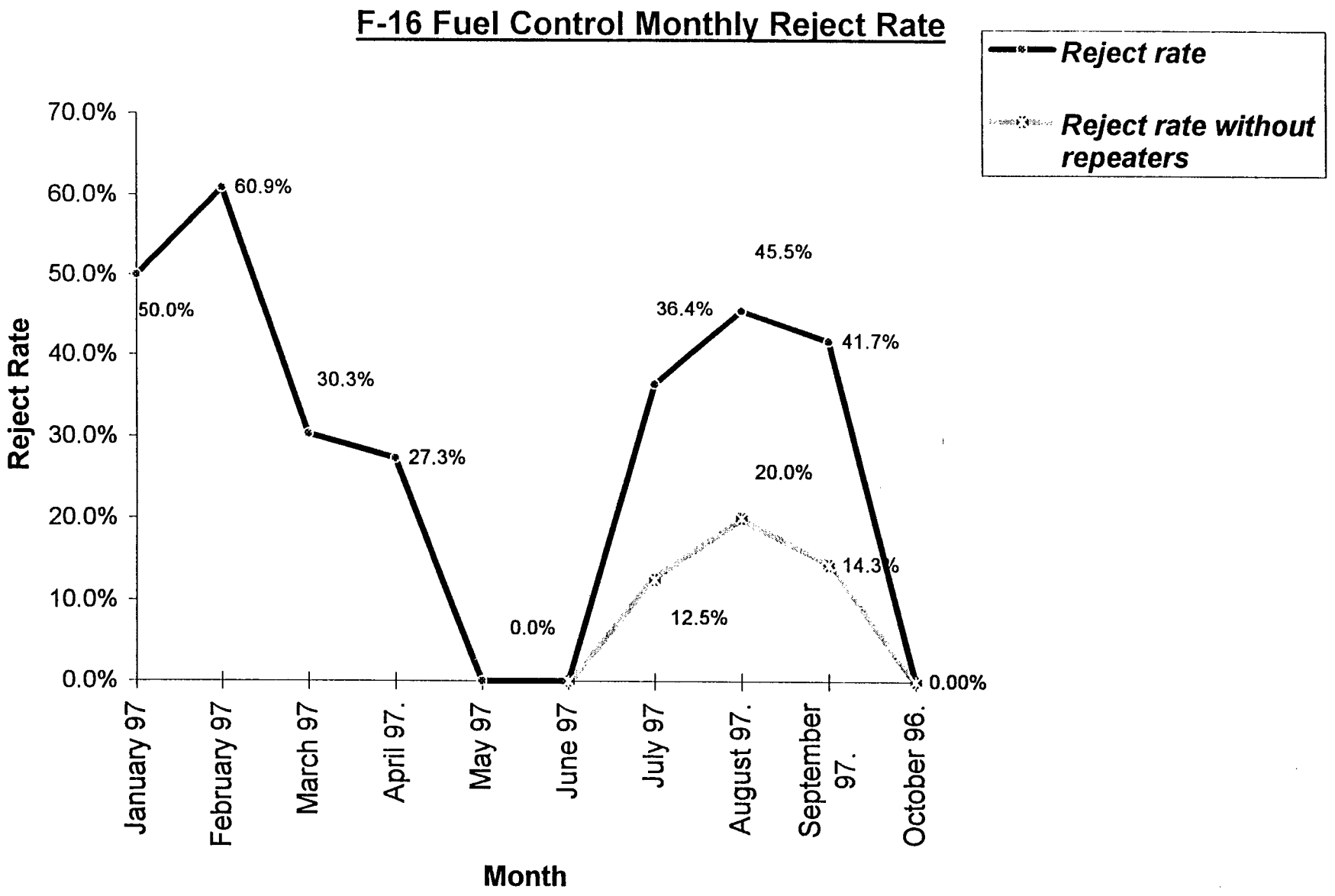
F-16 Fuel Control Monthly Reject Rate
Reject rate
Reject rate without repeaters
Reject Rate
70.0%
60.0%
50.0%
40.0%
30.0%
20.0%
10.0%
0.0%
60.9%
50.0%
30.3%
27.3%
0.0%
36.4%
45.5%
41.7%
20.0%
14.3%
12.5%
0.00%
January 97
February 97
March 97
April 97.
May 97
June 97
July 97
August 97.
September 97.
October 96.
Month

III. Other Fuel Controls:

In the meeting of 14 July 97, Mark Smith and Slimane Rechoum asked the team if there were any other candidate control number with a large reject rate. They have proposed to the project team to look into the C/N 66888-106. They think it may have a considerable reject rate. The following were the minutes for that meeting:

From: SLIMANE Rechoum
Sent: Monday, July 14, 1997 7:26 AM
To: SMITH Mark
Subject: F-16 Team meeting minutes of 10 July 97 at 0830

F-16 Team meeting minutes of 10 July 97 at 0830

1) Attendees:

Art C.Mendoza	LDCQ
Bill Navarijo	LDCQ
David Hinojosa	LDPPE
Ed Romo	LDPS
Harold Mitchell	LDPPC
Herman Sanchez	LDPP
Inocencio Sanchez	LDPS
Kevin Schabaker	LDPS
Mark Smith	LDCS
Paul Croom	LDPPC
Slimane Rechoum	LDCS

2) The team discussed gathering data to support the T.O. change in regards to adjusting the #8 screw. The testers have an action item to provide data on the next 10 items.

3) In May there were 25 items tested and 25 items passed with no rejects for 0% reject rate. This is a significant improvement from 56% between September 96 and February 97.

4) The team decided that fuel control # 66888-106 will be the next item for process improvement. Slimane Rechoum will collect and analyze data and present to the next meeting

5) The next meeting is scheduled for 12 August at 0930 in the LDPP branch conference room in building 345.

After analyzing the data, the following charts were generated shown in the next pages. The average reject rate over the last 7 months is 36.6% . The reject rate in the last moth is 66.7%. this rate cannot be tolerated even with a low production (3 failed out of 9 tested).

The defect Pareto chart shown indicates that only 2 out of 9 defect types are responsible of 70% of all rejects.

In the next meeting, we did not have the chance to go over these interesting results because the supervisor told us that no such fuel control is going to be produced during the quarter. Instead, he suggested

that the candidate would be fuel control C/N 07666A. Therefore, all relevant fuel controls available were tracked and emphasis was placed on the control numbers with high reject rates. The reject rates are summarized in the following table.

The most up to date data show that C/N 08559A has the largest average reject rate of 30.4%. The project team is looking into it.

Fuel Controls Reject Rates

C/N	Month	Tested	Sold	Reject	Monthly Reject Rate	Total tests	Total rejects	Average Reject Rate
00564A	January	13	5	8	61.5%	20	12	60.0%
	February	0	0	0	-			
	March	0	0	0	-			
	April.	5	2	3	60.0%			
	May	1	1	0	0.0%			
	June	1	0	1	100.0%			
	July	0	0	0	-			
	August	0	0	0	-			
	September	0	0	0	-			
	October	0	0	0	-			
07666A	January	31	28	3	9.7%	275	31	11.3%
	February	29	26	3	10.3%			
	March	27	24	3	11.1%			
	April	35	33	2	5.7%			
	May	19	19	0	0.0%			
	June	41	29	12	29.3%			
	July	38	34	4	10.5%			
	August	10	10	0	0.0%			
	September	39	36	3	7.7%			
	October	6	5	1	16.7%			
13494A	January	3	3	0	0.0%	18	2	11.1%
	February	0	0	0	-			
	March	3	3	0	0.0%			
	April	0	0	0	-			
	May	0	0	0	-			
	June	0	0	0	-			
	July	0	0	0	-			
	August	0	0	0	-			
	September	0	0	0	-			
	October	12	10	2	-			
08559A	January	16	16	0	0.0%	69	21	30.4%
	February	10	7	3	30.0%			
	March	9	4	5	55.6%			
	April	0	0	0	-			
	May	0	0	0	-			
	June	0	0	0	-			
	July	7	4	3	42.9%			
	August	4	3	1	25.0%			
	September	16	10	6	37.5%			
	October	7	4	3	42.9%			
66284A	January	21	13	8	38.1%	119	48	40.3%
	February	22	12	10	45.5%			
	March	15	6	9	60.0%			
	April	12	6	6	50.0%			
	May	10	8	2	20.0%			
	June	11	8	3	27.3%			
	July	24	17	7	29.2%			
	August	1	1	0	0.0%			
	September	0	0	0	-			
	October	3	0	3	-			
71280A	January	11	11	0	0.0%	41	4	9.8%
	February	8	7	1	12.5%			
	March	2	2	0	0.0%			
	April	10	10	0	0.0%			
	May	3	3	0	0.0%			
	June	0	0	0	-			
	July	4	2	2	50.0%			
	August	3	2	1	33.3%			
	September	0	0	0	-			
	October	0	0	0	-			
11209A	January	3	2	1	33.3%	79	9	11.4%
	February	6	6	0	0.0%			
	March	3	3	0	0.0%			
	April	18	14	4	22.2%			
	May	21	19	2	9.5%			
	June	6	6	0	0.0%			
	July	10	9	1	10.0%			
	August	4	3	1	25.0%			
	September	0	0	0	-			
	October	8	8	0	-			
23577A	September	7	6	1	14.3%	8	1	12.5%
	October	1	1	0	0.0%			

IV. APIS

Introduction:

The Automated Precision Inspection System (APIS) is a computerized precision measurement system. It is used to inspect dimensions of different critical mechanical parts. The quality of the inspected parts greatly depends on the APIS. Its critical accuracy makes it one the main areas where SPC can efficiently be applied.

Division Chief LD- John Stallings urged the project team in the meeting of March 97 to start implementing Statistical Process Control (SPC) on the Automatic Precision Inspection System (APIS).

Actions Taken:

After talking to the inspection section chief LD-- Homer Brooks, he showed the project team members around the inspection shop, the APIS machines, the APIS computer room, and the reports generated. He said, however, that the software is being upgraded, and it is better to wait until the new software is functional because most of the old data base files were wiped out. According to David Christopher, that should not take more than a three or four weeks. Six weeks later, Mr. Christopher was asked if the software has been implemented yet. A few more weeks, he replied. The complete software was not implemented yet. Apparently, it is a license issue. This went on for about six months.

In August 97, the project team, Dr. Roger Ford, Dr. Mark Smith, Kelly Jackson, and Slimane Rechoum, met with LDPAE Kevin D. Schnitzer and LDPAE David Christopher, and attempted to start applying SPC on the old data. David Christopher promised to provide us with accounts to access to their APIS computer files. A week later, we started working on their terminals using his account.

Results:

No relevant files were found in the VAX. David Christopher explained that he could not find the files either. The computer engineer who was archived the data was not working at the base anymore. Basically, the files are lost.

The computers and the software are being upgraded. The division chief Mr. Stallings has ordered the section chief Kevin Schnitzer and David Christopher to make sure the APIS be ready in no more than a month. That is by the end of October.

Conclusion:

In mid December, the software was still not installed yet. This is because the contractor who installed the hardware could not install the software. For this reason, the contract is being terminated. Kevin Schnitzer is now looking for a new contractor. He estimates that the new APIS will be ready within two months.

V. AMAD:

The project team decided to look into the AMAD shop to see if there was any need for our services. Data was gathered and the following reject rates were found:

AMAD Reject Rates

Month	Tested	Sold	Reject	Reject Rate
January 97	22	22	0	0.0%
February 97	25	25	0	0.0%
March 97	18	17	1	5.6%
April 97	26	24	2	7.7%
May 97	26	24	2	7.7%
June 97	13	12	1	7.7%

The reject rate was fairly low and the process seemed to be well in control, therefore there was no need to keep tracking it.

VI. Misidentified Parts From the Defense Logistic Agency:

In April 97, LDPAE Steve Gregory, a member of the DREP team, was concerned about the number of wrong parts he was receiving from the DLA. So he asked for the project team's services in order to find out about the percentage of mis-identified parts received from the DLA. The DLA incoming part logbook was referenced and the relevant data was located then put into the following table.

The results answered his questions. The average mis-identification rate was only 1.9%. This figure is fairly acceptable. A zero average rate is ideal, however, considering the complex protocols between the ALC and the DLA. Steve decided that it is advantageous to just tolerate it.

List of misidentified end items received from the DLA.

C/N	NSN(Master)	Mis-identified	Total	Percentage
12199-A	2995-01-048-9580	0	30	0.0%
10149-A	2995-00-492-1489	0	89	0.0%
10156-A	2995-00-337-5116	1	80	1.3%
10150-A	2995-00-337-5145	0	12	0.0%
12851-A	2995-01-139-6642	5	199	2.5%
10598-A	2995-01-077-6708	2	46	4.3%
10144-A	2995-00-920-1719	2	18	11.1%
10147-A	2995-00-951-3466	0	13	0.0%
42456-A	2995-01-140-2105	1	85	1.2%
10015-A	2995-00-851-3212	0	40	0.0%
10155-A	2995-00-856-9466	0	17	0.0%
10167-A	2995-00-856-9466	0	5	0.0%
39260-A	2995-01-187-4162	0	35	0.0%
43134-A	2995-00-998-5303	3	36	8.3%
80012-A	2995-01-187-4163	0	30	0.0%
	Total	14	735	
			Average	1.9%

VII. Electronic Engine Control (EEC)

Introduction:

The Electronic Engine Control (EEC) controls and optimizes the airplane engine efficiency in the F100 engines (used in the F-15 and F-16). The technical order instructs that the EEC's go through the following testing steps:

1. Initial inspection and preparation
2. Initial AGETS
3. Open loop vibration
4. Thermal cycling
5. Closed loop vibration
6. Extended range thermal test
7. Final functional
8. Final AGETS
9. Final inspection and preparation

If an EEC fails in any of the steps, it is sent to Troubleshooting and Repair. After the item is repaired, it is sent back to step *2. Initial AGETS* and has to pass all the other tests again.

Problem Statement:

LDCQ Raymond H. Gonzales, the QA in charge of the EEC's called the project team for a first informal meeting on 30 September 97. This was a consequence of a complaint raised by two of the mechanics. They were concerned about the maintenance procedures that were not properly followed. The main problems posed are:

- Some mechanics do not agree with the T.O. procedures. They prefer to send the EEC's back to the step where it failed and continue from there on, rather than sending it to step 2. The supervisor also pleads that the EEC's are over-stressed if they have to go again through the whole process every time they fail a testing step, the reason being that the EEC's are old and most of them have reached their expected life time.

- The test stands are not reliable. A few years ago, an electronics technician told the mechanics that if an EEC does not pass a test a first time, instead of failing it, they can redo the test again on the same or a different test stand. If the number of passes is larger than that of failures, then the item is good, otherwise they should send it back to the repair shop.

- The appraisal system takes into account only the number of EEC's produced. The mechanics who do not follow the T.O. procedures and skip steps to increase production are praised. The others whose primary concern is quality and reliability follow literally all T.O. steps are blamed to be slow.

On 2 October 1997, Dr. Mark Smith, Mr. Raymond Gonzales, and Slimane Rechoum met with the division chief LDA Vern Jauer and LDA Col. Wright Nodine in order to brief them about the employees' concerns. The division chief and the colonel wanted us to prove first that there is a problem, to explain our strategy , and most importantly not to take any unnecessary action. Time and resources did not allow further work to be conducted on this issue. However, the problems seemed significant enough to include in this report.

VIII. The Gas Turbine Engine:

Introduction:

In June 97, the project team started working on the Gas Turbine Engines (GTE). The supervisor of the GTE test shop Joe Vaquera, was very helpful. He provided us with all the data that we needed to analyze the reject for tested GTE end items.

Observations:

There were 13 GTE types that we tracked the data from January 97 up to November 97. The following conclusions were drawn:

The highest rejects, according to the indexed GTE Pareto Chart, are recorded for GTE types: 85-71, 85-72, 85-180H, 85-180L, 85-180C. The supervisor was asked about the reasons of rejects and he explained as summarized below.

- *GTE 85-71 and GTE 85-72:* a considerable number of them are Green Run IRAN's (Inspect and Repair As Necessary) or OCM's (On Condition Maintenance), in other words they are not overhauled. These items are tested as received. They are then repaired on the test stand if possible. Otherwise, they rejected. The records show rejected items for both IRAN's and overhauls at the same time without any distinction. The analysis done using these kind of data

is not reliable. For this reason, it was recommended Joe Vaquera to record overhauls, IRAN's and OCM's separately.

- *GTE 85-180H, GTE 85-180L, and GTE 85-180C:* most defects for these three gas turbine engines are cavity pressure. The supervisor justified that by the bad carbon seals they have been using recently. The new carbon seals do not conform to specification. The engineers are looking into that problem. He speculates that the new parts are supplied by a new manufacturer.

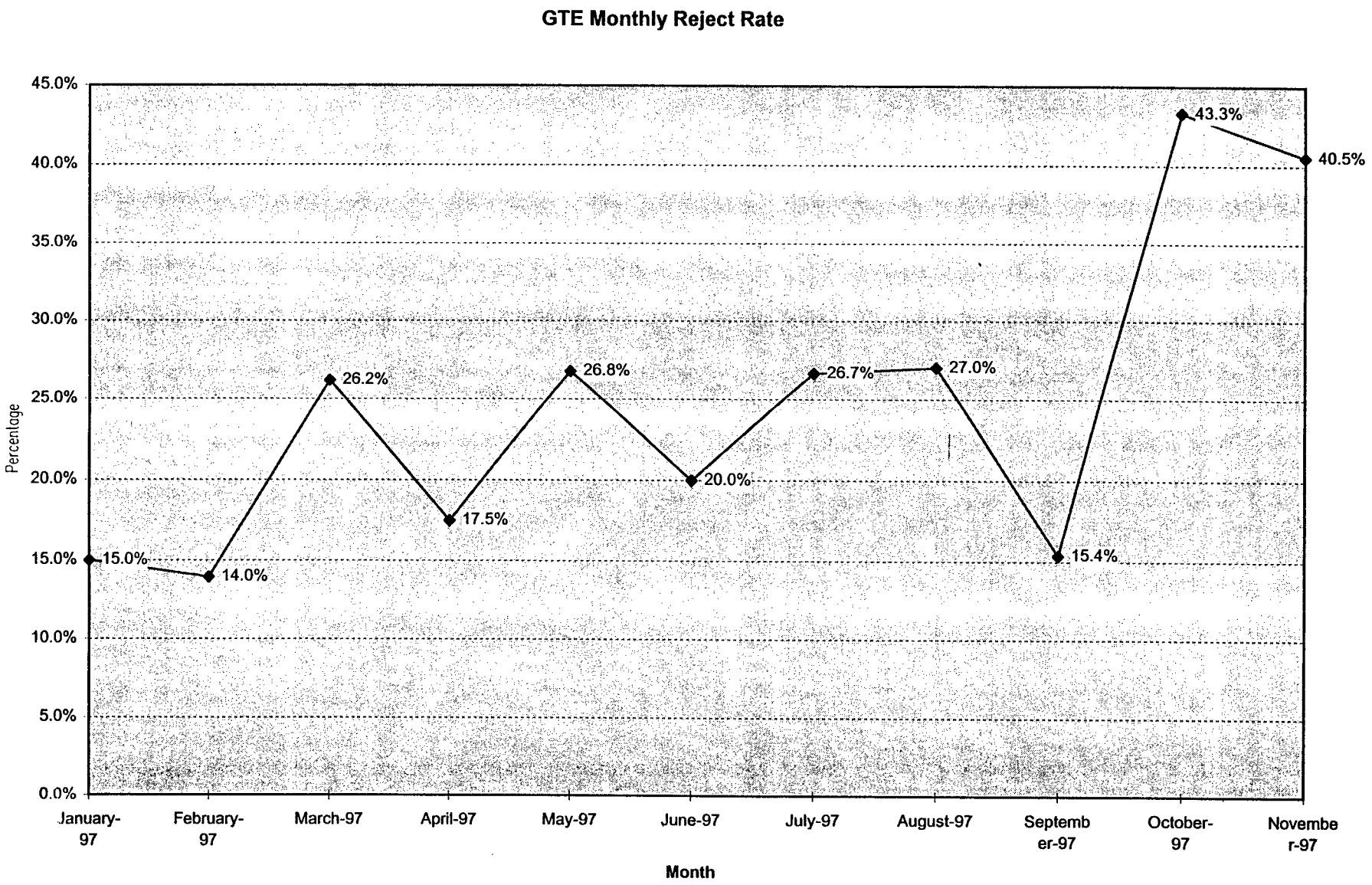
GTE Monthly Reject Rate
45.0%
40.0%
35.0%
30.0%
25.0%
20.0%
15.0%
10.0%
5.0%
0.0%
Percentage
15.0%
14.0%
26.2%
17.5%
26.8%
20.0%
26.7%
27.0%
15.4%
43.3%
40.5%
January-97
February-97
March-97
April-97
May-97
June-97
July-97
August-97
September-97
October-97
November-97
Month

GTE Production Chart

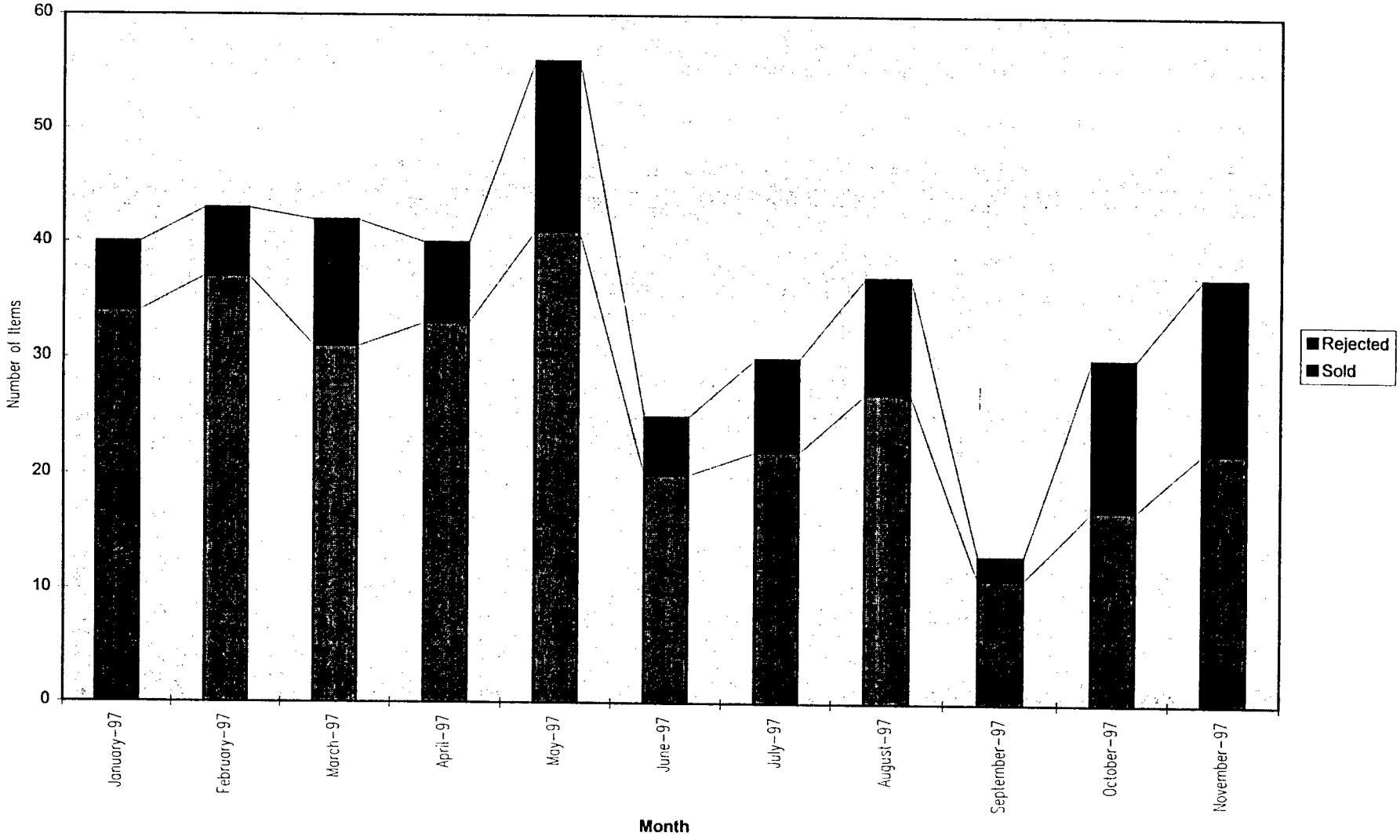

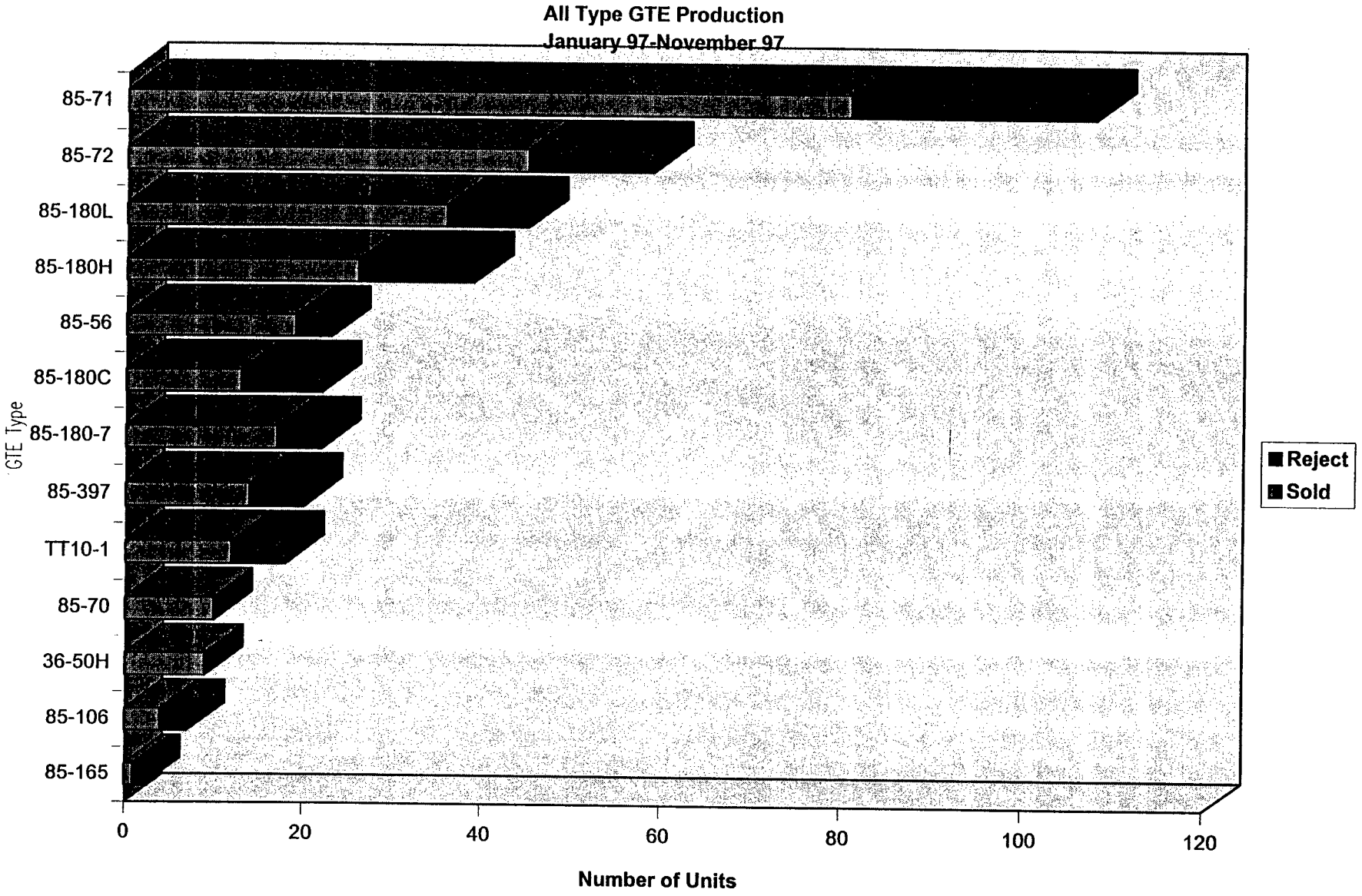
All Type GTE Production
January 97-November 97
GTE Type
85-71
85-72
85-180L
85-180H
85-56
85-180C
85-180-7
85-397
TT10-1
85-70
36-50H
85-106
85-165
0
20
40
60
80
100
120
Number of Units
Reject
Sold

GTE Pareto Chart

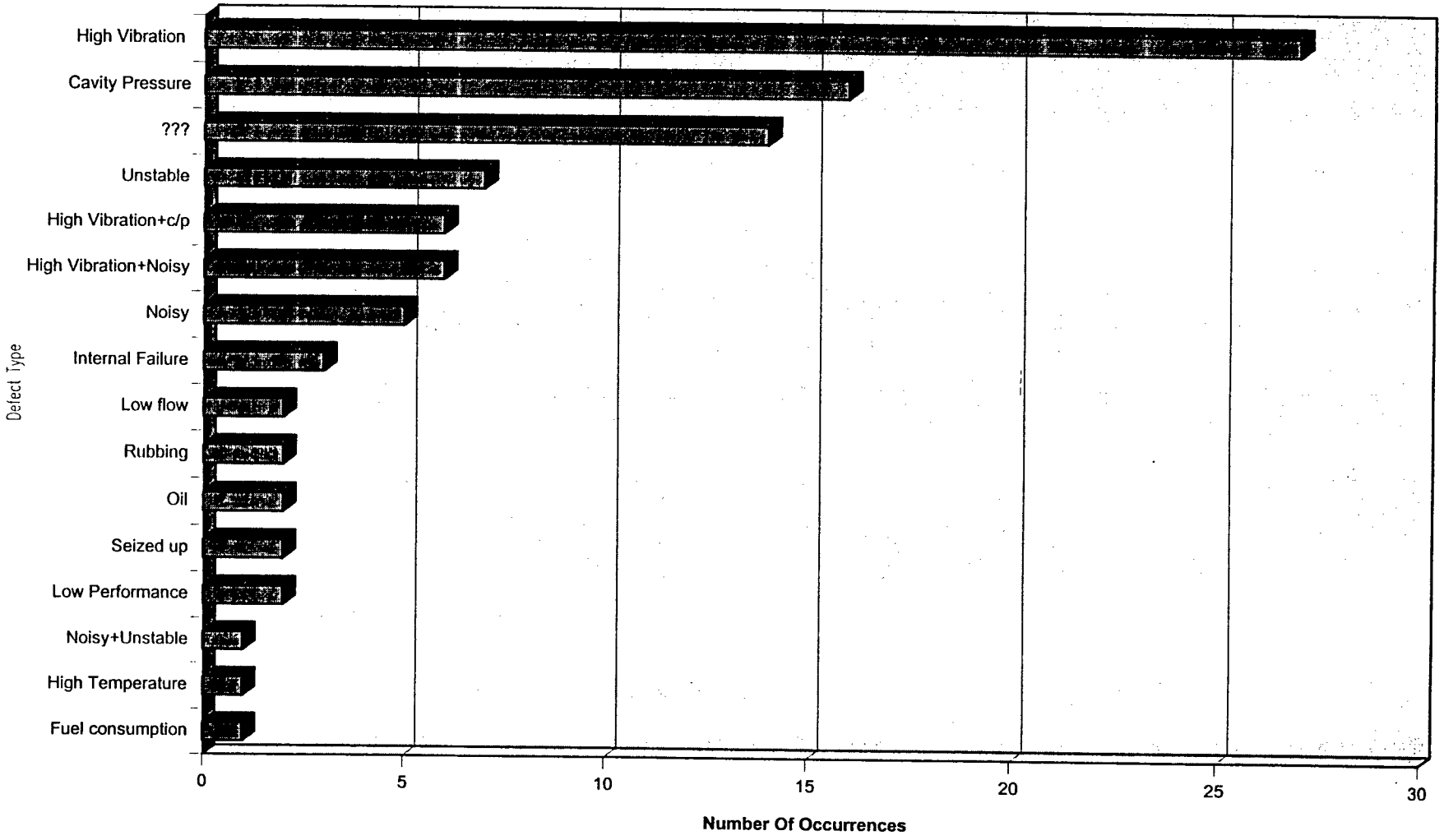

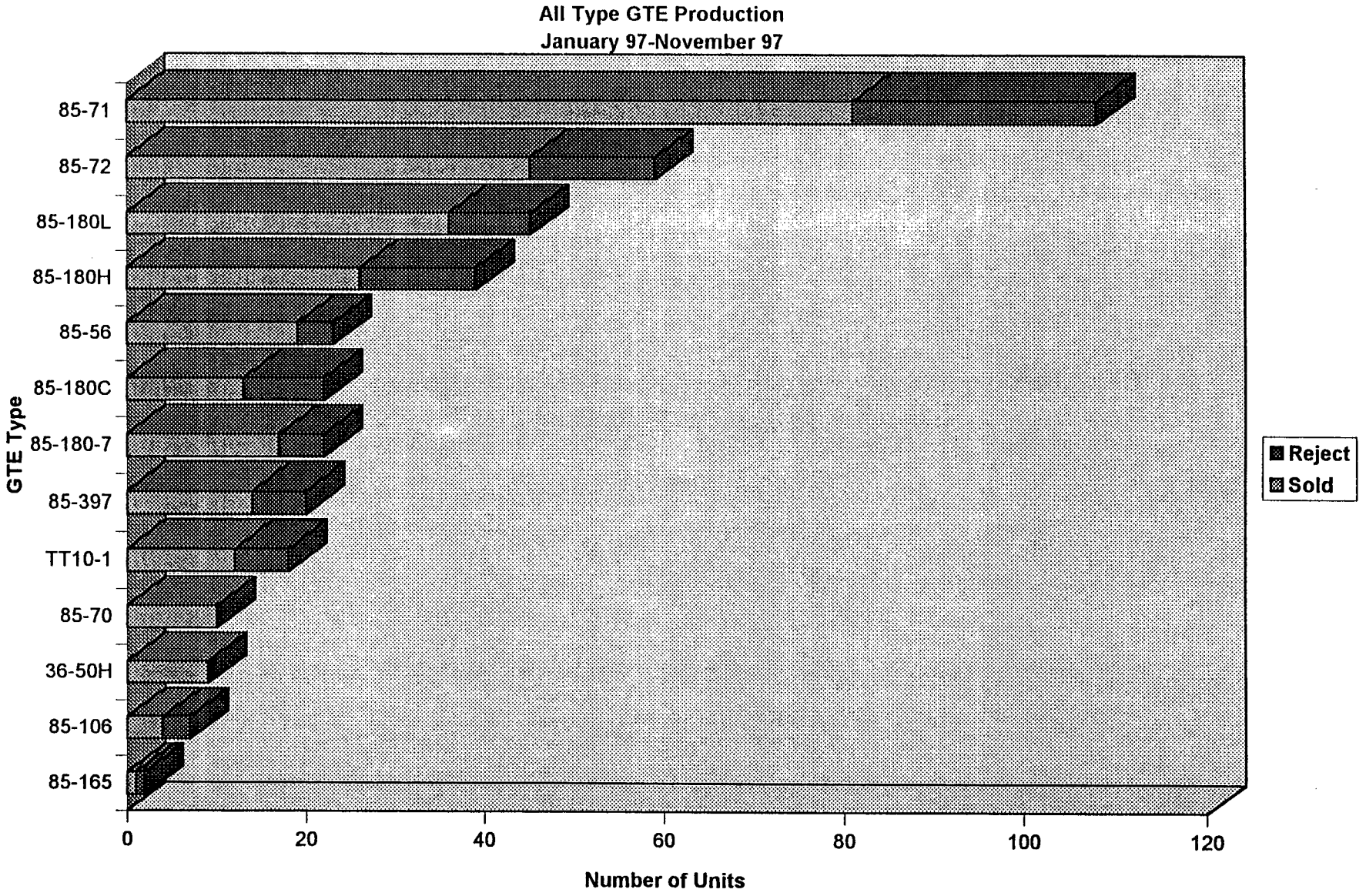
All Type GTE Production
January 97-November 97
GTE Type
85-71
85-72
85-180L
85-180H
85-56
85-180C
85-180-7
85-397
TT10-1
85-70
36-50H
85-106
85-165
0
20
40
60
80
100
120
Number of Units
Reject
Sold

GTE Reject Statistics

January 97 through November 97

GTE TYPE

Defect Type	36-50H	85-106	85-165	85-180-7	85-180C	85-180H	85-180L	85-397	85-56	85-70	85-71	85-72	TT10-1	Total	Percentage
Tested	9	7	2	22	22	39	45	20	23	10	108	59	18	384	
High Vibration		3	1	1	1	4	2	2			8	5		27	27.8%
???				2		1	1	2			3	2	3	14	14.4%
Cavity Pressure				1	4	4	5				1		1	16	16.5%
Unstable									1		6			7	7.2%
High Vibration+Noisy							1	1	1		2		1	6	6.2%
Noisy								1				4		5	5.2%
High Vibration+c/p				1	2	3								6	6.2%
Internal Failure					1							2		3	3.1%
Low Performance											2			2	2.1%
Seized up											2			2	2.1%
Oil									1			1		2	2.1%
Rubbing					1	1								2	2.1%
Fuel consumption													1	1	1.0%
High Temperature											1			1	1.0%
Low flow											2			2	2.1%
Noisy+Unstable									1					1	1.0%
Total	0	3	1	5	9	13	9	6	4	0	27	14	6	97	
Reject Rate	0%	43%	50%	23%	41%	33%	20%	30%	17%	0%	25%	24%	33%		

IX. Load Valves:

In April 97 branch chief LDPB Daniel Alvarado asked the project team to look into the situation of the Load Valve shop. He presumes the shop is suffering considerable reject rates. We then talked to the load valve supervisor LDPBH Frank Trevino to illustrate our operations in his shop. He surprised us with a very defensive attitude, thinking that we were working on ruining his career. We tried to convince him that his fears are unfounded and that all we want to do is to help him improve his production.

Mr. Trevino tried to convince us that the situation is in control and that he is well aware of the problems in his shop. According to him, what causes rejects most of the time are the disks that are out of round. The disks are rotated by an actuator radially inside a round barrel to control flow. A seal fits between the disk rim and the barrel. There would a leak if the disk or the barrel is not round, or if the seal is damaged.

The testing procedures in the shop are unusual. When a load valve is found to be defective, it is not logged as a reject. Instead, it is repaired on the test stand or in the shop. Only when the item passes all the tests that it recorded in the logbook. This way, all the logbook shows is sold items. In other words, a reject rate of 0%, even though, considerable effort and time is put in reworking failed items. Obviously, this kind of data cannot be used to do any statistics. In order to identify and solve the shop problems, we need to know about the shop internal rejects.

Project team members talked to some mechanics and testers individually to determine the reason for this kind of practice. They have simply answered if they reported rejects, the supervisor would penalize them. The supervisor responded he could be transferred if too many rejects are reported in his shop.

We tried to convince him that we were trying to help him produce better load valves without having to rework them. Finally, he seemed to agree to let the testers report the rejects correctly.

Data was gathered on all the load valves that were serviced in the shop. Those included the following control numbers: 65897A, 07613A, 13495A, 66269A, 08852A, and 67248A.

After gathering and analyzing three months worth of data, April through June, it became clear that the records were unusable. In the month of April, mechanics and/or the testers recorded some rejects along with the reject reasons. They told us, however, that some load valves are still being repaired on the test stand, and therefore, are not recorded as rejects. In May and June, on the other hand, no reject reasons were noted in the logbook.

X. The F-16 PTO Shafts:

The PTO shaft shop ran out of brand new parts and there was not enough funding to purchase more. Consequently, the mechanics had to use the old ones more often. The number of Quality Deficiency Reports (QDR) then increased significantly. This has unveiled some of the weaknesses within the shop. The project team and LDCQ Carlos Flores investigated the mechanics procedures and their equipment and came up with some valuable recommendations in their preliminary report.

F16 PTO Shaft. Engineering Report.

Problem Statement: The PTO Shaft is part of the Accessory Drive Gearbox (ADG) on the F16 jet engine. Recently, three PTO shafts were returned from the field, and reported as being deficient (QDR). Further investigation by Quality Assurance (QA) personnel has uncovered defects in more shafts here at the ALC.

Initial Findings: After visiting the PTO Shaft area, collecting the available data, observing the process of grinding/prepping the shafts, and charting the measurements taken using standard SPC techniques, the following was found. There will be more findings as investigation continues.

I. ***Journal Runout (Concentricity) Check Process is Inefficient/Imprecise:***

A. The runout check is performed by placing the shaft in a fixture on a table, then spinning the shaft by hand while a gauge rides along the journal. If the table moves at all, even if someone just leans on it, an inaccurate reading will result.

B. The tolerance on the runout is .0001. The gauge that is used to measure runout has smallest range increments of .0001. It is a very small needle movement. It could be interpreted as different readings by different people. A mechanic, who had measured runout on several shafts previously, found different readings the next day on the same shafts.

C. The gauge used to measure runout has not been calibrated since 1995. The calibration schedule is 18 months.

II. ***There is no documentation that the Grinder used to grind shafts has been checked for accuracy:***

A. There is no evidence of a PM schedule, or other such calibration cycle.

III. ***Large Diameter Journal Size is Usually Very Close to Lower T.O. Limit:***

A. X Bar Charts show that the shafts are within T.O. limits, they are usually very close to, or right on, the lower limit for journal size, as recommended by the T.O.

IV. ***Large Diameter Journal Runout (Concentricity) Measurements Show High Variance, and Process is Out of Control:***

A. The average (X Bar) runout measurement is out of T.O. limits for runout tolerance.

V. ***Small Diameter Journal Size Measurements Show High Variance:***

A. Although average journal size is close to the center of T.O. limits, there is still a high degree of variance in journal measurements.

Recommendations: The following are immediately apparent after initial investigation. More recommendations may come as investigation continues.

1. New instrumentation be provided to perform the runout measurements. This should include a more accurate gauge, preferably a digital gauge, that has increments of at most .00001". Additionally, the procedure should be performed on an absolutely stable platform/fixture setup.

2. QA/Engineering should check with the machine shop to see how they perform measurements on similar items.

3. The Grinder should be checked for accuracy. QA/Engineering and a machinist should do at least ten sample grinds and then verify them with a micrometer. Supervision should investigate the procedures for periodically verifying the accuracy of machine tools, and ensure this one is in compliance.

4. As an alternative, this process may be better performed in the machine shop by a Master machinist.

LDCQ Carlos Flores explained that they have bought 100 new PTO shafts and those need not be measured for Diameter and Runout. They are only balanced. The data are shown in the following charts.

F-16 PTO Shaft Large Diameter Control Chart

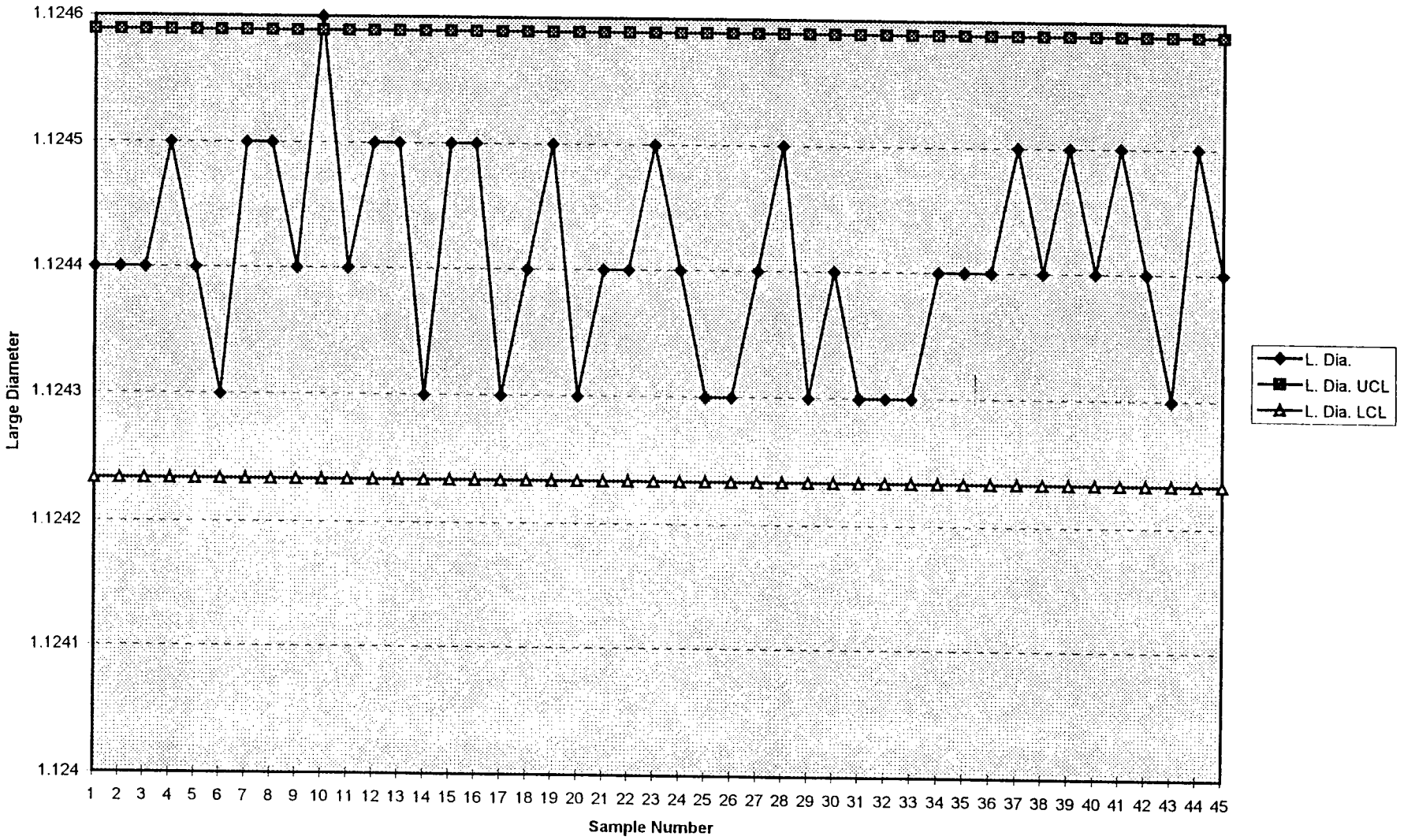

F-16 PTO Shaft Small Diameter Control Chart

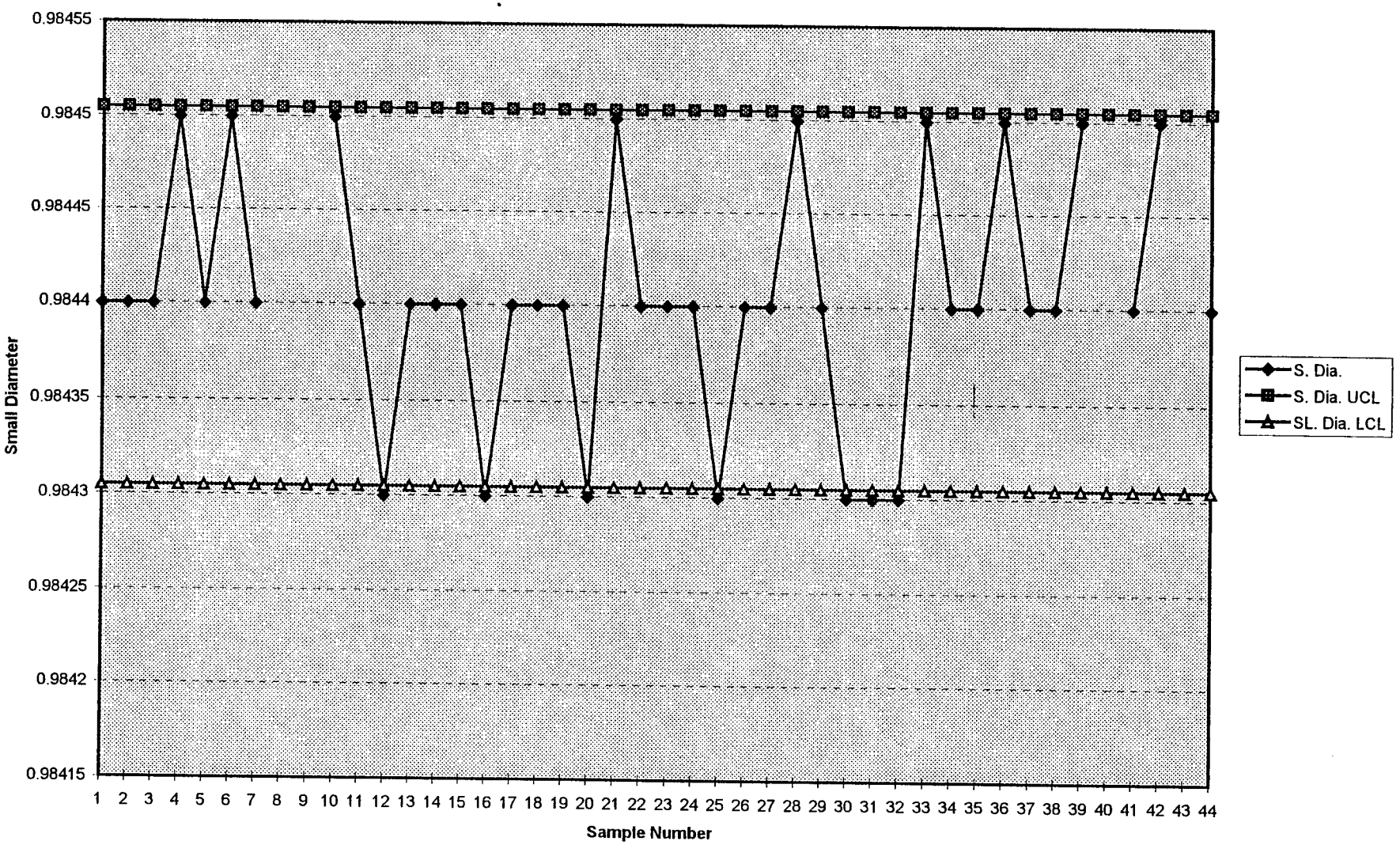

Conclusions and Observations

Some general conclusions and observations on the year long project team effort:

- Communication is very inefficient and the major cause of problems
- Reject rates can be reduced when people work in a cooperative manner, i.e. fuel control area
- Convincing middle supervision that statistical analysis is beneficial in finding out problems, in solving problems, and in keeping problems from reoccurring
- The QA person is the contact with the production area and must be the interpreter of SPC application
- SPC teams meet at the discretion of the QA specialist when problems arise
- Workers and people in the organization have an interest in making improvements

The general problems that exist in the LD Directorate leading to inefficiency and the non-use of statistical analysis including SPC:

- Low morale due to the knowledge of the base closing within the next few years
- Branch Level management's unwillingness to use an engineering approach to solving inefficiencies and problems that arise
- Lack of employees following their boss's orders
- QA is not interested in doing more because they know in order to solve problems they must have a greater work load
- Some QA specialists seem to think that their only function is to work QDRs
- Some supervisors are always on the defensive and blame someone else for the troubles – a lack of accountability
- Pressure on the mechanics and testers leads to shortcuts and inaccurate reporting
- There is no tracking of defective parts being done – the systems in place are either too complicated, changing too often to make them clear, or are misunderstood by those who are supposed to use them
- There is an overall resistance to change that sometimes borders on insubordination as in attendance at meetings and compliance with orders from bosses

General comments and recommendations on the positive results of the project team:

- Disposed of hundreds of rejected parts – found reasons for reject, found proper resolution and routing location, saw to it that part was routed correctly – procedures should be continued
- Implemented SPC work team meetings that should be continued
- Reduced kit part rejects in F-15 CGB and procedures should be continued
- Improved process in F-16 PTO Shafts and procedures should be continued
- Identified high reject rates on F5/T38 Gear Boxes
- Implemented SPC charting and control in CGB area and PTO area and charting should be continued
- Implemented various statistical analysis techniques such as Pareto analysis, cause/effect analysis, data gathering techniques and error tracking techniques as well as SPC and all should be continued

Associate did not participate in the program.